

# Cardiovascular Fluid Mechanics

- lecture notes -

**F.N. van de Vosse**  
**and**  
**M.E.H. van Dongen**

**(1998)**

Eindhoven University of Technology  
faculty of Mechanical Engineering (MaTe)  
faculty of Applied Physics (NT)



## **Preface**

As cardiovascular disease is a major cause of death in the western world, knowledge of cardiovascular pathologies, including heart valve failure and atherosclerosis is of great importance. This knowledge can only be gathered after well understanding the circulation of the blood. Also for the development and usage of diagnostic techniques, like ultrasound and magnetic resonance assessment of blood flow and vessel wall displacement, knowledge of the fluid mechanics of the circulatory system is indispensable. Moreover, awareness of cardiovascular fluid mechanics is of great help in endovascular treatment of diseased arteries, the design of vascular prostheses that can replace these arteries when treatment is not successful, and in the development of prosthetic heart valves. Finally, development and innovation of extra-corporal systems strongly relies on insight into cardiovascular fluid mechanics. The lecture notes focus on fluid mechanical phenomena that occur in the human cardiovascular system and aim to contribute to better understanding of the circulatory system.

In the introductory part of these notes a short overview of the circulatory system with respect to blood flow and pressure will be given. In chapter 1 a simple model of the vascular system will be presented despite the fact that the fluid mechanics of the cardiovascular system is complex due to the non-linear and non-homogeneous rheological properties of blood and arterial wall, the complex geometry and the pulsatile flow properties.

After this introduction, in chapter 2, a short review of the equations governing fluid mechanics is given. This includes the main concepts determining the constitutive equations for both fluids and solids. Using limiting values of the non-dimensional parameters, simplifications of these equations will be derived in subsequent chapters. A chapter on the fluid mechanics of the heart (chapter 3), which is an important topic with respect to cardiac diseases and heart valve dynamics, is not yet written and will be provided in a future version of this manuscript.

An important part, chapter 4, is dedicated to the description of Newtonian flow in straight, curved and bifurcating, rigid tubes. With the aid of characteristic dimensionless parameters the flow phenomena will be classified and related to specific physiological phenomena in the cardiovascular system. In this way difference between flow in the large arteries and flow in the micro-circulation and veins and the difference between flow in straight and curved arteries will be elucidated. It will be shown that the flow in branched tubes shows a strong resemblance to the flow in curved tubes.

Although flow patterns as derived from rigid tube models do give a good approximation of those that can be found in the vascular system, they will not provide information on pressure pulses and wall motion. In order to obtain this information a short introduction to vessel wall mechanics will be given and models for wall motion of distensible tubes as a function of a time dependent pressure load will be derived in chapter 5.

The flow in distensible tubes is determined by wave propagation of the pressure pulse. The main characteristics of the wave propagation including attenuation and reflection of waves at geometrical transitions are treated in chapter 6, using a one-dimensional wave propagation model.

As blood is a fluid consisting of blood cells suspended in plasma its rheological properties differ from that of a Newtonian fluid. In chapter 7 constitutive equations for Newtonian flow, generalized Newtonian flow, viscoelastic flow and the flow of suspensions will be dealt with. It will be shown that the viscosity of blood is shear and history dependent as a result of the presence of deformation and aggregation of the red blood cells that are suspended in plasma. The importance of non-Newtonian properties of blood for the flow in large and medium sized arteries will be discussed. Finally in chapter 8 the importance of the rheological (non-Newtonian) properties of blood, and especially its particulate character, for the flow in the micro-circulation will be elucidated. Velocity profiles as a function of the ratio between the vessel diameter and the diameter of red blood cells will be derived.

In order to obtain a better understanding of the physical meaning, many of the mathematical models that are treated are implemented in MATLAB. Descriptions of these implementations are available in a separate manuscript: 'Cardiovascular Fluid Mechanics - computational models'.

# Contents

<b>1</b>	<b>General introduction</b>	<b>1</b>
1.1	Introduction . . . . .	1
1.2	The cardiovascular system . . . . .	2
1.2.1	The heart . . . . .	2
1.2.2	The systemic circulation . . . . .	4
1.3	Pressure and flow in the cardiovascular system . . . . .	6
1.3.1	Pressure and flow waves in arteries . . . . .	6
1.3.2	Pressure and flow in the micro-circulation . . . . .	10
1.3.3	Pressure and flow in the venous system . . . . .	10
1.4	Simple model of the vascular system . . . . .	10
1.4.1	Periodic deformation and flow . . . . .	10
1.4.2	The windkessel model . . . . .	11
1.4.3	Vascular impedance . . . . .	12
1.5	Summary . . . . .	13
<b>2</b>	<b>Basic equations</b>	<b>15</b>
2.1	Introduction . . . . .	15
2.2	The state of stress and deformation . . . . .	16
2.2.1	Stress . . . . .	16
2.2.2	Displacement and deformation . . . . .	16
2.2.3	Velocity and rate of deformation . . . . .	19
2.2.4	Constitutive equations . . . . .	20
2.3	Equations of motion . . . . .	21
2.3.1	Reynolds' transport theorem . . . . .	21
2.3.2	Continuity equation . . . . .	22
2.3.3	The momentum equation . . . . .	23
2.3.4	Initial and boundary conditions . . . . .	24
2.4	Summary . . . . .	24
<b>3</b>	<b>Fluid mechanics of the heart</b>	<b>25</b>
3.1	Introduction . . . . .	25
3.2	Summary . . . . .	25

<b>4</b>	<b>Newtonian flow in blood vessels</b>	<b>27</b>
4.1	Introduction . . . . .	27
4.2	Incompressible Newtonian flow in general . . . . .	28
4.2.1	Incompressible viscous flow . . . . .	28
4.2.2	Incompressible in-viscid flow . . . . .	29
4.2.3	Incompressible boundary layer flow . . . . .	30
4.3	Steady and pulsatile Newtonian flow in straight tubes . . . . .	32
4.3.1	Fully developed flow . . . . .	32
4.3.2	Entrance flow . . . . .	39
4.4	Steady and pulsating flow in curved and branched tubes . . . . .	41
4.4.1	Steady flow in a curved tube . . . . .	41
4.4.2	Unsteady fully developed flow in a curved tube . . . . .	47
4.4.3	Flow in branched tubes . . . . .	49
4.5	Summary . . . . .	49
<b>5</b>	<b>Mechanics of the vessel wall</b>	<b>51</b>
5.1	Introduction . . . . .	51
5.2	Morphology . . . . .	52
5.3	Mechanical properties . . . . .	53
5.4	Incompressible elastic deformation . . . . .	56
5.4.1	Deformation of incompressible linear elastic solids . . . . .	56
5.4.2	Approximation for small strains . . . . .	57
5.5	Wall motion . . . . .	59
5.6	Summary . . . . .	61
<b>6</b>	<b>Wave phenomena in blood vessels</b>	<b>63</b>
6.1	Introduction . . . . .	63
6.2	Pressure and flow . . . . .	64
6.3	Fluid flow . . . . .	65
6.4	Wave propagation . . . . .	67
6.4.1	Derivation of a quasi one-dimensional model . . . . .	67
6.4.2	Wave speed and attenuation constant . . . . .	70
6.5	Wave reflection . . . . .	75
6.5.1	Wave reflection at discrete transitions . . . . .	75
6.5.2	Multiple wave reflection: effective admittance . . . . .	78
6.5.3	Vascular impedance and cardiac work . . . . .	81
6.6	Summary . . . . .	82
<b>7</b>	<b>Non-Newtonian flow in blood vessels</b>	<b>83</b>
7.1	Introduction . . . . .	83
7.2	Mechanical properties of blood . . . . .	84
7.2.1	Morphology . . . . .	84
7.2.2	Rheological properties of blood . . . . .	86
7.3	Newtonian models . . . . .	89
7.3.1	Constitutive equations . . . . .	89
7.3.2	Viscometric results . . . . .	90

7.4	Generalized Newtonian models . . . . .	90
7.4.1	Constitutive equations . . . . .	90
7.4.2	Viscometric results . . . . .	91
7.5	Viscoelastic models . . . . .	94
7.5.1	Constitutive equations . . . . .	94
7.5.2	Viscometric results . . . . .	97
7.6	Rheology of suspensions . . . . .	100
7.6.1	Constitutive equations . . . . .	100
7.6.2	Viscometric results . . . . .	102
7.7	Rheology of whole blood . . . . .	102
7.7.1	Experimental observations . . . . .	102
7.7.2	Constitutive equations . . . . .	104
7.8	Summary . . . . .	105
<b>8</b>	<b>Flow patterns in the micro-circulation</b>	<b>107</b>
8.1	Introduction . . . . .	107
8.2	Flow in small arteries and small veins: $D_v > 2D_c$ . . . . .	108
8.3	Velocity profiles . . . . .	109
8.3.1	Flow . . . . .	109
8.3.2	Effective viscosity . . . . .	109
8.3.3	Concentration . . . . .	110
8.3.4	Cell velocity . . . . .	111
8.4	Flow in arterioles and venules : $D_c < D_v < 2D_c$ . . . . .	112
8.4.1	Velocity profiles . . . . .	112
8.4.2	Flow . . . . .	113
8.4.3	Effective viscosity . . . . .	113
8.4.4	Concentration . . . . .	113
8.4.5	Cell velocity . . . . .	114
8.5	Flow in capillaries: $D_v < D_c$ . . . . .	114
8.6	Summary . . . . .	116



# Chapter 1

## General introduction

### 1.1 Introduction

The study of cardiovascular fluid mechanics is only possible with some knowledge of cardiovascular physiology. In this chapter a brief introduction to cardiovascular physiology will be given. Some general aspects of the fluid mechanics of the heart, the arterial system, the micro-circulation and the venous system as well as the most important properties of the vascular tree that determine the pressure and flow characteristics in the cardiovascular system will be dealt with. Although the fluid mechanics of the vascular system is complex due to complexity of geometry and pulsatility of the flow, a simple linear model of this system will be derived.

## 1.2 The cardiovascular system

The cardiovascular system takes care of convective transport of blood between the organs of the mammalian body in order to enable diffusive transport of oxygen, carbon oxide, nutrients and other solutes at cellular level in the tissues. Without this convective transport an appropriate exchange of these solutes would be impossible because of a too large diffusional resistance. An extended overview of physiological processes that are enabled by virtue of the cardiovascular system can be found in standard text books on physiology like Guyton (1967).

The circulatory system can be divided into two parts in series, the pulmonary circulation and the systemic circulation (see figure 1.1). Blood received by the right atrium (RA) from the venae cavae is pumped from the right ventricle (RV) of the heart into the pulmonary artery which strongly bifurcates in pulmonary arterioles transporting the blood to the lungs. The left atrium (LA) receives the oxygenated blood back from the pulmonary veins. Then the blood is pumped via the left ventricle (LV) into the systemic circulation. As from fluid mechanical point of view the main flow phenomena in the pulmonary circulation match the phenomena in the systemic circulation, in the sequel of this course only the systemic circulation will be considered.

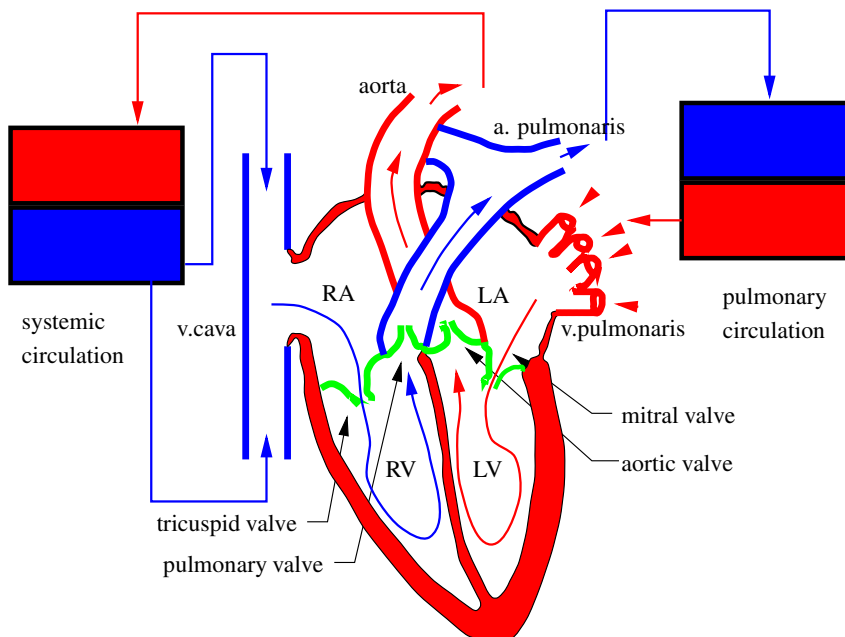


Figure 1.1: Schematic representation of the heart and the circulatory system. RA = right atrium, LA = left atrium, RV = right ventricle, LV = left ventricle.

### 1.2.1 The heart

The forces needed for the motion of the blood are provided by the heart, which serves as a four-chambered pump that propels blood around the circulatory system

(see figure 1.1). Since the mean pressure in the systemic circulation is approximately 13[kPa], which is more than three times the pressure in the pulmonary system ( $\approx 4$ [kPa]), the thickness of the left ventricular muscle is much larger than that of the right ventricle.

The ventricular and aortic pressure and aortic flow during the cardiac cycle are given in figure 1.2. Atrial contraction, induced by a stimulus for muscle contraction of the sinoatrial node, causes a filling of the ventricles with hardly any increase of the ventricular pressure. In the left heart the mitral valve is opened and offers very low resistance. The aortic valve is closed. Shortly after this, at the onset of systole the two ventricles contract simultaneously controlled by a stimulus generated by the atrioventricular node. At the same time the mitral valve closes (mc) and a sharp pressure rise in the left ventricle occurs. At the moment that this ventricular pressure exceeds the pressure in the aorta, the aortic valve opens (ao) and blood is ejected into the aorta. The ventricular and aortic pressure first rise and then fall as a result of a combined action of ventricular contraction forces and the resistance and compliance of the systemic circulation. Due to this pressure fall (or actually the corresponding flow deceleration) the aortic valve closes (ac) and the pressure in the ventricle drops rapidly, the mitral valve opens (mo), while the heart muscle relaxes (diastole).

Since, in the heart, both the blood flow velocities as well as the geometrical length scales are relatively large, the fluid mechanics of the heart is strongly determined by inertial forces which are in equilibrium with pressure forces.

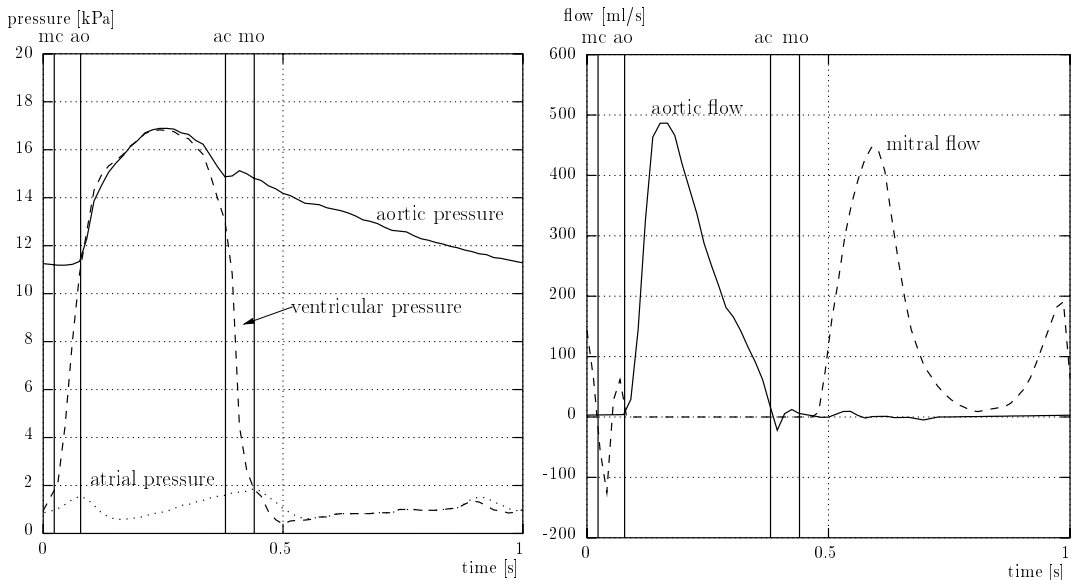


Figure 1.2: Pressure in the left atrium, left ventricle and the aorta (left) and flow through the mitral valve and the aorta (right) as a function of time during one cardiac cycle (after Milnor, 1989). With times: mc = mitral valve closes, ao = aortic valve opens, ac = aortic valve closes and mo = mitral valve opens.

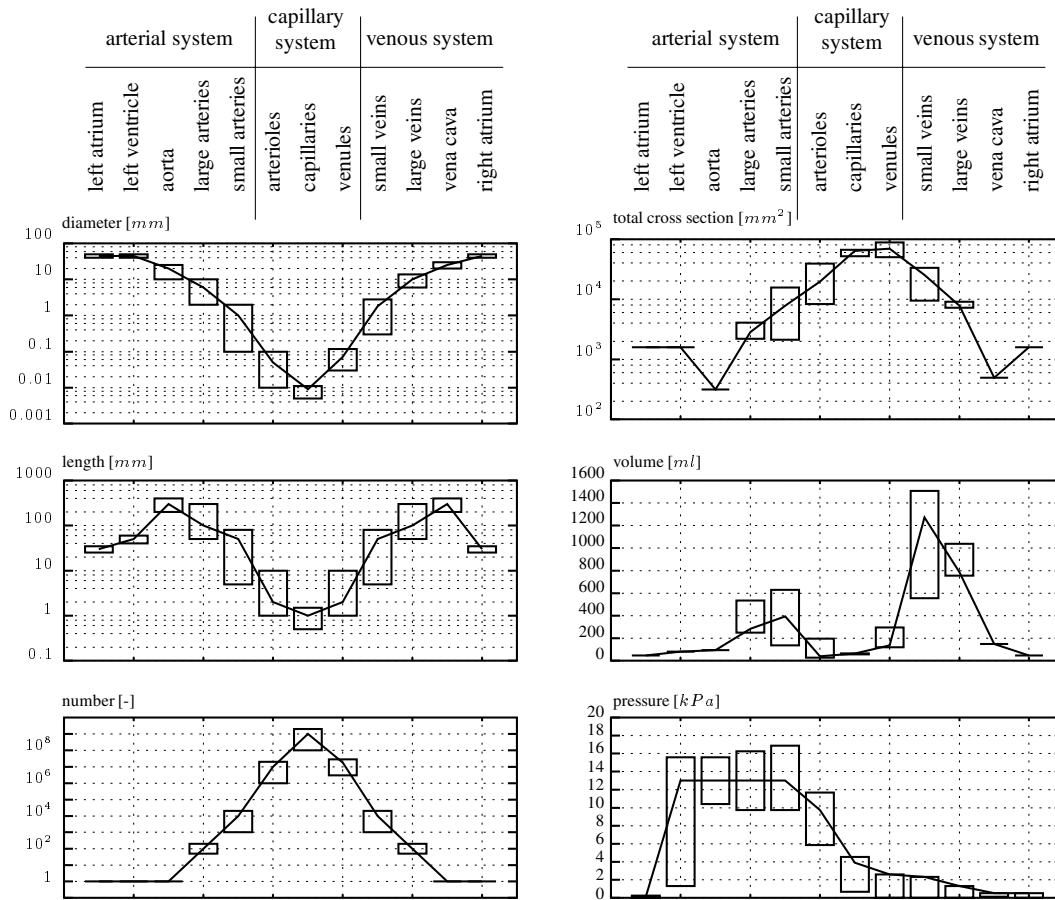


Figure 1.3: Rough estimates of the diameter, length and number of vessels, their total cross-section and volume and the pressure in the vascular system.

### 1.2.2 The systemic circulation

The systemic circulation can be divided into three parts: the arterial system, the capillary system and the venous system. The main characteristics of the systemic circulation are depicted schematically in figure 1.3.

From figure 1.3 it can be seen that the diameter of the blood vessels strongly decrease from the order of  $0.5 - 20 [mm]$  in the arterial system to  $5 - 500 [\mu m]$  in the capillary system. The diameters of the vessels in the venous system in general are slightly larger than those in the arterial system. The length of the vessels also strongly decreases and increases going from the arterial system to the venous system but only changes in two decades. Most dramatic changes can be found in the number of vessels that belong to the different compartments of the vascular system. The number of vessels in the capillary system is of order  $O(10^6)$  larger than in the arterial and venous system. As a consequence, the total cross section in the capillary system is about 1000 times larger than in the arterial and the venous system, enabling an efficient exchange of solutes in the tissues by diffusion. Combination of the different

dimensions mentioned above shows that the total volume of the venous system is about 2 times larger than the volume of the arterial system and much larger than the total volume of the capillary system. As can be seen from the last figure, the mean pressure falls gradually as blood flows into the systemic circulation. The pressure amplitude, however, shows a slight increase in the proximal part of the arterial system.

The **arterial system** is responsible for the transport of blood to the tissues. Besides the transport function of the arterial system the pulsating flow produced by the heart is also transformed to a more-or-less steady flow in the smaller arteries. Another important function of the arterial system is to maintain a relatively high arterial pressure. This is of importance for a proper functioning of the brain and kidneys. This pressure can be kept at this relatively high value because the distal end of the arterial system strongly bifurcates into vessels with small diameters (arterioles) and hereby forms a large peripheral resistance. The smooth muscle cells in the walls are able to change the diameter and hereby the resistance of the arterioles. In this way the circulatory system can adopt the blood flow to specific parts in accordance to momentary needs (vasoconstriction and vasodilatation). Normally the heart pumps about 5 liters of blood per minute but during exercise the heart minute volume can increase to 25 liters. This is partly achieved by an increase of the heart frequency but is mainly made possible by local regulation of blood flow by vasoconstriction and vasodilatation of the distal arteries (arterioles). Unlike the situation in the heart, in the arterial system, also viscous forces may become of significant importance as a result of a decrease in characteristic velocity and length scales (diameters of the arteries).

Leaving the arterioles the blood flows into the **capillary system**, a network of small vessels. The walls consist of a single layer of endothelial cells lying on a basement membrane. Here an exchange of nutrients with the interstitial liquid in the tissues takes place. In physiology, capillary blood flow is mostly referred to as micro circulation. The diameter of the capillaries is so small that the whole blood may not be considered as a homogeneous fluid anymore. The blood cells are moving in a single file (train) and strongly deform. The plasma acts as a lubrication layer. The fluid mechanics of the capillary system hereby strongly differs from that of the arterial system and viscous forces dominate over inertia forces in their equilibrium with the driving pressure forces.

Finally the blood is collected in the **venous system** (venules and veins) in which the vessels rapidly merge into larger vessels transporting the blood back to the heart. The total volume of the venous system is much larger than the volume of the arterial system. The venous system provides a storage function which can be controlled by constriction of the veins (venoconstriction) that enables the heart to increase the arterial blood volume. As the diameters in the venous system are of the same order of magnitude as in the arterial system, inertia forces may become influential again. Both characteristic velocities and pressure amplitudes, however, are lower than in the arterial system. As a consequence, in the venous system, instationary inertia

forces will be of less importance than in the arterial system. Moreover, the pressure in the venous system is that low that gravitational forces become of importance. The geometrical dimensions referred to above and summarized in figure 1.3 show that the vascular tree is highly bifurcating and will be geometrically complex. Flow phenomena related with curvature and bifurcation of the vessels (see chapter 4) can not be neglected. As in many cases the length of the vessels is small compared to the length needed for fully developed flow, also entrance flow must be included in studies of cardiovascular fluid mechanics.

## 1.3 Pressure and flow in the cardiovascular system

### 1.3.1 Pressure and flow waves in arteries

The pressure in the aorta significantly changes with increasing distance from the heart. The peak of the pressure pulse delays downstream indicating wave propagation along the aorta with a certain wave speed. Moreover, the shape of the pressure pulse changes and shows an increase in amplitude, a steepening of the front and only a moderate fall of the mean pressure (see figure 1.4).

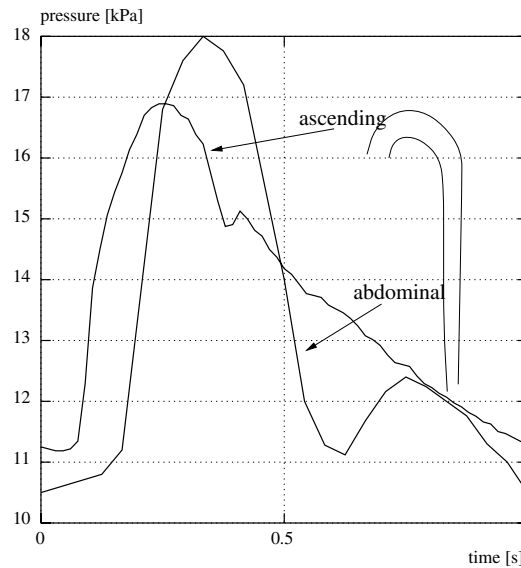


Figure 1.4: Typical pressure waves at two different sites in the aorta

This wave phenomenon is a direct consequence of the distensibility of the arterial wall, allowing a partial storage of the blood injected from the heart due to an increase of the pressure and the elastic response of the vessel walls. The cross-sectional area of the vessels depend on the pressure difference over the wall. This pressure difference is called the transmural pressure and is denoted by  $p_{tr}$ . This transmural pressure consists of several parts. First, there exists a hydrostatic part proportional to the density of the blood inside  $\rho$ , the gravity force  $g$  and the height  $h$ . This hydrostatic part is a result of the fact that the pressure outside the vessels is closely to atmospheric. Next, the pressure is composed of a time independent

part  $p_0$  and a periodic, time dependent part  $p$ . So the transmural pressure can be written as:

$$p_{tr} = \rho q h + p_0 + p \quad (1.1)$$

Due to the complex nonlinear anisotropic and viscoelastic properties of the arterial wall, the relation between the transmural pressure and the cross sectional area  $A$  of the vessel is mostly nonlinear and can be rather complicated. Moreover it varies from one vessel to the other. Important quantities with respect to this relation, used in physiology, are the compliance or alternatively the distensibility of the vessel. The compliance  $C$  is defined as:

$$C = \frac{\partial A}{\partial p} \quad (1.2)$$

The distensibility  $D$  is defined by the ratio of the compliance and the cross sectional area and hereby is given by:

$$D = \frac{1}{A} \frac{\partial A}{\partial p} = \frac{C}{A} \quad (1.3)$$

In the sequel of this course these quantities will be related to the material properties of the arterial wall. For thin walled tubes, with radius  $a$  and wall thickness  $h$ , without longitudinal strain, e.g., it can be derived that:

$$D = \frac{2a}{h} \frac{1 - \mu^2}{E} \quad (1.4)$$

Here  $\mu$  denotes Poisson's ratio and  $E$  Young's modulus. From this we can see that besides the properties of the material of the vessel ( $E, \mu$ ) also geometrical properties ( $a, h$ ) play an important role.

The value of the ratio  $a/h$  varies strongly along the arterial tree. The veins are more distensible than the arteries. Mostly, in some way, the pressure-area relationship, i.e. the compliance or distensibility, of the arteries or veins that are considered, have to be determined from experimental data. A typical example of such data is given in figure 1.5 where the relative transmural pressure  $p/p_0$  is given as a function of the relative cross-sectional area  $A/A_0$ . As depicted in this figure, the compliance changes with the pressure load since at relatively high transmural pressure, the collagen fibres in the vessel wall become stretched and prevent the artery from further increase of the circumferential strain.

The flow is driven by the gradient of the pressure and hereby determined by the propagation of the pressure wave. Normally the pressure wave will have a pulsating periodic character. In order to describe the flow phenomena we distinguish between steady and unsteady part of this pulse. Often it is assumed that the unsteady part can be described by means of a linear theory, so that we can introduce the concept of pressure and flow waves which be superpositions of several harmonics:

$$p = \sum_{n=1}^N p_n e^{ni\omega t} \quad q = \sum_{n=1}^N q_n e^{ni\omega t} \quad (1.5)$$

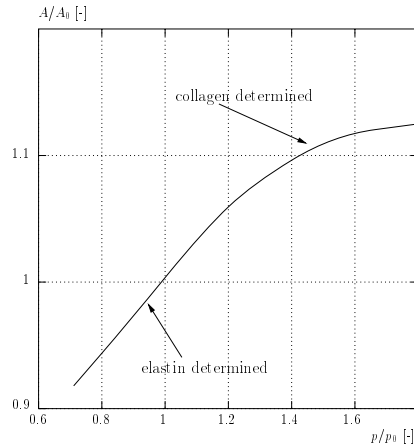


Figure 1.5: Typical relation between the relative transmurial pressure  $p/p_0$  and the relative cross-sectional area  $A/A_0$  of an artery.

Here  $p_n$  and  $q_n$  are the complex Fourier coefficients and hereby  $p$  and  $q$  are the complex pressure and the complex flow,  $\omega$  denotes the angular frequency of the basic harmonic. Actual pressure and flow can be obtained by taking the real part of these complex functions. Normally spoken 6 to 10 harmonics are sufficient to describe the most important features of the pressure wave. Table 1.3.1 is adopted from Milnor (1989) and represents the modulus and phase of the first 10 harmonics of the pressure and flow in the aorta. The corresponding pressure and flow are given in figure 1.6.

	$q$ in $ml/s$		$p$ in $mmHg$	
harmonic	modulus	phase	modulus	phase
0	110	0	85	0
1	202	-0.78	18.6	-1.67
2	157	-1.50	8.6	-2.25
3	103	-2.11	5.1	-2.61
4	62	-2.46	2.9	-3.12
5	47	-2.59	1.3	-2.91
6	42	-2.91	1.4	-2.81
7	31	+2.92	1.2	+2.93
8	19	+2.66	0.4	-2.54
9	15	+2.73	0.6	-2.87
10	15	+2.42	0.6	+2.87

Table 1.1: First 10 harmonics of the pressure and flow in the aorta (from Milnor, 1989).

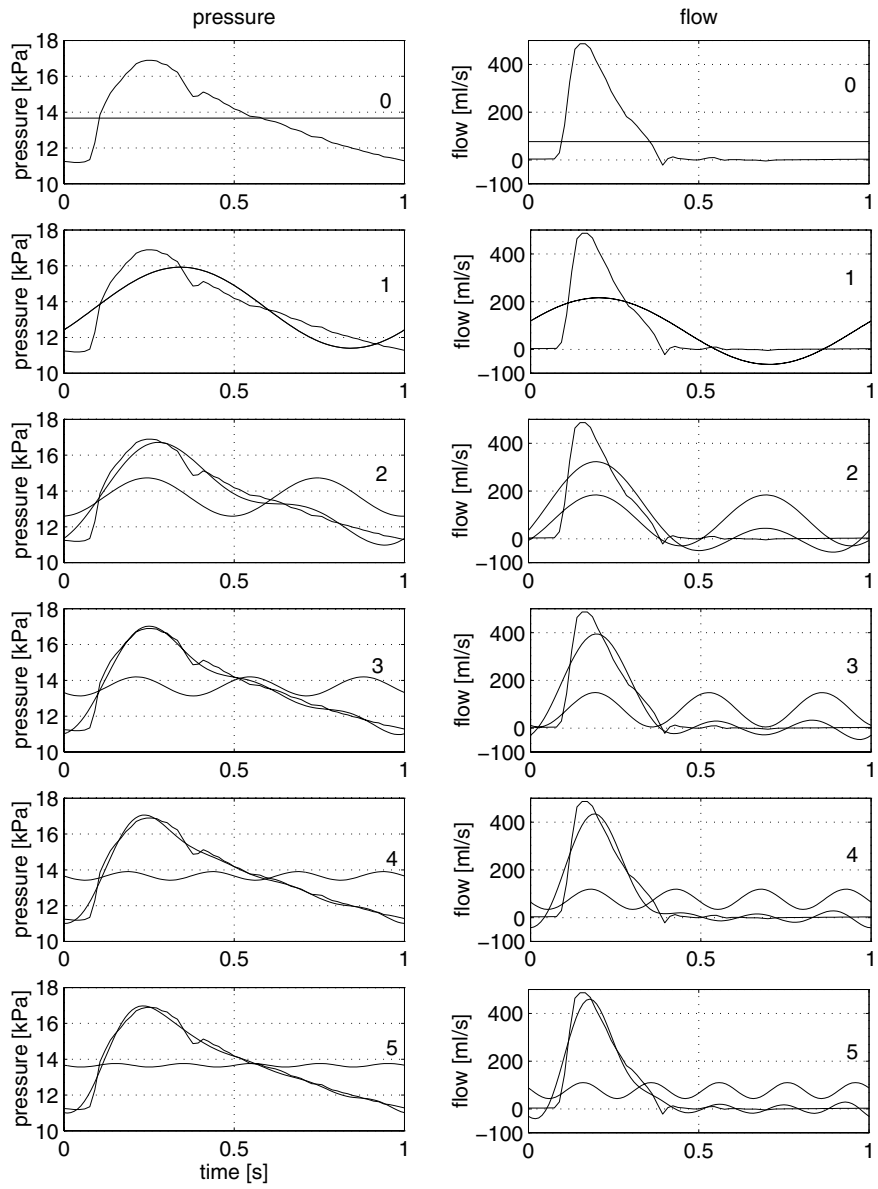


Figure 1.6: Pressure and flow in the aorta based on the data given in table 1.3.1

### 1.3.2 Pressure and flow in the micro-circulation

The micro-circulation is a strongly bifurcating network of small vessels and is responsible for the exchange of nutrients and gases between the blood and the tissues. Mostly blood can leave the arterioles in two ways. The first way is to follow a metarteriole towards a specific part of the tissue and enter the capillary system. This second way is to bypass the tissue by entering an arterio venous anastomosis that shortcuts the arterioles and the venules. Smooth muscle cells in the walls of the metarterioles, precapillary sphincters at the entrance of the capillaries and glomus bodies in the anastomoses regulate the local distribution of the flow. In contrast with the arteries the pressure in the micro-vessels is more or less constant in time yielding an almost steady flow. This steadiness, however, is strongly disturbed by the 'control actions' of the regulatory system of the micro-circulation. As the dimensions of the blood cells are of the same order as the diameter of the micro-vessels the flow and deformation properties of the red cells must be taken into account in the modeling of the flow in the micro-circulation (see chapter 4).

### 1.3.3 Pressure and flow in the venous system

The morphology of the systemic veins resemble arteries. The wall however is not as thick as in the arteries of the same diameter. Also the pressure in a vein is much lower than the pressure in an artery of the same size. In certain situations the pressure can be so low that in normal functioning the vein will have an elliptic cross-sectional area or even will be collapsed for some time. Apart from its different wall thickness and the relatively low pressures, the veins distinguish from arteries by the presence of valves to prevent back flow.

## 1.4 Simple model of the vascular system

### 1.4.1 Periodic deformation and flow

In cardiovascular fluid dynamics the flow often may be considered as periodic if we assume a constant duration of each cardiac cycle. In many cases, i.e. if the deformation and the flow can be described by a linear theory, the displacements and velocity can be decomposed in a number of harmonics using a Fourier transform:

$$v = \sum_{n=0}^N \hat{v}_n e^{in\omega t} \quad (1.6)$$

Here  $\hat{v}_n$  are the complex Fourier coefficients,  $\omega$  denotes the angular frequency of the basic harmonic. Note that a complex notation of the velocity is used exploiting the relation:

$$e^{i\omega t} = \cos(\omega t) + i \sin(\omega t) \quad (1.7)$$

with  $i = \sqrt{-1}$ . The actual velocity can be obtained by taking the real part of the complex velocity. By substitution of relation (1.6) in the governing equations that describe the flow, often an analytical solution can be derived for each harmonic.

Superposition of these solution then will give a solution for any periodic flow as long as the equations are linear in the solution  $v$ .

### 1.4.2 The windkessel model

Incorporating some of the physiological properties described above several models for the cardiovascular system has been derived in the past. The most simple model is the one that is known as the *windkessel* model. In this model the aorta is represented by a simple compliance  $C$  (elastic chamber) and the peripheral blood vessels are assumed to behave as a rigid tube with a constant resistance ( $R_p$ ) (see left hand side of figure 1.7). The pressure  $p_a$  in the aorta as a function of the left ventricular flow  $q_a$  then is given by:

$$q_a = C \frac{\partial p_a}{\partial t} + \frac{p_a}{R_p} \tag{1.8}$$

or after Fourier transformation:

$$\hat{q}_a = (i\omega C + \frac{1}{R_p}) \hat{p}_a \tag{1.9}$$

In the right hand side of figure 1.7 experimental data ((Milnor, 1989) of the flow in the aorta (top figure) is plotted as a function of time. This flow is used as input for the computation of the pressure from (1.8) and compared with experimental data (dotted resp. solid line in figure 1.7). The resistance  $R_p$  and compliance  $C$  were obtained from a least square fit and turned out to be  $R_p = 0.18[kPa \cdot s/ml]$  and  $C = 11.5[ml/kPa]$ .

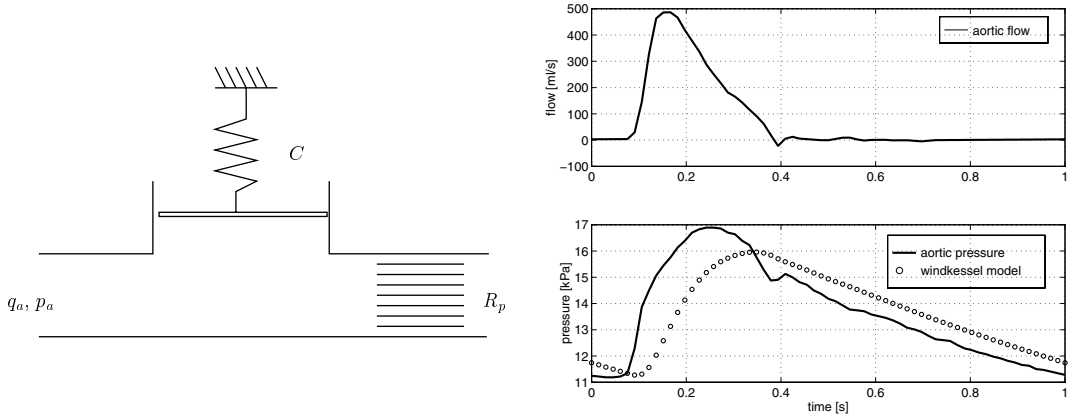


Figure 1.7: Windkessel model of the cardiovascular system (left). Aortic flow and pressure (data from Milnor, 1989) as function of time with pressure obtained from the windkessel model indicated with the dotted line.

During the diastolic phase of the cardiac cycle the aortic flow is relatively low and (1.8) can be approximated by:

$$\frac{\partial p_a}{\partial t} \approx \frac{1}{R_p C} p_a \quad \text{during diastole} \tag{1.10}$$

with solution  $p_a \approx p_{as}e^{-t/R_p C}$  with  $p_{as}$  peak systolic pressure. This approximate solution reasonably corresponds with experimental data.

During the systolic phase of the flow the aortic flow is much larger than the peripheral flow ( $q_a \gg p_a/R_p$ ) yielding:

$$\frac{\partial p_a}{\partial t} \approx \frac{1}{C}q_a \quad \text{during systole} \quad (1.11)$$

with solution  $p_a \approx p_{ad} + (1/C) \int q_a dt$  with  $p_{ad}$  the diastolic pressure. Consequently a phase difference between pressure and flow is expected. Experimental data, however, show  $p_a \approx p_{ad} + kq_a$ , so pressure and flow are more or less in-phase (see figure 1.7). Notwithstanding the significant phase error in the systolic phase, this simple Windkessel model is often used to derive the cardiac work at given flow. Note that for linear time-periodic systems, better fits can be obtained using the complex notation (1.9) with frequency dependent resistance ( $R_p(\omega)$ ) and compliance  $C(\omega)$ .

In chapter 6 of this course we will show that this model has strong limitations and is in contradiction with important features of the vascular system.

### 1.4.3 Vascular impedance

As mentioned before the flow of blood is driven by the force acting on the blood induced by the gradient of the pressure. The relation of these forces to the resulting motion of blood is expressed in the longitudinal impedance:

$$Z_L = \frac{\partial \hat{p}}{\partial z} / \hat{q} \quad (1.12)$$

The longitudinal impedance is a complex number defined by complex pressures and complex flows. It can be calculated by frequency analysis of the pressure gradient and the flow that have been recorded simultaneously. As it expresses the flow induced by a local pressure gradient, it is a property of a small (infinitesimal) segment of the vascular system and depends on local properties of the vessel. The longitudinal impedance plays an important role in the characterization of vascular segments. It can be measured by a simultaneous determination of the pulsatile pressure at two points in the vessel with a known small longitudinal distance apart from each other together with the pulsatile flow. In the chapter 6, the longitudinal impedance will be derived mathematically using a linear theory for pulsatile flow in rigid and distensible tubes. A second important quantity is the input impedance defined as the ratio of the pressure and the flow at a specific cross-section of the vessel:

$$Z_i = \hat{p} / \hat{q} \quad (1.13)$$

The input impedance is not a local property of the vessel but a property of a specific site in the vascular system. If some input condition is imposed on a certain site in the system, then the input impedance only depends on the properties of the entire vascular tree distal to the cross-section where it is measured. In general the input impedance at a certain site depends on both the proximal and distal vascular tree. The compliance of an arterial segment is characterized by the transverse impedance defined by:

$$Z_T = \hat{p} / \frac{\partial \hat{q}}{\partial z} \approx -\hat{p} / i\omega \hat{A} \quad (1.14)$$

This relation expresses the flow drop due to the storage of the vessel caused by the radial motion of its wall ( $A$  being the cross-sectional area) at a given pressure (note that  $i\omega\hat{A}$  represents the partial time derivative  $\partial A/\partial t$ ). In chapter 6 it will be shown that the impedance-functions as defined here can be very useful in the analysis of wave propagation and reflection of pressure and flow pulses traveling through the arterial system.

## 1.5 Summary

In this chapter a short introduction to cardiovascular fluid mechanics is given. A simple (windkessel) model has been derived based on the knowledge that the cardiovascular systems is characterized by an elastic part (large arteries) and a flow resistance (micro circulation) In this model it is ignored that the fluid mechanics of the cardiovascular system is characterized by complex geometries and complex constitutive behavior of the blood and the vessel wall. The vascular system, however, is strongly bifurcating and time dependent (pulsating) three-dimensional entrance flow will occur. In the large arteries the flow will be determined by both viscous and inertia forces and movement of the nonlinear viscoelastic anisotropic wall may be of significant importance. In the smaller arteries viscous forces will dominate and non-Newtonian viscoelastic properties of the blood may become essential in the description of the flow field.

In the next chapter the basic equations that govern the fluid mechanics of the cardiovascular system (equations of motion and constitutive relations) will be derived. With the aid of characteristic dimensionless numbers these equations often can be simplified and solved for specific sites of the vascular system. This will be the subject of the subsequent chapters.



## Chapter 2

# Basic equations

### 2.1 Introduction

In this section the equations that govern the deformation of a solid and motion of a fluid will be given. For isothermal systems these can be derived from the equations of conservation of mass and momentum. For non-isothermal systems the motion is also determined by the conservation of energy. Using limiting values of the non-dimensional parameters, simplifications of these equations can be derived that will be used in subsequent chapters. For a detailed treatment of general fluid dynamics and boundary layer flow the reader is referred to Batchelor (1967) and Schlichting (1960) respectively. More details concerning non-Newtonian and viscoelastic fluid flow can be found in chapter 7 and in Bird *et al.* (1960, 1987).

## 2.2 The state of stress and deformation

### 2.2.1 Stress

If an arbitrary body with volume  $\Omega(t)$  is in mechanical equilibrium, then the sum of all forces acting on the body equals zero and the body will neither accelerate, nor deform. If we cut the body with a plane  $\Gamma_c$  with normal  $\mathbf{n}$ , we need a surface force in order to prevent deformation and acceleration of the two parts (see figure 2.1). In each point this surface force can be represented by the product of a stress vector  $\mathbf{s}$  and an infinitesimal surface element  $d\Gamma_c$ . The stress vector  $\mathbf{s}$  will vary with the location in and the normal direction of the cutting plane and can be defined according to:

$$\mathbf{s} = \mathbf{n} \cdot \boldsymbol{\sigma} \quad (2.1)$$

The tensor  $\boldsymbol{\sigma}$  is the Cauchy stress tensor and completely determines the state of stress of the body and, different from  $\mathbf{s}$ , does not depend on the orientation of the cutting plane. Note that at the boundary of the volume  $\Omega$  the Cauchy stress tensor defines the surface force or surface stress acting on the the body. This surface stress can be decomposed in a normal stress acting in normal direction of the surface and a shear stress acting in tangential direction.

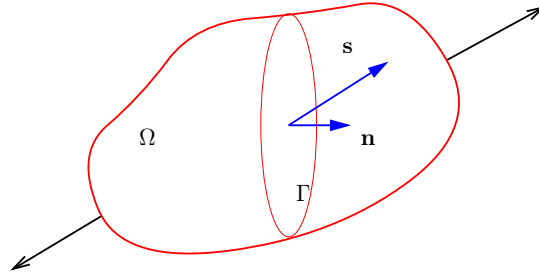


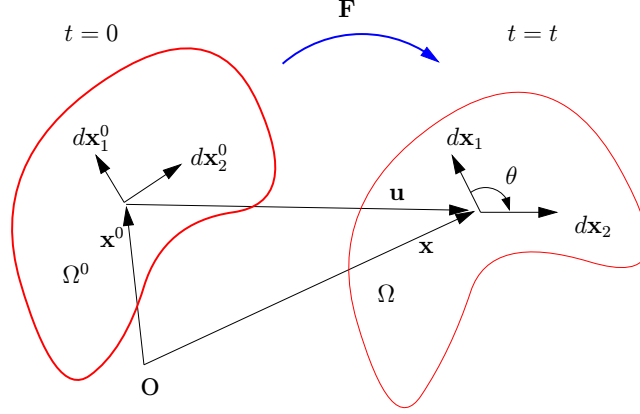
Figure 2.1: Volume  $\Omega$  cut by a plane  $\Gamma_c$  with normal  $\mathbf{n}$ .

### 2.2.2 Displacement and deformation

In the previous section the state of stress of a body is defined by introducing a stress tensor. Also a measure for the deformation of the body can be defined by a tensor: the deformation gradient tensor  $\mathbf{F}$ . If a continuous body deforms from one state  $\Omega^0$  to another  $\Omega$ , this deformation is determined by the **displacement vector** of all material points  $\mathbf{x}^0$  of the body:

$$\mathbf{u}(\mathbf{x}^0, t) = \mathbf{x}(\mathbf{x}^0, t) - \mathbf{x}^0. \quad (2.2)$$

Note that we have identified each material point  $\xi$  of the body with its position vector  $\mathbf{x}(\xi)$  at time  $t = t^0$  (i.e.  $\mathbf{x}(\xi, 0) = \mathbf{x}^0(\xi)$ ). So the position vector  $\mathbf{x}$  of a material point depends on the initial position  $\mathbf{x}^0$  and the time  $t$ . For convenience, from now on we will omit the  $\xi$ -dependency in the notation and will denote with  $\mathbf{x} = \mathbf{x}(\mathbf{x}^0, t)$  the position vectors of all material points  $\xi$  at time  $t$  (note:  $\mathbf{x}(\mathbf{x}^0, 0) = \mathbf{x}^0$ ).

Figure 2.2: Volume  $\Omega$  before and after deformation.

Each infinitesimal material vector  $d\mathbf{x}^0$  in the reference state  $\Omega^0$  will stay infinitesimal after deformation but will stretch and rotate to a new vector  $d\mathbf{x}$  (see figure 2.2 where the infinitesimal vectors  $d\mathbf{x}_1$  and  $d\mathbf{x}_2$  are given). The relation between  $d\mathbf{x}^0$  and  $d\mathbf{x}$  can be defined by the deformation gradient tensor  $\mathbf{F}$  defined by:

$$d\mathbf{x} = (\nabla^0 \mathbf{x})^c \cdot d\mathbf{x}^0 \equiv \mathbf{F} \cdot d\mathbf{x}^0 \quad (2.3)$$

**Remark :**

The operator  $\nabla^0$  is the gradient operator with respect to the initial reference frame. In Cartesian coordinates this yields:

$$\mathbf{F} = (\nabla^0 \mathbf{x})^c = \begin{bmatrix} \frac{\partial x_1}{\partial x_1^0} & \frac{\partial x_1}{\partial x_2^0} & \frac{\partial x_1}{\partial x_3^0} \\ \frac{\partial x_2}{\partial x_1^0} & \frac{\partial x_2}{\partial x_2^0} & \frac{\partial x_2}{\partial x_3^0} \\ \frac{\partial x_3}{\partial x_1^0} & \frac{\partial x_3}{\partial x_2^0} & \frac{\partial x_3}{\partial x_3^0} \end{bmatrix} \quad (2.4)$$

Also the notation  $\mathbf{F} = \frac{\partial \mathbf{x}}{\partial \mathbf{x}^0}$  is often used yielding  $d\mathbf{x} = \frac{\partial \mathbf{x}}{\partial \mathbf{x}^0} \cdot d\mathbf{x}^0$ .

If we want to construct constitutive equations, we want to relate the state of deformation  $\mathbf{F}$  to the state of stress  $\boldsymbol{\sigma}$ . If we would simply take  $\boldsymbol{\sigma} = \boldsymbol{\sigma}(\mathbf{F})$  then in general a simple rotation of the whole body  $\Omega$  would introduce a change of state of the stress  $\boldsymbol{\sigma}$ . This of course is physical nonsense. True deformation consists of stretch and shear and should not contain translation and rotation. The stretch of the material vector  $d\mathbf{x}^0$  is given by:

$$\begin{aligned} \lambda &= \frac{\|d\mathbf{x}\|}{\|d\mathbf{x}^0\|} = \sqrt{\frac{d\mathbf{x} \cdot d\mathbf{x}}{\|d\mathbf{x}^0\| \|d\mathbf{x}^0\|}} = \sqrt{\frac{\mathbf{F} \cdot d\mathbf{x}^0 \cdot \mathbf{F} \cdot d\mathbf{x}^0}{\|d\mathbf{x}^0\| \|d\mathbf{x}^0\|}} \\ &= \sqrt{\frac{d\mathbf{x}^0 \cdot \mathbf{F}^c \cdot \mathbf{F} \cdot d\mathbf{x}^0}{\|d\mathbf{x}^0\| \|d\mathbf{x}^0\|}} = \sqrt{\mathbf{e}^0 \cdot \mathbf{F}^c \cdot \mathbf{F} \cdot \mathbf{e}^0} \end{aligned} \quad (2.5)$$

with  $\mathbf{e}^0 = d\mathbf{x}^0 / \|d\mathbf{x}^0\|$  the unit vector in the direction of  $d\mathbf{x}^0$  and  $\mathbf{F}^c$  the transpose of  $\mathbf{F}$ . The shear deformation between two initially perpendicular material vectors  $d\mathbf{x}_1^0$  and  $d\mathbf{x}_2^0$  is determined by the angle  $\theta$  between the vectors after deformation (see figure 2.2):

$$\begin{aligned} \cos(\theta) &= \frac{d\mathbf{x}_1 \cdot d\mathbf{x}_2}{\sqrt{d\mathbf{x}_1 \cdot d\mathbf{x}_1} \sqrt{d\mathbf{x}_2 \cdot d\mathbf{x}_2}} \\ &= \frac{\mathbf{e}_1^0 \cdot \mathbf{F}^c \cdot \mathbf{F} \cdot \mathbf{e}_2^0}{\sqrt{\mathbf{e}_1^0 \cdot \mathbf{F}^c \cdot \mathbf{F} \cdot \mathbf{e}_1^0} \sqrt{\mathbf{e}_2^0 \cdot \mathbf{F}^c \cdot \mathbf{F} \cdot \mathbf{e}_2^0}} \end{aligned} \quad (2.6)$$

Equations (2.5) and (2.6) show that true deformation can be described by the Cauchy-Green deformation tensor  $\mathbf{C}$  given by:

$$\mathbf{C} = \mathbf{F}^c \cdot \mathbf{F} \quad (2.7)$$

Note that in the derivation of the stretch  $\lambda$  and the shear  $\theta$  the vectors  $d\mathbf{x}$ ,  $d\mathbf{x}_1$  and  $d\mathbf{x}_2$  are eliminated using the definition of the deformation gradient tensor  $\mathbf{F}$ . This means that the stretch and shear is defined with respect to the initial geometry  $\Omega^0$ . This is common in solid mechanics where the initial state is mostly well known and free of stress.

In a similar way one can derive:

$$\lambda = \frac{\|d\mathbf{x}\|}{\|d\mathbf{x}^0\|} = \sqrt{\mathbf{e} \cdot \mathbf{F} \cdot \mathbf{F}^c \cdot \mathbf{e}} \quad (2.8)$$

and:

$$\cos(\theta) = \frac{\mathbf{e}_1 \cdot \mathbf{F} \cdot \mathbf{F}^c \cdot \mathbf{e}_2}{\sqrt{\mathbf{e}_1 \cdot \mathbf{F} \cdot \mathbf{F}^c \cdot \mathbf{e}_1} \sqrt{\mathbf{e}_2 \cdot \mathbf{F} \cdot \mathbf{F}^c \cdot \mathbf{e}_2}} \quad (2.9)$$

Note that now the stretch and shear is defined with respect to the new (deformed) geometry, which is more suitable for fluids but also commonly used for rubber-like solids.

The tensor product

$$\mathbf{B} = \mathbf{F} \cdot \mathbf{F}^c \quad (2.10)$$

is called the Finger tensor.

**Remark :**

The Finger tensor can also be derived by decomposing the deformation gradient tensor into a stretching part  $\mathbf{U}$  and a rotation  $\mathbf{R}$ :

$$\mathbf{F} = \mathbf{U} \cdot \mathbf{R} \quad (2.11)$$

By multiplying  $\mathbf{F}$  with its transpose ( $\mathbf{F} \cdot \mathbf{F}^c = \mathbf{U} \cdot \mathbf{R} \cdot (\mathbf{U} \cdot \mathbf{R})^c = \mathbf{U} \cdot \mathbf{R} \cdot \mathbf{R}^c \cdot \mathbf{U}^c = \mathbf{U} \cdot \mathbf{U}^c$ ), the rotation is removed since for rotation  $\mathbf{R} \cdot \mathbf{R}^c = \mathbf{I}$  must hold.

Unlike the deformation gradient tensor  $\mathbf{F}$  the Cauchy-Green deformation tensor  $\mathbf{C} = \mathbf{F}^c \cdot \mathbf{F}$  and the Finger tensor  $\mathbf{B} = \mathbf{F} \cdot \mathbf{F}^c$  both can be used to construct constitutive relations relating the state of deformation with the state of stress without introducing spurious stresses after simple rotation.

### 2.2.3 Velocity and rate of deformation

In fluid mechanics not only the deformation but also the rate of deformation is of importance. The rate of deformation depends on the relative velocity  $d\mathbf{v}$  between two points defined by the material vector  $d\mathbf{x}$ . The velocity of material points  $\mathbf{x} = \mathbf{x}(\mathbf{x}^0, t)$  is defined by the rate of displacement:

$$\begin{aligned} \mathbf{v}(\mathbf{x}^0, t) &= \dot{\mathbf{u}}(\mathbf{x}^0, t) \\ &= \lim_{\Delta t \rightarrow 0} \frac{\mathbf{u}(\mathbf{x}^0, t + \Delta t) - \mathbf{u}(\mathbf{x}^0, t)}{\Delta t} \end{aligned} \quad (2.12)$$

Together with the definition of the displacement (2.2) this yields:

$$\begin{aligned} \mathbf{v}(\mathbf{x}^0, t) &= \lim_{\Delta t \rightarrow 0} \frac{\mathbf{x}(\mathbf{x}^0, t + \Delta t) - \mathbf{x}(\mathbf{x}^0, t)}{\Delta t} \\ &= \dot{\mathbf{x}}(\mathbf{x}^0, t) \end{aligned} \quad (2.13)$$

The rate of change of a infinitesimal material vector  $d\mathbf{x}$  follows from (2.3) and reads:

$$d\mathbf{v} = d\dot{\mathbf{x}} = \dot{\mathbf{F}} \cdot d\mathbf{x}^0 \quad (2.14)$$

The infinitesimal velocity can also be related to the infinitesimal material vector according to:

$$d\mathbf{v} = \frac{\partial \mathbf{v}}{\partial \mathbf{x}} \cdot d\mathbf{x} + \frac{\partial \mathbf{v}}{\partial t} dt \quad (2.15)$$

and for a fixed instant of time ( $dt = 0$ ):

$$d\mathbf{v} = \frac{\partial \mathbf{v}}{\partial \mathbf{x}} \cdot d\mathbf{x} \equiv \mathbf{L} \cdot d\mathbf{x} \quad (2.16)$$

$\mathbf{L}$  is called the velocity gradient tensor.

Using (2.16) this yields  $\mathbf{L} \cdot d\mathbf{x} = d\mathbf{v} = d\dot{\mathbf{x}} = \dot{\mathbf{F}} \cdot d\mathbf{x}^0 = \dot{\mathbf{F}} \cdot \mathbf{F}^{-1} d\mathbf{x}$ , showing that the tensor  $\dot{\mathbf{F}}$  is defined by the tensor product of the velocity gradient tensor and the deformation gradient tensor:

$$\dot{\mathbf{F}} = \mathbf{L} \cdot \mathbf{F} \quad (2.17)$$

The velocity gradient tensor  $\mathbf{L}$  is often written as the dyadic product of the gradient vector  $\nabla$  and the velocity vector  $\mathbf{v}$ :

$$\mathbf{L} = \frac{\partial \mathbf{v}}{\partial \mathbf{x}} = (\nabla \mathbf{v})^c \quad (2.18)$$

If we want to relate the rate of deformation to the state of stress we must decompose  $\mathbf{L}$  into a part that describes the rate of deformation and a part that represents the rate of rotation. This is achieved by the following decomposition:

$$\mathbf{L} = \mathbf{D} + \mathbf{\Omega} \quad (2.19)$$

with:

$$\mathbf{D} = \dot{\mathbf{U}} = \frac{1}{2}(\mathbf{L} + \mathbf{L}^c) = \frac{1}{2}(\nabla \mathbf{v} + (\nabla \mathbf{v})^c) \quad (2.20)$$

$$\mathbf{\Omega} = \dot{\mathbf{R}} = \frac{1}{2}(\mathbf{L} - \mathbf{L}^c) = \frac{1}{2}(\nabla \mathbf{v} - (\nabla \mathbf{v})^c) \quad (2.21)$$

$2\mathbf{D}$  (also written as  $\dot{\gamma}$ ) is the **rate of deformation** or rate of strain tensor and  $\mathbf{\Omega}$  is the **vorticity** or spin tensor. This can be derived readily if we realize that in (2.14) we are only interested in the instantaneous rate of separation of points, i.e. we consider a deformation that takes place in an infinitesimal period of time  $dt$  so  $\mathbf{x}^0 \rightarrow \mathbf{x}$ . In that case we have after combination of (2.11) and (2.17):

$$\lim_{\mathbf{x}^0 \rightarrow \mathbf{x}} \mathbf{L} \cdot \mathbf{F} = \lim_{\mathbf{x}^0 \rightarrow \mathbf{x}} (\dot{\mathbf{U}} \cdot \mathbf{R} + \mathbf{U} \cdot \dot{\mathbf{R}}) \quad (2.22)$$

Since  $\mathbf{L}$ ,  $\dot{\mathbf{U}}$  and  $\dot{\mathbf{R}}$  are defined in the current reference state they only depend on  $\mathbf{x}$  and  $t$  and do not depend on  $\mathbf{x}^0$  we get:

$$\mathbf{L} \cdot \lim_{\mathbf{x}^0 \rightarrow \mathbf{x}} \mathbf{F} = \dot{\mathbf{U}} \cdot \lim_{\mathbf{x}^0 \rightarrow \mathbf{x}} \mathbf{R} + \lim_{\mathbf{x}^0 \rightarrow \mathbf{x}} \mathbf{U} \cdot \dot{\mathbf{R}} \quad (2.23)$$

and thus by virtue of  $\lim_{\mathbf{x}^0 \rightarrow \mathbf{x}} \mathbf{F} = \lim_{\mathbf{x}^0 \rightarrow \mathbf{x}} \mathbf{U} = \lim_{\mathbf{x}^0 \rightarrow \mathbf{x}} \mathbf{R} = \mathbf{I}$ :

$$\mathbf{L} = \dot{\mathbf{U}} + \dot{\mathbf{R}} \quad (2.24)$$

So, the velocity gradient tensor  $\mathbf{L}$  is the sum of the rate of stretching tensor  $\dot{\mathbf{U}}$  and the rate of rotation tensor  $\dot{\mathbf{R}}$ .

## 2.2.4 Constitutive equations

For later use in deriving constitutive equations the following relations are given:

$$\begin{aligned} \dot{\mathbf{B}} &= \dot{\mathbf{F}} \cdot \mathbf{F}^c + \mathbf{F} \cdot \dot{\mathbf{F}}^c \\ &= \mathbf{L} \cdot \mathbf{F} \cdot \mathbf{F}^c + \mathbf{F} \cdot \mathbf{F}^c \cdot \mathbf{L}^c \\ &= \mathbf{L} \cdot \mathbf{B} + \mathbf{B} \cdot \mathbf{L}^c \end{aligned} \quad (2.25)$$

from which it follows that

$$\dot{\mathbf{B}} = 2\mathbf{D} \quad (2.26)$$

Constitutive equations for solids are oftenly constructed using a relation between the stress tensor  $\boldsymbol{\sigma}$  and the Finger tensor  $\mathbf{B}$ :  $\boldsymbol{\sigma} = \boldsymbol{\sigma}(\mathbf{B})$ . Fluids are mostly described by a relation between the stress tensor  $\boldsymbol{\sigma}$  and the time derivative of the Finger tensor  $\dot{\mathbf{B}}$  or by virtue of (2.26):  $\boldsymbol{\sigma} = \boldsymbol{\sigma}(\mathbf{D})$ . Incompressible media (fluid or solid) on which to a constant pressure force is exerted will not deform. Still the state of stress will change whenever the external pressure changes. This property can be incorporated in the constitutive equations by taking:

$$\boldsymbol{\sigma} = -p\mathbf{I} + \boldsymbol{\tau}(\mathbf{B}) \quad \text{and} \quad \boldsymbol{\sigma} = -p\mathbf{I} + \boldsymbol{\tau}(\mathbf{D}) \quad \text{resp.} \quad (2.27)$$

The tensor  $\boldsymbol{\tau}$  is called the extra stress tensor.

The most simple versions are found for incompressible linear elastic solids that can be described  $\boldsymbol{\sigma} = -p\mathbf{I} + G\mathbf{B}$  and incompressible Newtonian fluids where  $\boldsymbol{\sigma} = -p\mathbf{I} + 2\eta\mathbf{D}$  with  $p$  the pressure,  $G$  the shear modulus and  $\eta$  the dynamic viscosity.

Viscoelastic materials (fluids or solids) in general are characterized by a constitutive equation of the form:  $\boldsymbol{\tau} = \boldsymbol{\tau}(\mathbf{B}, \dot{\mathbf{B}}, \ddot{\mathbf{B}}, \dots)$ . In the sections that follow these relations between stress and strain will be used in different forms.

## 2.3 Equations of motion

The equations needed for the determination of the variables pressure ( $p$ ) and velocity ( $\mathbf{v}$ ) can be derived by requiring conservation of mass, momentum and energy of fluid moving through a small control volume  $\Omega$ . A general procedure to obtain these equations is provided by the transport theorem of Reynolds.

### 2.3.1 Reynolds' transport theorem

Consider an arbitrary volume  $\Omega = \Omega(t)$  with boundary surface  $\Gamma = \Gamma(t)$  not necessarily moving with the fluid and let  $\Psi(\mathbf{x}, t)$  be a scalar, vector or tensor function of space and time defined in  $\Omega(t)$ . The volume integral:

$$\int_{\Omega(t)} \Psi(\mathbf{x}, t) d\Omega \quad (2.28)$$

is a well defined function of time only. The rate of change of  $\Psi$  in  $\Omega(t)$  is given by:

$$\begin{aligned} \frac{d}{dt} \int_{\Omega(t)} \Psi(\mathbf{x}, t) d\Omega = \\ \lim_{\Delta t \rightarrow 0} \frac{1}{\Delta t} \left[ \int_{\Omega(t+\Delta t)} \Psi(\mathbf{x}, t + \Delta t) d\Omega - \int_{\Omega(t)} \Psi(\mathbf{x}, t) d\Omega \right]. \end{aligned} \quad (2.29)$$

If the boundary  $\Gamma(t)$  moves with velocity  $\mathbf{v}_\Gamma$  this will introduce a flux of  $\Psi$  proportional to  $\mathbf{v}_\Gamma \cdot \mathbf{n}$ . As a consequence:

$$\int_{\Omega(t+\Delta t)} \Psi(\mathbf{x}, t + \Delta t) d\Omega = \int_{\Omega(t)} \Psi(\mathbf{x}, t + \Delta t) d\Omega + \Delta t \int_{\Gamma(t)} \Psi(\mathbf{x}, t + \Delta t) \mathbf{v}_\Gamma \cdot \mathbf{n} d\Gamma \quad (2.30)$$

The rate of change of  $\Psi$  then can be written as:

$$\begin{aligned} \frac{d}{dt} \int_{\Omega(t)} \Psi d\Omega &= \lim_{\Delta t \rightarrow 0} \frac{1}{\Delta t} \left[ \int_{\Omega(t)} \Psi(\mathbf{x}, t + \Delta t) d\Omega + \right. \\ &\quad \left. \Delta t \int_{\Gamma(t)} \Psi(\mathbf{x}, t + \Delta t) \mathbf{v}_\Gamma \cdot \mathbf{n} d\Gamma - \int_{\Omega(t)} \Psi(\mathbf{x}, t) d\Omega \right] \\ &= \int_{\Omega(t)} \lim_{\Delta t \rightarrow 0} \frac{1}{\Delta t} [\Psi(\mathbf{x}, t + \Delta t) d\Omega - \Psi(\mathbf{x}, t) d\Omega] + \\ &\quad \int_{\Gamma(t)} \lim_{\Delta t \rightarrow 0} \Psi(\mathbf{x}, t + \Delta t) \mathbf{v}_\Gamma \cdot \mathbf{n} d\Gamma \end{aligned} \quad (2.31)$$

or equivalently:

$$\frac{d}{dt} \int_{\Omega(t)} \Psi d\Omega = \int_{\Omega(t)} \frac{\partial \Psi(\mathbf{x}, t)}{\partial t} d\Omega + \int_{\Gamma(t)} \Psi(\mathbf{x}, t) \mathbf{v}_\Gamma \cdot \mathbf{n} d\Gamma \quad (2.32)$$

In order to derive differential forms of the conservation laws the transport theorem (also called the Leibnitz formula) is often used in combination with the Gauss-Ostrogradskii theorem:

$$\int_{\Omega(t)} (\nabla \cdot \mathbf{v}) d\Omega = \int_{\Gamma(t)} (\mathbf{v} \cdot \mathbf{n}) d\Gamma \quad (2.33)$$

$$\int_{\Omega(t)} (\mathbf{a}(\nabla \cdot \mathbf{v}) + (\mathbf{v} \cdot \nabla) \mathbf{a}) d\Omega = \int_{\Gamma(t)} \mathbf{a}(\mathbf{v} \cdot \mathbf{n}) d\Gamma \quad (2.34)$$

$$\int_{\Omega(t)} (\nabla \cdot \boldsymbol{\tau}^c) d\Omega = \int_{\Gamma(t)} (\boldsymbol{\tau} \cdot \mathbf{n}) d\Gamma \quad (2.35)$$

### 2.3.2 Continuity equation

Consider an arbitrary control volume  $\Omega(t)$  with boundary  $\Gamma(t)$  and outer normal  $\mathbf{n}(\mathbf{x}, t)$  (see figure 2.3). This control volume is placed in a velocity field  $\mathbf{v}(\mathbf{x}, t)$ .

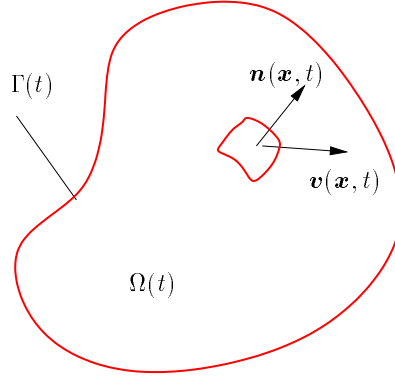


Figure 2.3: Control volume  $\Omega(t)$  with boundary  $\Gamma(t)$  and outer normal  $\mathbf{n}(\mathbf{x}, t)$ .

Conservation of mass requires that the rate of change of mass of fluid within the control volume  $\Omega(t)$  is equal to the flux of mass across the boundary  $\Gamma(t)$ :

$$\frac{d}{dt} \int_{\Omega(t)} \rho d\Omega + \int_{\Gamma(t)} \rho(\mathbf{v} - \mathbf{v}_\Gamma) \cdot \mathbf{n} d\Gamma = 0 \quad (2.36)$$

The first term can be rewritten with Leibnitz formula. Applying the Gauss-Ostrogradskii divergence theorem this yields:

$$\int_{\Omega(t)} \left[ \frac{\partial \rho}{\partial t} + \nabla \cdot (\rho \mathbf{v}) \right] d\Omega = 0 \quad (2.37)$$

Since this equation must hold for all arbitrary control volumes  $\Omega(t)$ , the following differential form can be derived:

$$\frac{\partial \rho}{\partial t} + \nabla \cdot (\rho \mathbf{v}) = 0 \quad (2.38)$$

This differential form of the equation for conservation of mass is called the continuity equation.

### 2.3.3 The momentum equation

Consider again the control volume  $\Omega(t)$  with boundary  $\Gamma(t)$  and outer normal  $\mathbf{n}(\mathbf{x}, t)$  placed in a velocity field  $\mathbf{v}(\mathbf{x}, t)$ . The rate of change of linear momentum summed with the flux of momentum through the boundary  $\Gamma(t)$  is equal to the sum of the external volume and boundary forces.

$$\frac{d}{dt} \int_{\Omega(t)} \rho \mathbf{v} d\Omega + \int_{\Gamma(t)} \rho \mathbf{v} (\mathbf{v} - \mathbf{v}_\Gamma) \cdot \mathbf{n} d\Gamma = \int_{\Omega(t)} \rho \mathbf{f} d\Omega + \int_{\Gamma(t)} \mathbf{s} d\Gamma \quad (2.39)$$

Here  $\mathbf{f}$  denotes the body force per unit of mass and  $\mathbf{s}$  denotes the stress vector acting on the boundary  $\Gamma$  of  $\Omega$ . If again the control volume is considered to be fixed in space one can apply the Gauss-Ostrogradskii divergence theorem. Then, making use of the Cauchy stress tensor  $\boldsymbol{\sigma}$  defined by (see (2.1):

$$\mathbf{s} = \mathbf{n} \cdot \boldsymbol{\sigma} \quad (2.40)$$

equation (2.39) yields:

$$\int_{\Omega(t)} \left[ \frac{\partial \rho \mathbf{v}}{\partial t} + \rho \mathbf{v} (\nabla \cdot \mathbf{v}) + (\mathbf{v} \cdot \nabla) \rho \mathbf{v} \right] d\Omega = \int_{\Omega(t)} [\rho \mathbf{f} + \nabla \cdot \boldsymbol{\sigma}] d\Omega \quad (2.41)$$

After substitution of the continuity equation (2.38) the differential form of (2.41) will be the momentum equation:

$$\rho \frac{\partial \mathbf{v}}{\partial t} + \rho (\mathbf{v} \cdot \nabla) \mathbf{v} = \rho \mathbf{f} + \nabla \cdot \boldsymbol{\sigma} \quad (2.42)$$

### 2.3.4 Initial and boundary conditions

Without going into the mathematics needed to prove that a unique solution of the equations of motion (2.38) and (2.42) exists, the boundary conditions that are needed to solve these equations can be deduced from the integral formulation of the continuity and momentum equations (2.36) and (2.39) respectively. From the momentum equation (2.39) it can be seen that both the velocity and the stress vector could be prescribed on the boundary. Since these quantities are related by virtue of a constitutive equation, only one of them (for each coordinate direction) should be used. So for each local boundary coordinate direction one can describe either its velocity  $\mathbf{v}$  or its stress vector  $\mathbf{s}$ . Defining  $\mathbf{n}$  as the outer normal and  $\mathbf{t}_i$  ( $i = 1, 2$ ) the tangential unit vectors to the boundary  $\Gamma$  this yields:

in normal direction:

the Dirichlet condition:

$$(\mathbf{v} \cdot \mathbf{n}) = v_{n\Gamma}$$

or Neumann condition:

$$(\boldsymbol{\sigma} \cdot \mathbf{n}) \cdot \mathbf{n} = (\mathbf{s} \cdot \mathbf{n}) \quad (2.43)$$

in tangential directions:

the Dirichlet conditions:

$$(\mathbf{v} \cdot \mathbf{t}_i) = v_{t_i\Gamma} \quad i = 1, 2$$

or Neumann conditions:

$$(\boldsymbol{\sigma} \cdot \mathbf{n}) \cdot \mathbf{t}_i = (\mathbf{s} \cdot \mathbf{t}_i)$$

For time-dependent problems initial conditions for velocity and stress must be given as well.

## 2.4 Summary

In this chapter the basic equations that govern incompressible solid deformation and fluid flow are derived. After introducing the deformation tensor  $\mathbf{F}$  it has been shown that the Finger tensor  $\mathbf{B} = \mathbf{F} \cdot \mathbf{F}^c$  can be used to construct physically permitted constitutive equations for both solids and fluids. For incompressible media, these constitutive equations then are of the form  $\boldsymbol{\sigma} = -p\mathbf{I} + \boldsymbol{\tau}(\mathbf{B}, \mathbf{D})$  with  $\boldsymbol{\sigma}$  the Cauchy stress tensor,  $p$  the pressure,  $\boldsymbol{\tau}$  the extra stress tensor and  $\mathbf{D} = \frac{1}{2}\dot{\mathbf{B}}$  the rate of deformation tensor. The equations of motion have been derived.

## **Chapter 3**

# **Fluid mechanics of the heart**

### **3.1 Introduction**

This chapter will be added in a future version of these lecture notes.

### **3.2 Summary**



## Chapter 4

# Newtonian flow in blood vessels

### 4.1 Introduction

In this section the flow patterns in rigid straight, curved and branching tubes will be considered. First, fully developed flow in straight tubes will be dealt with and it will be shown that this uni-axial flow is characterized by two dimensionless parameters, the Reynolds number  $Re$  and the Womersley number  $\alpha$ , that distinguish between flow in large and small vessels. Also derived quantities, like wall shear stress and vascular impedance, can be expressed as a function of these parameters.

For smaller tube diameters (micro-circulation), however, the fluid can not be taken to be homogeneous anymore and the dimensions of the red blood cells must be taken into account (see chapter 8). In the entrance regions of straight tubes, the flow is more complicated. Estimates of the length of these regions will be derived for steady and pulsatile flow.

The flow in curved tubes is not uni-axial but exhibits secondary flow patterns perpendicular to the axis of the tube. The strength of this secondary flow field depends on the curvature of the tube which is expressed in another dimensionless parameter: the Dean number. Finally it will be shown that the flow in branched tubes shows a strong resemblance to the flow in curved tubes.

## 4.2 Incompressible Newtonian flow in general

### 4.2.1 Incompressible viscous flow

For incompressible isothermal flow the density  $\rho$  is constant in space and time and the mass conservation or continuity equation is given by:

$$\nabla \cdot \mathbf{v} = 0 \quad (4.1)$$

In a viscous fluid, besides pressure forces also viscous forces contribute to the stress tensor and in general the total stress tensor can be written as (see chapter 2):

$$\boldsymbol{\sigma} = -p\mathbf{I} + \boldsymbol{\tau}(\dot{\mathbf{B}}). \quad (4.2)$$

In order to find solutions of the equations of motion the viscous stress tensor  $\boldsymbol{\tau}$  has to be related to the kinematics of the flow by means of a constitutive equation depending on the rheological properties of the fluid. In this section only Newtonian fluids will be discussed briefly.

#### Newtonian flow

In Newtonian flow there is a linear relation between the viscous stress  $\boldsymbol{\tau}$  and the rate of deformation tensor  $\dot{\boldsymbol{\gamma}}$  according to:

$$\boldsymbol{\tau} = 2\eta\mathbf{D} = \eta\dot{\boldsymbol{\gamma}} \quad (4.3)$$

with  $\eta$  the dynamic viscosity and the rate of deformation tensor defined as:

$$\dot{\boldsymbol{\gamma}} = \nabla\mathbf{v} + (\nabla\mathbf{v})^c. \quad (4.4)$$

Substitution in the momentum equation yields the Navier-Stokes equations:

$$\begin{cases} \rho \frac{\partial \mathbf{v}}{\partial t} + \rho(\mathbf{v} \cdot \nabla)\mathbf{v} = \rho\mathbf{f} - \nabla p + \eta\nabla^2\mathbf{v} \\ \nabla \cdot \mathbf{v} = 0 \end{cases} \quad (4.5)$$

After introduction of the non-dimensional variables:  $\mathbf{x}^* = \mathbf{x}/L$ ,  $\mathbf{v}^* = \mathbf{v}/V$ ,  $t^* = t/\theta$ ,  $p^* = p/\rho V^2$  and  $\mathbf{f}^* = \mathbf{f}/g$ , the dimensionless Navier-Stokes equations for incompressible Newtonian flow become (after dropping the superscript \*):

$$\begin{cases} Sr \frac{\partial \mathbf{v}}{\partial t} + (\mathbf{v} \cdot \nabla)\mathbf{v} = \frac{1}{Fr^2}\mathbf{f} - \nabla p + \frac{1}{Re}\nabla^2\mathbf{v} \\ \nabla \cdot \mathbf{v} = 0 \end{cases} \quad (4.6)$$

With the dimensionless parameters:

$$\begin{aligned} Sr &= \frac{L}{\theta V} && \text{Strouhal number} \\ Re &= \frac{\rho V L}{\eta} && \text{Reynolds number} \\ Fr &= \frac{V}{\sqrt{gL}} && \text{Froude number} \end{aligned} \quad (4.7)$$

### 4.2.2 Incompressible in-viscid flow

For incompressible isothermal flow the density  $\rho$  is constant in space and time and the mass conservation or continuity equation is given by:

$$\nabla \cdot \mathbf{v} = 0 \quad (4.8)$$

In an in-viscid fluid, the only surface force is due to the pressure, which acts normal to the surface. In that case the stress tensor can be written as:

$$\boldsymbol{\sigma} = -p\mathbf{I} \quad (4.9)$$

The momentum and continuity equations then lead to the Euler equations:

$$\begin{cases} \rho \frac{\partial \mathbf{v}}{\partial t} + \rho(\mathbf{v} \cdot \nabla)\mathbf{v} = \rho\mathbf{f} - \nabla p \\ \nabla \cdot \mathbf{v} = 0 \end{cases} \quad (4.10)$$

If the Euler equations are rewritten using the vector identity  $(\mathbf{v} \cdot \nabla)\mathbf{v} = \frac{1}{2}\nabla(\mathbf{v} \cdot \mathbf{v}) + \boldsymbol{\omega} \times \mathbf{v}$  with the rotation  $\boldsymbol{\omega} = \nabla \times \mathbf{v}$ , an alternative formulation for the momentum equations then is given by:

$$\rho \frac{\partial \mathbf{v}}{\partial t} + \frac{1}{2}\rho\nabla(\mathbf{v} \cdot \mathbf{v}) + \boldsymbol{\omega} \times \mathbf{v} = \rho\mathbf{f} - \nabla p \quad (4.11)$$

It can readily derived that  $\mathbf{v} \cdot (\boldsymbol{\omega} \times \mathbf{v}) = 0$  so taking the inner product of (4.11) with  $\mathbf{v}$  yields:

$$\mathbf{v} \cdot \left( \rho \frac{\partial \mathbf{v}}{\partial t} + \frac{1}{2}\rho\nabla(\mathbf{v} \cdot \mathbf{v}) - \rho\mathbf{f} + \nabla p \right) = 0 \quad (4.12)$$

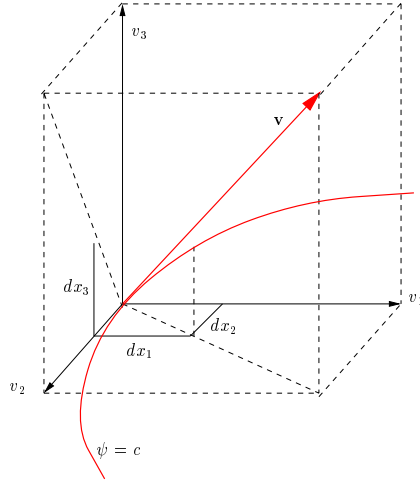


Figure 4.1: Definition of a streamline  $\psi = c$ .

Streamlines are defined as a family of lines that at time  $t$  is a solution of:

$$\frac{dx_1}{v_1(\mathbf{x}, t)} = \frac{dx_2}{v_2(\mathbf{x}, t)} = \frac{dx_3}{v_3(\mathbf{x}, t)} \quad (4.13)$$

As depicted in figure 4.1 the tangent of these lines is everywhere parallel to  $\mathbf{v}$ . If the flow is steady and only potential body forces  $\mathbf{f} = -\nabla F$ , like the gravity force  $\mathbf{g}$ , are involved, equation (4.12) yields

$$\mathbf{v} \cdot \nabla \left( \frac{1}{2} \rho (\mathbf{v} \cdot \mathbf{v}) + \rho F + p \right) \equiv \nabla H = 0 \quad (4.14)$$

As, by virtue of this,  $\nabla H \perp \mathbf{v}$ , along streamlines this results in the Bernoulli equation:

$$\frac{1}{2} \rho (\mathbf{v} \cdot \mathbf{v}) + p + \rho F = \text{const} \quad (4.15)$$

### Irotational flow

For irrotational flow ( $\boldsymbol{\omega} = \nabla \times \mathbf{v} = \mathbf{0}$ ) Bernoulli's equation holds for the complete flow domain. Moreover, since  $\mathbf{v}$  can be written as:

$$\mathbf{v} = \nabla \psi \text{ and thus due to incompressibility } \nabla^2 \psi = 0 \quad (4.16)$$

it follows that:

$$\rho \frac{\partial \psi}{\partial t} + \frac{1}{2} \rho (\mathbf{v} \cdot \mathbf{v}) + p + \rho F = \text{const} \quad (4.17)$$

### Boundary conditions

Using the constitutive equation (4.9) the boundary conditions described in section 2.3.4 reduce to:

in normal direction:

$$\begin{aligned} \text{the Dirichlet condition: } & (\mathbf{v} \cdot \mathbf{n}) = v_{n\Gamma} \\ \text{or Neumann condition: } & (\boldsymbol{\sigma} \cdot \mathbf{n}) \cdot \mathbf{n} = p \end{aligned} \quad (4.18)$$

in tangential directions:

$$\begin{aligned} \text{the Dirichlet conditions: } & (\mathbf{v} \cdot \mathbf{t}_i) = v_{t_i\Gamma} \quad i = 1, 2 \\ \text{or Neumann conditions: } & (\boldsymbol{\sigma} \cdot \mathbf{n}) \cdot \mathbf{t}_i = 0 \end{aligned}$$

## 4.2.3 Incompressible boundary layer flow

### Newtonian boundary layer flow

The viscous stress for incompressible flow

$$\boldsymbol{\tau} = \eta \dot{\boldsymbol{\gamma}} \quad (4.19)$$

is only large if velocity gradients are large especially if the viscosity is not too high. For flow along a smooth boundary parallel to the flow direction the viscous forces are only large in the boundary layer (see figure 4.2).

If the boundary layer thickness  $\delta$  is small compared to a typical length scale of the flow an estimate of the order of magnitude of the terms and neglecting  $\mathcal{O}(\delta/L)$  gives

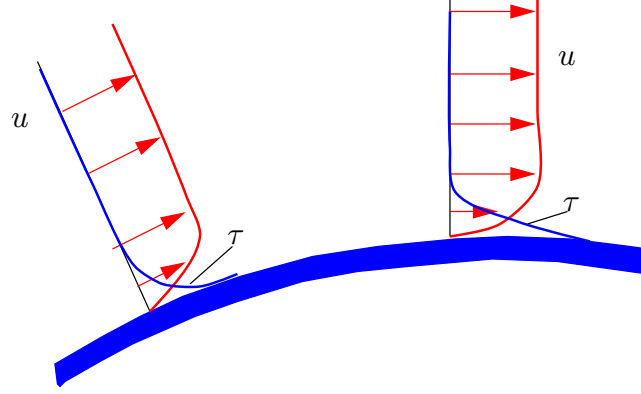


Figure 4.2: Velocity and stress distribution in a boundary layer.

the equations of motion:

$$\begin{cases} \frac{\partial v_1}{\partial x_1} + \frac{\partial v_2}{\partial x_2} = 0 \\ \rho \frac{\partial v_1}{\partial t} + \rho v_1 \frac{\partial v_1}{\partial x_1} + \rho v_2 \frac{\partial v_1}{\partial x_2} = -\frac{\partial p}{\partial x_1} + \eta \frac{\partial^2 v_1}{\partial x_2^2} \\ \frac{\partial p}{\partial x_2} = 0 \end{cases} \quad (4.20)$$

Outside the boundary layer the flow is assumed to be in-viscid and application of Bernoulli in combination with the second equation of (4.20) gives:

$$-\frac{\partial p}{\partial x_1} = \rho V \frac{\partial V}{\partial x_1} \quad (4.21)$$

### Initial and boundary conditions

This set of equations requires initial conditions:

$$v_1(x_{10}, x_2, 0) = v_1^0(x_1, x_2) \quad (4.22)$$

and boundary conditions:

$$\begin{aligned} v_1(x_{10}, x_2, t) &= v_{10}(x_2, t) \\ v_1(x_1, 0, t) &= 0 \\ v_1(x_1, \delta, t) &= V(x_1, t) \end{aligned} \quad (4.23)$$

The boundary layer thickness  $\delta$  can often be estimated by stating that at  $x_2 = \delta$  the viscous forces  $\mathcal{O}(\eta V / \rho \delta^2)$  are of the same magnitude as the stationary inertia forces  $\mathcal{O}(V^2 / L)$  or in-stationary inertia forces  $\mathcal{O}(V / \theta)$ .

## 4.3 Steady and pulsatile Newtonian flow in straight tubes

### 4.3.1 Fully developed flow

#### Governing equations

To analyze fully developed Newtonian flow in rigid tubes consider the Navier-Stokes equations in a cylindrical coordinate system:

$$\begin{cases} \frac{\partial v_r}{\partial t} + v_r \frac{\partial v_r}{\partial r} + v_z \frac{\partial v_r}{\partial z} = -\frac{1}{\rho} \frac{\partial p}{\partial r} + \nu \left( \frac{\partial}{\partial r} \left( \frac{1}{r} \frac{\partial}{\partial r} (r v_r) \right) + \frac{\partial^2 v_r}{\partial z^2} \right) \\ \frac{\partial v_z}{\partial t} + v_r \frac{\partial v_z}{\partial r} + v_z \frac{\partial v_z}{\partial z} = -\frac{1}{\rho} \frac{\partial p}{\partial z} + \nu \left( \frac{1}{r} \frac{\partial}{\partial r} \left( r \frac{\partial}{\partial r} (v_z) \right) + \frac{\partial^2 v_z}{\partial z^2} \right) \\ \frac{1}{r} \frac{\partial}{\partial r} (r v_r) + \frac{\partial v_z}{\partial z} = 0 \end{cases} \quad (4.24)$$

Since the velocity in circumferential direction equals zero ( $v_\phi = 0$ ), the momentum equation and all derivatives in  $\phi$ -direction are omitted. For fully developed flow the derivatives of the velocity in axial direction  $\frac{\partial}{\partial z}$  and the velocity component in radial direction  $v_r$  are zero and equations (4.24) simplify to:

$$\frac{\partial v_z}{\partial t} = -\frac{1}{\rho} \frac{\partial p}{\partial z} + \frac{\nu}{r} \frac{\partial}{\partial r} \left( r \frac{\partial v_z}{\partial r} \right) \quad (4.25)$$

Now a dimensionless velocity can be defined as  $v_z^* = v_z/V$ , the coordinates can be made dimensionless using the radius of the tube, i.e.  $r^* = r/a$  and  $z^* = z/a$ , the pressure can be scaled as  $p^* = p/\rho V^2$  and the time can be scaled using  $t^* = \omega t$ . Dropping the asterix, the equation of motion reads:

$$\alpha^2 \frac{\partial v_z}{\partial t} = -Re \frac{\partial p}{\partial z} + \frac{1}{r} \frac{\partial}{\partial r} \left( r \frac{\partial v_z}{\partial r} \right) \quad (4.26)$$

with  $Re$  the Reynolds number given by

$$Re = \frac{aV}{\nu} \quad (4.27)$$

and  $\alpha$  the Womersley number defined as:

$$\alpha = a \sqrt{\frac{\omega}{\nu}} \quad (4.28)$$

So two dimensionless parameters are involved : the Womersley number  $\alpha$  defining the ratio of the instationary inertia forces and the viscous forces and the Reynolds number  $Re$  that is in this case nothing more then a scaling factor for the pressure gradient. The pressure could also be scaled according to  $p^* = p/(a^2/\eta V)$  yielding one single parameter  $\alpha$ .

In table 4.3.1 the Womersley numbers for several sites in the arterial system are given. These values show that in the aorta and in the largest arteries inertia dominated flow and in arterioles and capillaries friction dominated flow may be expected.

	a [mm]	$\alpha$ [-]
aorta	10	10
large arteries	4	4
small arteries	1	1
arterioles	0.1	0.1
capillaries	0.01	0.01

Table 4.1: Estimated Womersley number at several sites of the arterial system based on the first harmonic of the flow. A kinematic of  $5 \cdot 10^{-3} [Pa \cdot s]$ , a density of  $10^3 [kg \cdot m^{-3}]$  and a frequency of  $1 [Hz]$  are assumed.

In most part of the arteries an intermediate value of  $\alpha$  is found and both inertia and viscous friction are important.

For the venous system a similar dependence of the Womersley number is found but it must be noted that inertia is less important due to the low amplitude of the first and higher harmonics with respect to the mean flow.

### Velocity profiles

For flow in a rigid tube (see figure 4.3) with radius  $a$  the boundary condition  $v(a, t) = 0$  is used to impose a no slip condition.

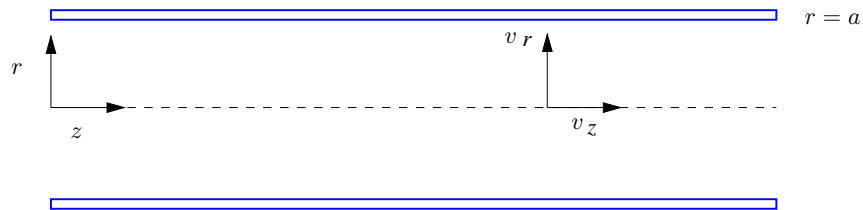


Figure 4.3: Rigid tube with radius  $a$

We will assume a harmonic pressure gradient and will search for harmonic solutions:

$$\frac{\partial p}{\partial z} = \frac{\partial \hat{p}}{\partial z} e^{i\omega t} \quad (4.29)$$

and

$$v_z = \hat{v}_z(r) e^{i\omega t} \quad (4.30)$$

The solution of an arbitrary periodic function then can be constructed by superposition of its harmonics. This is allowed because the equation to solve (4.26) is linear in  $v_z$ .

Now two asymptotic cases can be defined. For small Womersley numbers there is an equilibrium of viscous forces and the driving pressure gradient. For large Womersley numbers, however, the viscous forces are small compared to the instationary inertia forces and there will be an equilibrium between the inertia forces and the driving pressure gradient. Both cases will be considered in more detail.

**Small Womersley number flow.** If  $\alpha \ll 1$  equation (4.26) (again in dimension-full form) yields:

$$0 = -\frac{1}{\rho} \frac{\partial p}{\partial z} + \frac{\nu}{r} \frac{\partial}{\partial r} \left( r \frac{\partial v_z}{\partial r} \right) \quad (4.31)$$

Substitution of (4.29) and (4.30) yields:

$$\nu \frac{\partial^2 \hat{v}_z(r)}{\partial r^2} + \frac{\nu}{r} \frac{\partial \hat{v}_z(r)}{\partial r} = \frac{1}{\rho} \frac{\partial \hat{p}}{\partial z} \quad (4.32)$$

with solution:

$$v_z(r, t) = -\frac{1}{4\eta} \frac{\partial \hat{p}}{\partial z} (a^2 - r^2) e^{i\omega t} \quad (4.33)$$

So, for low values of the Womersley number a quasi-static Poiseuille profile is found. It oscillates  $180^\circ$  out of phase with the pressure gradient. The shape of the velocity profiles is depicted in the left graph of figure 4.4.

**Large Womersley number flow.** If the  $\alpha \gg 1$  equation (4.26) yields:

$$\frac{\partial v_z}{\partial t} = -\frac{1}{\rho} \frac{\partial p}{\partial z} \quad (4.34)$$

Substitution of (4.29) and (4.30) yields:

$$i\omega \hat{v}_z(r) = -\frac{1}{\rho} \frac{\partial \hat{p}}{\partial z} \quad (4.35)$$

with solution:

$$v_z(r, t) = \frac{i}{\rho\omega} \frac{\partial \hat{p}}{\partial z} e^{i\omega t} \quad (4.36)$$

Now, for high values of the Womersley number, an oscillating plug flow is found which is  $90^\circ$  out of phase with the pressure gradient (right graph of figure 4.4). The flow is dominated by inertia.

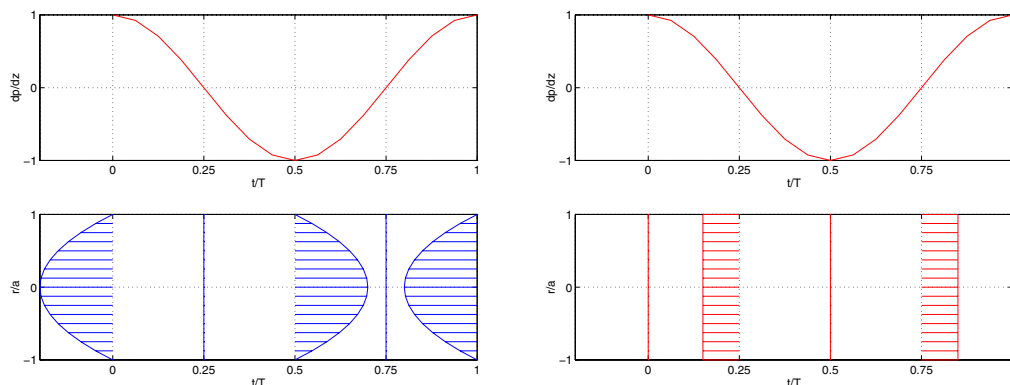


Figure 4.4: Pressure gradient (top) and corresponding velocity profiles (bottom) as a function of time for small (left) and large (right) Womersley numbers.

**Arbitrary Womersley number flow.** Substitution of (4.29) and (4.30) in equation (4.25) yields:

$$\nu \frac{\partial^2 \hat{v}_z(r)}{\partial r^2} + \frac{\nu}{r} \frac{\partial \hat{v}_z(r)}{\partial r} - i\omega \hat{v}_z(r) = \frac{1}{\rho} \frac{\partial \hat{p}}{\partial z} \quad (4.37)$$

Substitution of

$$s = i^{3/2} \alpha r / a \quad (4.38)$$

in the homogeneous part of this equation yields the equation of Bessel for  $n = 0$ :

$$\frac{\partial^2 \hat{v}_z}{\partial s^2} + \frac{1}{s} \frac{\partial \hat{v}_z}{\partial s} + \left(1 - \frac{n^2}{s^2}\right) \hat{v}_z = 0 \quad (4.39)$$

with solution given by the Bessel functions of the first kind:

$$J_n(s) = \sum_{k=0}^{\infty} \frac{(-1)^k}{k!(n+k)!} \left(\frac{s}{2}\right)^{2k+n} \quad (4.40)$$

so:

$$J_0(s) = \sum_{k=0}^{\infty} \frac{(-1)^k}{k!k!} \left(\frac{s}{2}\right)^{2k} = 1 - \left(\frac{s}{2}\right)^2 + \frac{1}{1^2 2^2} \left(\frac{s}{2}\right)^4 - \frac{1}{1^2 2^2 3^2} \left(\frac{s}{2}\right)^6 + \dots \quad (4.41)$$

(see Abramowitz and Stegun, 1964).

Together with the particular solution :

$$\hat{v}_z^p = \frac{i}{\rho\omega} \frac{\partial \hat{p}}{\partial z} \quad (4.42)$$

we have:

$$\hat{v}_z(s) = K J_0(s) + \hat{v}_z^p \quad (4.43)$$

Using the boundary condition  $\hat{v}_z(a) = 0$  then yields:

$$K = -\frac{\hat{v}_z^p}{J_0(i^{3/2}\alpha)} \quad (4.44)$$

and finally:

$$\hat{v}_z(r) = \frac{i}{\rho\omega} \frac{\partial \hat{p}}{\partial z} \left[ 1 - \frac{J_0(i^{3/2}\alpha r/a)}{J_0(i^{3/2}\alpha)} \right] \quad (4.45)$$

These are the well known Womersley profiles (Womersley, 1957) displayed in figure 4.5. As can be seen from this figure, the Womersley profiles for intermediate Womersley numbers are characterized by a phase-shift between the flow in the boundary layer and the flow in the central core of the tube. Actually, in the boundary layer viscous forces dominate the inertia forces and the flow behaves like the flow for small Womersley numbers. For high enough Womersley numbers, in the central core, inertia forces are dominant and flattened profiles that are shifted in phase are found. The thickness of the instationary boundary layer is determined by the Womersley number. This will be discussed in more detail in section 4.3.2.

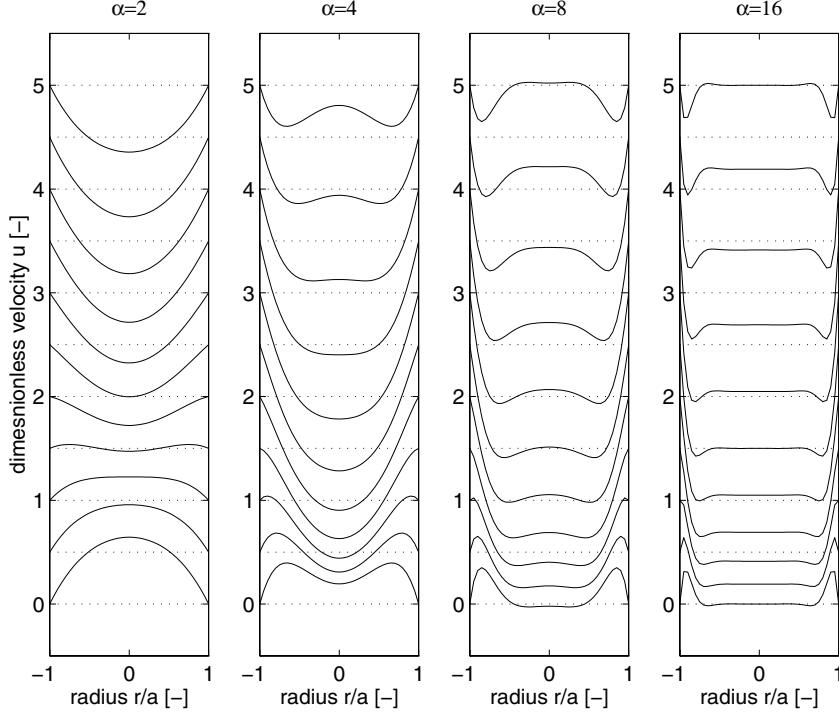


Figure 4.5: Womersley profiles for different Womersley numbers ( $\alpha = 2, 4, 8, 16$ )

### Wall shear stress

Using the property of Bessel functions (see Abramowitz and Stegun, 1964)

$$\frac{\partial J_0(s)}{\partial s} = -J_1(s) \quad (4.46)$$

and the definition of the Womersley function

$$F_{10}(\alpha) = \frac{2J_1(i^{3/2}\alpha)}{i^{3/2}\alpha J_0(i^{3/2}\alpha)} \quad (4.47)$$

the wall shear stress defined as:

$$\tau_w = -\eta \frac{\partial v_z}{\partial r} \Big|_{r=a} \quad (4.48)$$

can be derived as:

$$\tau_w = -\frac{a}{2} F_{10}(\alpha) \frac{\partial p}{\partial z} = F_{10}(\alpha) \tau_w^p \quad (4.49)$$

with  $\tau_w^p$  the wall shear stress for Poiseuille flow. In figure 4.6 the function  $F_{10}(\alpha)$  and thus a dimensionless wall shear stress  $\tau_w/\tau_w^p$  is given as a function of  $\alpha$ .

**remark :**

$$J_1(s) = \sum_{k=0}^{\infty} \frac{(-1)^k}{k!(1+k)!} \left(\frac{s}{2}\right)^{2k+1} = \left(\frac{s}{2}\right) - \frac{1}{1^2 2} \left(\frac{s}{2}\right)^3 + \frac{1}{1^2 2^2 3} \left(\frac{s}{2}\right)^5 + \dots \quad (4.50)$$

In many cases, for instance to investigate limiting values for small and large values of  $\alpha$ , it is convenient to approximate the Womersley function with:

$$F_{10}(\alpha) \approx \frac{(1 + \beta)^{1/2}}{(1 + \beta)^{1/2} + 2\beta} \quad \text{with} \quad \beta = \frac{i\alpha^2}{16} \quad (4.51)$$

This approximation is plotted with dotted lines in figure 4.6. For small values of the Womersley number ( $\alpha < 3$ ) the following approximation derived from (4.51) can be used:

$$F_{10}(\alpha) \approx \frac{1}{1 + 2\beta} = \frac{1}{1 + i\alpha^2/8} \quad (4.52)$$

whereas for large values ( $\alpha > 15$ ) one may use:

$$F_{10}(\alpha) \approx \frac{1}{2}\beta^{-1/2} = \frac{(1 - i)\sqrt{2}}{\alpha} \quad (4.53)$$

These two approximations are plotted with dashed lines in figure 4.6. Note that the dimensionless wall shear stress for large values of  $\alpha$  approximates zero and not  $\infty$  that one could conclude from the steep gradients in the velocity profiles in figure 4.5.

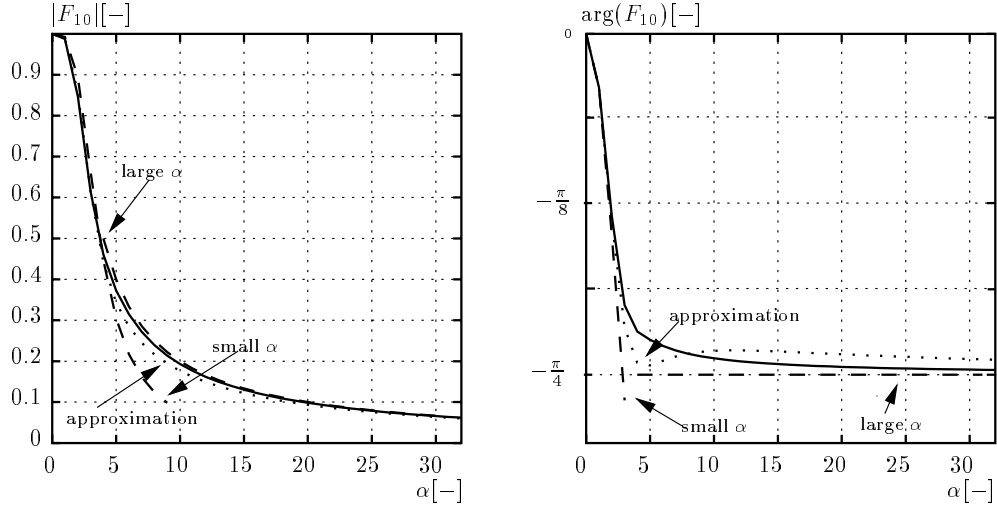


Figure 4.6: Modulus (left) and argument (right) of the function  $F_{10}(\alpha)$  or  $\tau_w/\tau_w^p$  as a function of  $\alpha$ . The approximations are indicated with dotted and dashed lines.

The mean flow  $q$  can be derived using the property (Abramowitz and Stegun, 1964):

$$s \frac{\partial J_n(s)}{\partial s} = -n J_n(s) + s J_{n-1}(s) \quad (4.54)$$

For  $n = 1$  it follows that:

$$s J_0(s) ds = d(s J_1(s)) \quad (4.55)$$

and together with  $J_1(0) = 0$  the flow becomes:

$$\begin{aligned} q &= \int_0^a \hat{v}_z 2\pi r dr = i \frac{\pi a^2}{\rho \omega} [1 - F_{10}(\alpha)] \frac{\partial p}{\partial z} \\ &= [1 - F_{10}(\alpha)] \hat{q}_\infty \\ &= \frac{8i}{\alpha^2} [1 - F_{10}(\alpha)] \hat{q}_p \end{aligned} \quad (4.56)$$

with

$$\hat{q}_\infty = \frac{i\pi a^2}{\rho \omega} \frac{\partial \hat{p}}{\partial z} \quad \text{and} \quad \hat{q}_p = \frac{\pi a^4}{8\eta} \frac{\partial \hat{p}}{\partial z} \quad (4.57)$$

Combining equation (4.49) with equation (4.56) by elimination of  $\frac{\partial p}{\partial z}$  finally yields:

$$\tau_w = \frac{a}{2A} i\omega \rho \frac{F_{10}(\alpha)}{1 - F_{10}(\alpha)} q \quad (4.58)$$

With  $A = \pi a^2$  the cross-sectional area of the tube. In the next chapter this expression for the wall shear stress will be used to approximate the shear forces that the fluid exerts on the wall of the vessel.

### Vascular impedance

The longitudinal impedance defined as:

$$Z_L = -\frac{\partial p}{\partial z} / q \quad (4.59)$$

can be derived directly from equation (4.56) and reads:

$$Z_L = i\omega \frac{\rho}{\pi a^2} \frac{1}{1 - F_{10}(\alpha)} \quad (4.60)$$

For a Poiseuille profile the longitudinal impedance is defined by integration of (4.33) and is given by:

$$Z_p = \frac{8\eta}{\pi a^4} \quad (4.61)$$

From this it can be derived that the impedance of a rigid tube for oscillating flow related to the impedance for steady flow (Poiseuille resistance) is given by the following equation:

$$\frac{Z_L}{Z_p} = \frac{i\alpha^2}{8} \frac{1}{1 - F_{10}(\alpha)} \quad (4.62)$$

In figure 4.7 the relative impedance is plotted as a function of the Womersley number  $\alpha$ . The relative longitudinal impedance is real for  $\alpha \ll 1$  and becomes imaginary for  $\alpha \rightarrow \infty$ . This expresses the fact that for low frequencies (or small diameters)

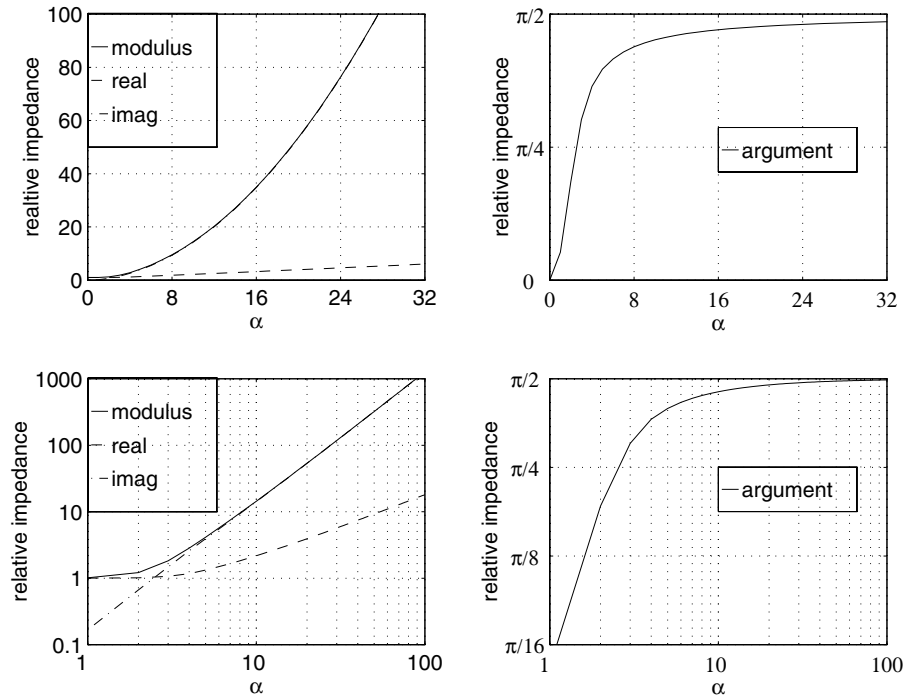


Figure 4.7: The relative impedance for oscillating flow in a tube (linear scale at the top and logarithmic scale at the bottom) as a function of  $\alpha$ .

the viscous forces are dominant, whereas for high frequencies (or large diameters) inertia is dominant and the flow behaves as an inviscid flow.

For small values of  $\alpha$  the relative impedance results in (see 4.52):

$$\frac{Z_L(\alpha < 3)}{Z_p} \approx 1 + \frac{i\alpha^2}{8} \quad (4.63)$$

Viscous forces then dominate and the pressure gradient is in phase with the flow and does not (strongly) depend on  $\alpha$ . For large values of  $\alpha$  (4.53) gives:

$$\frac{Z_L(\alpha > 15)}{Z_p} \approx \frac{i\alpha^2}{8} \quad (4.64)$$

indicating that the pressure gradient is out of phase with the flow and increases quadratically with  $\alpha$ .

### 4.3.2 Entrance flow

In general the flow in blood vessels is not fully developed. Due to transitions and bifurcations the velocity profile has to develop from a certain profile at the entrance of the tube (see figure 4.8).

In order to obtain an idea of the length needed for the flow to develop, the flow with a characteristic velocity  $V$  along a smooth boundary with characteristic length  $L$  is

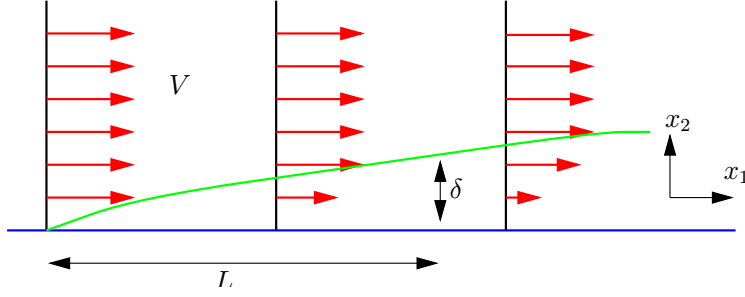


Figure 4.8: Development of a boundary layer

considered. Viscous forces only play an important role in the small boundary layer with thickness  $\delta$ . Outside the boundary layer the flow is assumed to be inviscid so that Bernoulli's law can be applied. From this configuration simplified Navier-Stokes equations can be derived by assuming that  $\delta \ll L$  (see 4.20) and the order of magnitude of its terms can be estimated:

$$\left\{ \begin{array}{l} \frac{\partial v_1}{\partial x_1} + \frac{\partial v_2}{\partial x_2} = 0 \\ O\left(\frac{V}{L}\right) \quad O\left(\frac{v}{\delta}\right) \\ \rho \frac{\partial v_1}{\partial t} + \rho v_1 \frac{\partial v_1}{\partial x_1} + \rho v_2 \frac{\partial v_1}{\partial x_2} = -\frac{\partial p}{\partial x_1} + \eta \frac{\partial^2 v_1}{\partial x_1^2} + \eta \frac{\partial^2 v_1}{\partial x_2^2} \\ O(\omega V) \quad O\left(\frac{V^2}{L}\right) \quad O\left(\frac{V^2}{L}\right) \quad O\left(\frac{1}{\rho} \frac{\partial p}{\partial x}\right) \quad O\left(\frac{\nu V}{L^2}\right) \quad O\left(\frac{\nu V}{\delta^2}\right) \end{array} \right. \quad (4.65)$$

This shows clearly that the diffusive forces are determined by second order derivatives of the velocity normal to the boundary. Moreover it can be seen that the stationary inertia forces are of the same order of magnitude as the viscous forces (which is the case at the boundary layer  $x_2 = \delta$ ) as long as:

$$O\left(\frac{\nu V}{\delta^2}\right) = O\left(\frac{V^2}{L}\right) \quad (4.66)$$

### Steady flow

If the entrance length of the flow in a tube is defined as the length needed for the boundary layer to contain the complete cross section, i.e.  $\delta = a$ , then the ratio of the entrance length and the radius of the tube follows from the equation above as:

$$\frac{L_e}{a} = O\left(\frac{aV}{\nu}\right) \quad (4.67)$$

Or with the definition of the Reynolds number  $Re = 2aV/\nu$  the dimensionless entrance length  $L_e/2a$  is found to be proportional to the Reynolds number:

$$\frac{L_e}{2a} = O(Re) \quad (4.68)$$

In Schlichting (1960) one can find that for laminar flow, for  $L_e : v(L_e, 0) = 0.99 \cdot 2V$ :

$$\frac{L_e}{2a} = 0.056 Re \quad (4.69)$$

For steady flow in the carotid artery, for instance,  $Re = 300$ , and thus  $L_e \approx 40a$ . This means that the flow will never become fully developed since the length of the carotid artery is much less than 40 times its radius. In arterioles and smaller vessels, however,  $Re < 10$  and hereby  $L_e < a$ , so fully developed flow will be found in many cases.

### Oscillating flow

For oscillating flow the inlet length is smaller as compared to the inlet length for steady flow. This can be seen from the following. The unsteady inertia forces are of the same magnitude as the viscous forces when:

$$O(V\omega) = O\left(\frac{\nu V}{\delta^2}\right) \quad (4.70)$$

and thus:

$$\delta = O\left(\sqrt{\frac{\nu}{\omega}}\right) \quad (4.71)$$

This means that for fully developed oscillating flow a boundary layer exists with a relative thickness of:

$$\frac{\delta}{a} = O(\alpha^{-1}) \quad (4.72)$$

If, for oscillating flow, the inlet length is defined as the length for which the viscous forces still are of the same magnitude as the stationary inertia forces, i.e.:

$$O\left(\frac{\nu V}{\delta^2}\right) = O\left(\frac{V^2}{L_e}\right) \quad (4.73)$$

then together with (4.72) the inlet length is of the order

$$L_e = O\left(\frac{V\delta^2}{\nu}\right) = O\left(\frac{a}{\alpha^2} Re\right) \quad (4.74)$$

Note that this holds only for  $\alpha > 1$ . For  $\alpha < 1$  the boundary layer thickness is restricted to the radius of the tube and we obtain an inlet length of the same magnitude as for steady flow.

## 4.4 Steady and pulsating flow in curved and branched tubes

### 4.4.1 Steady flow in a curved tube

#### Steady entrance flow in a curved tube

The flow in a curved tube is determined by an equilibrium of convective forces, pressure forces and viscous forces. Consider, the entrance flow in a curved tube

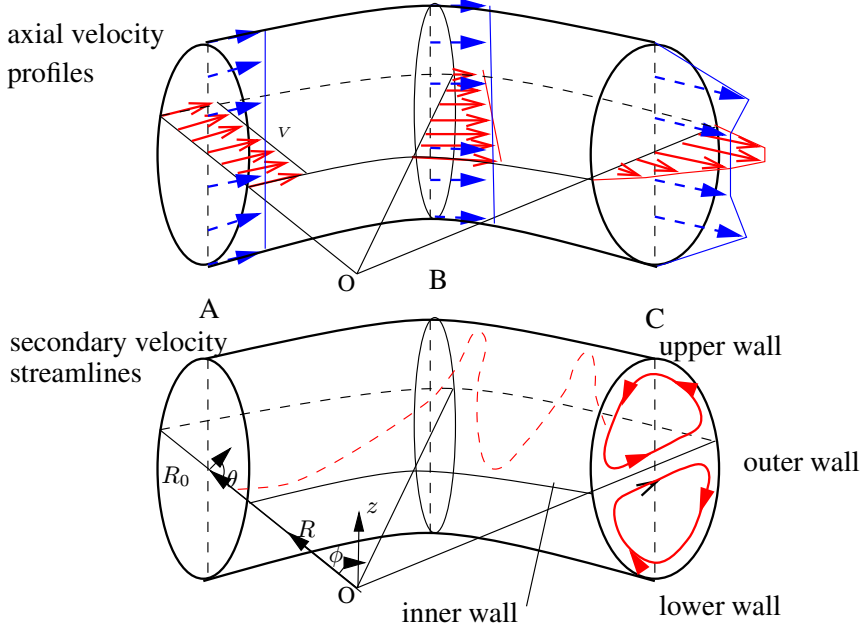


Figure 4.9: Axial velocity profiles, secondary velocity streamlines and helical motion of particles for entrance flow in a curved tube.

with radius  $a$  and a radius of curvature  $R_0$ . With respect to the origin  $O$  we can define a cylindrical coordinate system  $(R, z, \phi)$ . At the entrance (A:  $R_0 - a < R < R_0 + a$ ,  $-a < z < a$ ,  $\phi = 0$ ) a uniformly distributed irrotational (plug) flow  $v_\phi = V$  (see figure 4.9) is assumed. As long as the boundary layer has not yet developed ( $R_0\phi \ll 0.1aRe$ ) the viscous forces are restricted to a very thin boundary layer and the velocity is restricted to one component,  $v_\phi$ . The other components ( $v_R$  and  $v_z$ ) are small compared to  $v_\phi$ . In the core the flow is inviscid so Bernoulli's law can be applied:

$$p + \frac{1}{2}\rho v_\phi^2 = \text{constant} \quad (4.75)$$

With  $p$  the pressure, and  $\rho$  the density of the fluid. The momentum equation in  $R$ -direction shows an equilibrium of pressure forces and centrifugal forces:

$$\frac{\partial p}{\partial R} = \frac{\rho v_\phi^2}{R} \quad (4.76)$$

As a consequence, the pressure is largest at the outer wall and smallest at the inner wall. Together with Bernoulli's law it follows that the velocity will become largest at the inner wall and lowest at the outer wall of the tube (see figure 4.9 location (B)). Indeed, elimination of the pressure from (4.75) and (4.76) yields:

$$\frac{\partial v_\phi}{\partial R} = -\frac{v_\phi}{R} \quad (4.77)$$

and thus:

$$v_\phi = \frac{k_1}{R} \quad (4.78)$$

The constant  $k_1$  can be determined from the conservation of mass in the plane of symmetry ( $z = 0$ ):

$$2aV = \int_{R_0-a}^{R_0+a} v_\phi(R') dR' = k_1 \ln \frac{R_0+a}{R_0-a} \quad (4.79)$$

and thus:

$$k_1 = \frac{2aV}{\ln \frac{1+\delta}{1-\delta}} \quad (4.80)$$

with  $\delta = a/R_0$ . So in the entrance region ( $\phi \ll 0.1\delta Re$ ) initially the following velocity profile will develop:

$$v_\phi(R) = \frac{2aV}{R \ln \frac{1+\delta}{1-\delta}} \quad (4.81)$$

It is easy to derive that for small values of  $\delta$  this reduces to  $v_\phi(R) = (R_0/R)V$ . Note that the velocity profile does only depend on  $R$  and does not depend on the azimuthal position  $\theta$  in the tube. In terms of the toroidal coordinate system  $(r, \theta, \phi)$  we have:

$$R(r, \theta) = R_0 - r \cos \theta \quad (4.82)$$

and the velocity profile given in (4.81) is:

$$\begin{aligned} v_\phi(r, \theta) &= \frac{2aV}{(R_0 - r \cos \theta) \ln \frac{1+\delta}{1-\delta}} \\ &= \frac{2\delta V}{(1 - \delta(r/a) \cos \theta) \ln \frac{1+\delta}{1-\delta}} \end{aligned} \quad (4.83)$$

Again for small values of  $\delta$  this reduces to  $v_\phi(r, \theta) = V/(1 - \delta(r/a) \cos \theta)$ .

Going more downstream, due to viscous forces a boundary layer will develop along the walls of the tube and will influence the complete velocity distribution. Finally the velocity profile will look like the one that is sketched at position C. This profile does depend on the azimuthal position. In the plane of symmetry it will have a maximum that is shifted to the outer wall. In the direction perpendicular to the plane of symmetry an M-shaped profile will be found (see figure 4.9). This velocity distribution can only be explained if we also consider the secondary flow field, i.e. the velocity components in the plane of a cross-section ( $\phi = \text{constant}$ ) of the tube perpendicular to the axis.

Viscous forces will diminish the axial velocity in the boundary layer along the wall of the curved tube. As a result, the equilibrium between the pressure gradient in  $R$ -direction and the centrifugal forces will be disturbed. In the boundary layers we will have  $\frac{\rho V^2}{R} < \frac{\partial p}{\partial R}$  and in the central core  $\frac{\rho V^2}{R} > \frac{\partial p}{\partial R}$ . Consequently the fluid particles in the central core will accelerate towards the outer wall, whereas fluid particles in the boundary layer will accelerate in opposite direction. In this way a secondary

vortex will develop as indicated in figure 4.9. This motion of fluid particles from the inner wall towards the outer wall in the core and along the upper and lower walls back to the inner wall will have consequences for the axial velocity distribution. Particles with a relatively large axial velocity will move to the outer wall and due to convective forces, the maximum of the axial velocity will shift in the same direction. On the other hand, particles in the boundary layer at the upper and lower walls will be transported towards the inner wall and will convect a relatively low axial velocity. In this way in the plane of symmetry an axial velocity profile will develop with a maximum at the outer wall, and a minimum at the inner wall. For large curvatures or large Reynolds numbers even negative axial velocity at the inner wall can occur due to boundary layer separation.

Once the maximum of the axial velocity is located near the outer wall, the secondary flow will transport particles with a relatively large axial velocity along the upper and lower walls and a C-shaped axial velocity contour will develop. This can clearly be seen in figure 4.10 where for different curvatures of the tube contour plots of the axial velocity and streamlines of the secondary velocity are given. Note that the combination of the axial and secondary flow results in a helical movement of the fluid particles (see figure 4.9). While moving in downstream direction the particles move from the inner wall towards the outer wall and back to the inner wall along the upper (or lower) wall.

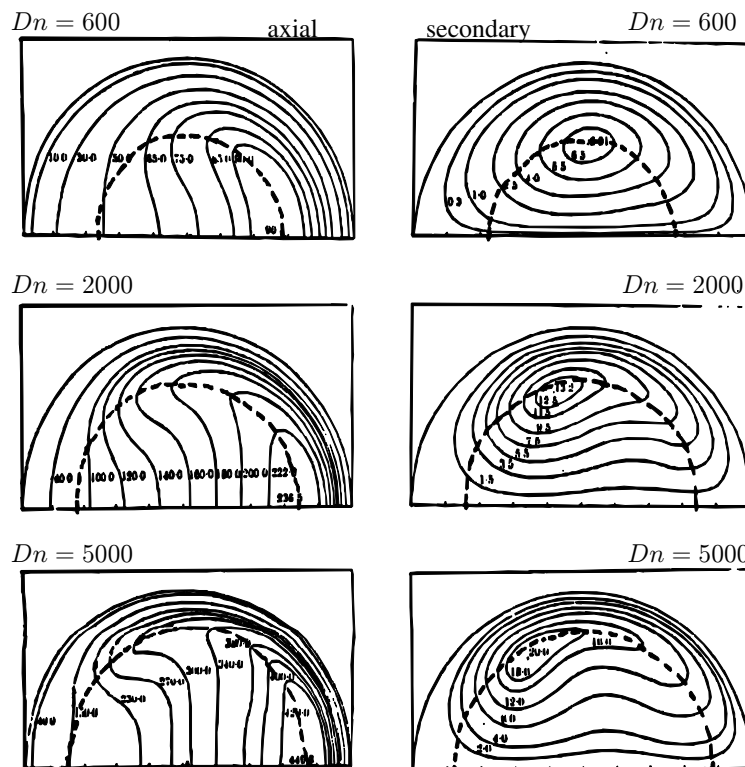


Figure 4.10: Contour plots of axial (left) and streamline plots of secondary (right) fully developed steady flow in a curved tube for Dean numbers of 600 (top), 2000 (middle) and 5000 (bottom) as computed by (Collins and Dennis, 1975).

### Steady fully developed flow in a curved tube

In order to obtain a more quantitative description of the flow phenomena it is convenient to use the toroidal coordinate system  $(r, \theta, \phi)$  as is depicted in figure 4.9. The corresponding velocity components are  $v_r$ ,  $v_\theta$  and  $v_\phi$ . The Navier-Stokes equations in toroidal coordinates read (Ward-Smith, 1980):

in  $r$ -direction:

$$\begin{aligned} & \frac{\partial v_r}{\partial t} + \frac{1}{rB} \left[ \frac{\partial}{\partial r}(rBv_r^2) + \frac{\partial}{\partial \theta}(Bv_rv_\theta) + \frac{\partial}{\partial \phi}(\delta rv_\phi v_r) - Bv_\theta^2 - \delta r \cos \theta v_\phi^2 \right] = \\ & - \frac{\partial p}{\partial r} + \frac{1}{Re} \left\{ \frac{1}{rB} \left[ \frac{\partial}{\partial r}(rB \frac{\partial v_r}{\partial r}) + \frac{\partial}{\partial \theta}(\frac{B}{r} \frac{\partial v_r}{\partial \theta}) + \frac{\partial}{\partial \phi}(\frac{\delta^2 r}{B} \frac{\partial v_r}{\partial \phi}) \right] - \right. \\ & \left. \frac{1}{r^2}(2 \frac{\partial v_\theta}{\partial \theta} + v_r) + \frac{\delta \sin \theta v_\theta}{rB} + \frac{\delta^2 \cos \theta}{B^2}(v_\theta \sin \theta - v_r \cos \theta - 2 \frac{\partial v_\phi}{\partial \phi}) \right\} \end{aligned} \quad (4.84)$$

in  $\theta$ -direction:

$$\begin{aligned} & \frac{\partial v_\theta}{\partial t} + \frac{1}{rB} \left[ \frac{\partial}{\partial r}(rBv_rv_\theta) + \frac{\partial}{\partial \theta}(Bv_\theta^2) + \frac{\partial}{\partial \phi}(\delta rv_\phi v_\theta) + Bv_rv_\theta + \delta r \sin \theta v_\phi^2 \right] = \\ & - \frac{\partial p}{\partial \theta} + \frac{1}{Re} \left\{ \frac{1}{rB} \left[ \frac{\partial}{\partial r}(rB \frac{\partial v_\theta}{\partial r}) + \frac{\partial}{\partial \theta}(\frac{B}{r} \frac{\partial v_\theta}{\partial \theta}) + \frac{\partial}{\partial \phi}(\frac{\delta^2 r}{B} \frac{\partial v_\theta}{\partial \phi}) \right] + \right. \\ & \left. \frac{1}{r^2}(2 \frac{\partial v_r}{\partial \theta} - v_\theta) - \frac{\delta \sin \theta v_r}{rB} - \frac{\delta^2 \sin \theta}{B^2}(v_\theta \sin \theta - v_r \cos \theta - 2 \frac{\partial v_\phi}{\partial \phi}) \right\} \end{aligned} \quad (4.85)$$

in  $\phi$ -direction:

$$\begin{aligned} & \frac{\partial v_\phi}{\partial t} + \frac{1}{rB} \left[ \frac{\partial}{\partial r}(rBv_\phi v_r) + \frac{\partial}{\partial \theta}(Bv_\phi v_\theta) + \frac{\partial}{\partial \phi}(\delta rv_\phi^2) + \delta rv_\phi(v_r \cos \theta - v_\theta \sin \theta) \right] = \\ & - \frac{\delta}{B} \frac{\partial p}{\partial \phi} + \frac{1}{Re} \left\{ \frac{1}{rB} \left[ \frac{\partial}{\partial r}(rB \frac{\partial v_\phi}{\partial r}) + \frac{\partial}{\partial \theta}(\frac{B}{r} \frac{\partial v_\phi}{\partial \theta}) + \frac{\partial}{\partial \phi}(\frac{\delta^2 r}{B} \frac{\partial v_\phi}{\partial \phi}) \right] + \right. \\ & \left. \frac{2\delta^2}{B^2} \left( \frac{\partial v_r}{\partial \phi} \cos \theta - \frac{\partial v_\theta}{\partial \phi} \sin \theta - \frac{v_\phi}{2} \right) \right\} \end{aligned} \quad (4.86)$$

continuity:

$$\frac{\partial}{\partial r}(rBv_r) + \frac{\partial}{\partial \theta}(Bv_\theta) + \frac{\partial}{\partial \phi}(\delta rv_\phi) = 0 \quad (4.87)$$

with

$$\delta = \frac{a}{R_0} \quad \text{and} \quad B = 1 + \delta r \cos \theta$$

For fully developed flow all derivatives in  $\phi$  direction are zero ( $\frac{\partial}{\partial \phi} = 0$ ). This of course does not hold for the driving force  $\frac{\partial p}{\partial \phi}$ . If we scale according to:

$$r^* = \frac{r}{a}, \quad p^* = \frac{p}{\rho V^2}, \quad v_r^* = \frac{v_r}{V}, \quad v_\theta^* = \frac{v_\theta}{V}, \quad v_\phi^* = \frac{v_\phi}{V} \quad (4.88)$$

the continuity equation and the momentum equation in  $r$ -direction read after dropping the asterix:

$$\frac{\partial v_r}{\partial r} + \frac{v_r}{r} \left[ \frac{1 + 2\delta r \cos \theta}{1 + \delta r \cos \theta} \right] + \frac{1}{r} \frac{\partial v_\theta}{\partial \theta} - \frac{\delta v_\theta \sin \theta}{1 + \delta r \cos \theta} = 0 \quad (4.89)$$

and

$$\begin{aligned} v_r \frac{\partial v_r}{\partial r} + \frac{v_\theta}{r} \frac{\partial v_r}{\partial \theta} - \frac{v_\theta^2}{r} - \delta \frac{v_\phi^2 \cos \theta}{1 + \delta r \cos \theta} = \\ - \frac{\partial p}{\partial r} + \frac{1}{Re} \left[ \left( \frac{1}{r} \frac{\partial}{\partial \theta} - \frac{\delta \sin \theta}{1 + \delta r \cos \theta} \right) \left( \frac{1}{r} \frac{\partial v_r}{\partial \theta} - \frac{\partial v_\theta}{\partial r} - \frac{v_\theta}{r} \right) \right] \end{aligned} \quad (4.90)$$

The two important dimensionless parameters that appear are the curvature ratio  $\delta$  and the Reynolds number  $Re$  defined as:

$$\delta = \frac{a}{R_0} \quad \text{and} \quad Re = \frac{2aV}{\nu} \quad (4.91)$$

with  $a$  the radius and  $R_0$  the curvature of the tube. If we restrict ourselves to the plane of symmetry ( $\theta = 0, \pi$ ,  $\cos \theta = \pm 1$  and  $v_\theta = 0$ ) we have for the momentum equation:

$$v_r \frac{\partial v_r}{\partial r} - \delta \frac{\pm v_\phi^2}{1 \pm \delta r} = - \frac{\partial p}{\partial r} + \frac{1}{Re} \left[ \left( \frac{1}{r} \frac{\partial}{\partial \theta} \right) \left( \frac{1}{r} \frac{\partial v_r}{\partial \theta} - \frac{\partial v_\theta}{\partial r} \right) \right] \quad (4.92)$$

If we consider small curvatures ( $\delta \ll 1$ ) only, knowing that  $v_\phi = O(1)$  and  $r$  is already scaled and in the interval  $[0, 1]$ , the momentum equation yields  $v_r \frac{\partial v_r}{\partial r} = O(\delta v_\phi^2) = O(\delta)$  and thus  $O(v_r) = \delta^{1/2}$ . From the continuity equation (4.89) it can be seen that  $v_r$  and  $v_\theta$  scale in the same way, i.e.  $O(v_r) = O(v_\theta)$ , and thus also  $O(v_\theta) = \delta^{1/2}$ . If instead of using (4.88) we would use:

$$r^* = \frac{r}{a}, \quad p^* = \frac{p}{\delta \rho V^2}, \quad v_r^* = \frac{v_r}{\delta^{1/2} V}, \quad v_\theta^* = \frac{v_\theta}{\delta^{1/2} V}, \quad v_\phi^* = \frac{v_\phi}{V} \quad (4.93)$$

The continuity equation and momentum equation in  $r$ -direction for  $\delta \ll 1$  would be (again after dropping the asterix):

$$\frac{\partial v_r}{\partial r} + \frac{v_r}{r} + \frac{1}{r} \frac{\partial v_\theta}{\partial \theta} = 0 \quad (4.94)$$

and

$$\begin{aligned} v_r \frac{\partial v_r}{\partial r} + \frac{v_\theta}{r} \frac{\partial v_r}{\partial \theta} - \frac{v_\theta^2}{r} - v_\phi^2 \cos \theta = \\ - \frac{\partial p}{\partial r} + \frac{1}{\delta^{1/2} Re} \left[ \frac{1}{r} \frac{\partial}{\partial \theta} \left( \frac{1}{r} \frac{\partial v_r}{\partial \theta} - \frac{\partial v_\theta}{\partial r} - \frac{v_\theta}{r} \right) \right] \end{aligned} \quad (4.95)$$

From this we can see that for small curvature another dimensionless parameter, the Dean number, can be defined as:

$$Dn = \delta^{1/2} Re. \quad (4.96)$$

The secondary flow depends on two important parameters, the Reynolds number  $Re$  and the curvature  $\delta$  or the Dean number  $Dn$  and the curvature  $\delta$ . The last combination is often used because for small curvature only the Dean number is of importance.

For large Dean numbers the viscous term in (4.95) can be neglected in the core of the secondary flow field and one can talk about a boundary layer of the secondary flow. The thickness  $\delta_s$  of this boundary layer can be derived from the momentum equation in  $\theta$ -direction:

$$v_r \frac{\partial v_\theta}{\partial r} + \frac{v_\theta}{r} \frac{\partial v_\theta}{\partial \theta} - \frac{v_r v_\theta}{r} + \delta \frac{v_\phi^2 \sin \theta}{1 + \delta r \cos \theta} = -\frac{1}{r} \frac{\partial p}{\partial \theta} + \frac{1}{\delta^{1/2} Re} \left[ \left( \frac{\partial}{\partial r} + \frac{\delta \cos \theta}{1 + \delta r \cos \theta} \right) \left( \frac{\partial v_\theta}{\partial r} + \frac{v_\theta}{r} - \frac{1}{r} \frac{\partial v_r}{\partial r} \right) \right] \quad (4.97)$$

If we assume that at  $r = a - \delta_s$  the viscous and inertia forces are of the same order of magnitude we have:

$$\frac{\delta_s}{a} = O(Dn^{-1/2}) \quad (4.98)$$

In figure 4.10 the boundary layer of the secondary flow is indicated with a dashed line and indeed decreases with increasing Dean numbers.

#### 4.4.2 Unsteady fully developed flow in a curved tube

In unsteady flow in a curved tube the secondary flow will have the same orientation as in stationary flow. The reason for this is that the centrifugal forces are not sensitive for the direction of the axial velocity ( $f_c \propto v_\phi^2$ ). For high frequencies, or better large Womersley numbers, like in the case for straight tubes an instationary boundary layer will develop such that in the central core the flow will behave more or less inviscid whereas at the boundary viscous forces are dominant. For oscillatory flow this may lead to a secondary flow field as is depicted in figure 4.11. In the core the secondary vortex will have an opposite direction as in the boundary layer where the direction corresponds with the one in steady flow. In contradiction to the flow in a straight tube, however, for flow in a curved tube the superposition of several harmonics is not allowed because the governing equations are strongly non-linear.

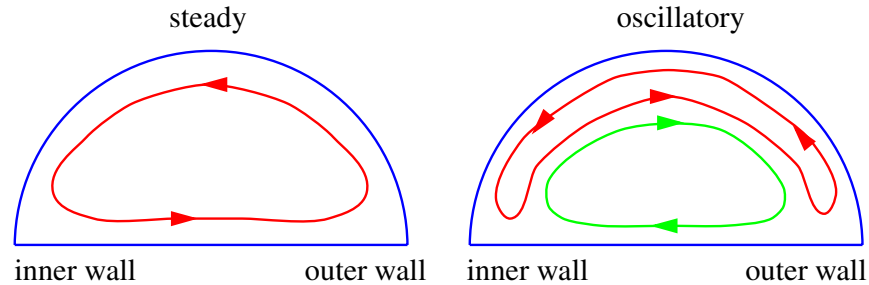


Figure 4.11: Streamline patterns of fully developed secondary flow in steady (left) and oscillatory (right) flow in a curved tube.

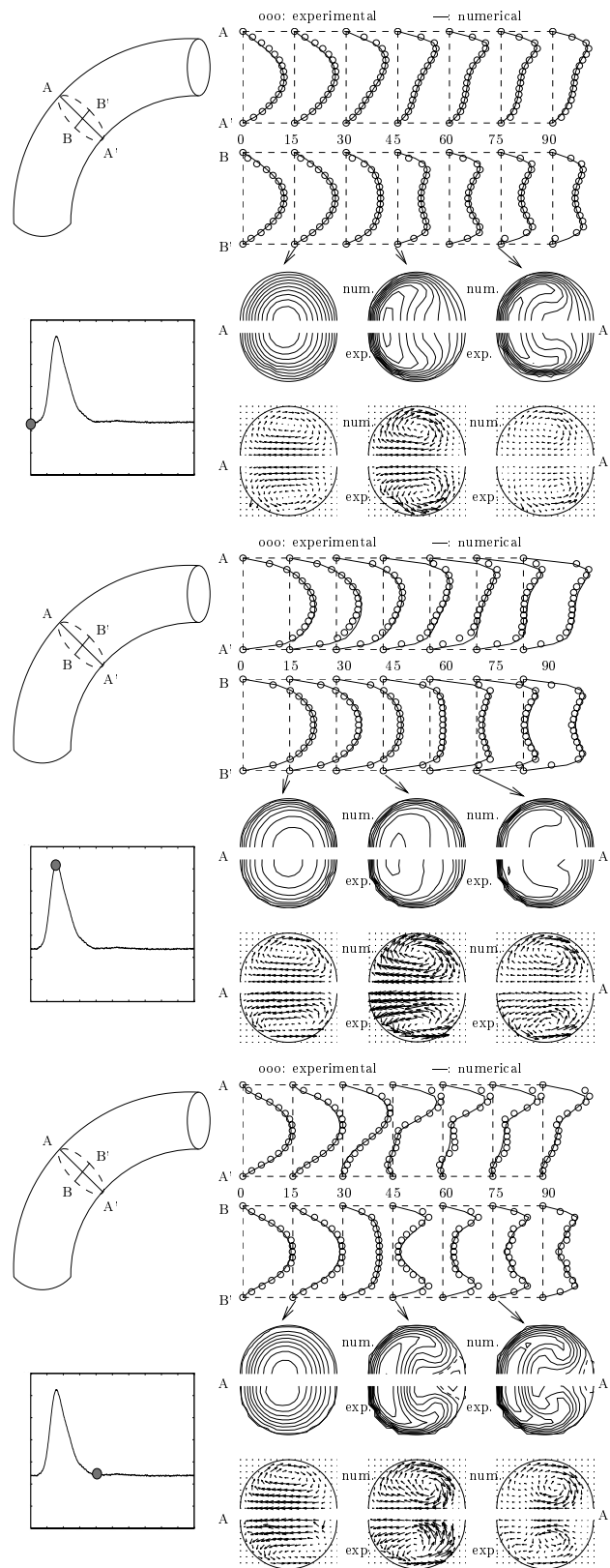


Figure 4.12: Computational (FEM) and experimental (LDA) results of pulsatile flow in a curved tube: end diastolic (top), peak systolic (middle) and end systolic (bottom).

In pulsating flow this second vortex will not be that pronounced as in oscillating flow but some influence can be depicted. This is shown in the figure 4.12 where the results of a finite element computation of pulsating flow in a curved tube are given together with experimental (laser Doppler) data.

#### 4.4.3 Flow in branched tubes

The flow in branched tubes (bifurcations) shows the same phenomena as in curved tubes. Actually the bifurcation can be considered as a two joined curved tubes. Of course there are also differences with curved tube flow due to the bifurcation point (apex) which will induce an extra asymmetry (see figure 4.13).

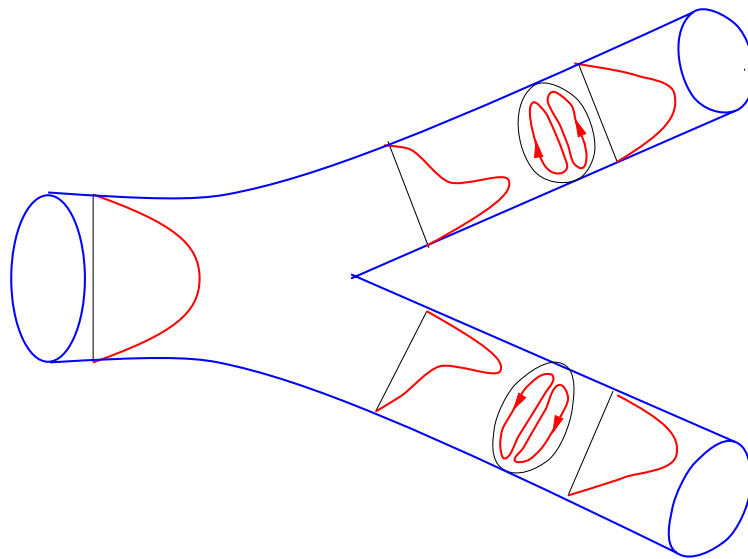


Figure 4.13: Axial velocity and streamline patterns of flow in a bifurcation.

Detailed knowledge about the flow phenomena in curved and branched tubes is of great physiological and clinical importance. The prediction of areas of high and low shear rates and wall shear stress, the prediction of flow instabilities related to high shear rates as occur at the interface between the areas with high and low axial velocity can help to interpret clinical data from ultra-sound Doppler measurements and MRI images and can help to get insight in the development of atherosclerosis. In many case advanced methods in computational fluid dynamics (CFD) are needed to obtain more then the qualitative information as is given in this section. An example of this is given in figure 4.14 where the results of computations of the flow in the internal carotid artery is given together with experimental results obtained with laser Doppler anemometry.

## 4.5 Summary

Flow patterns in rigid straight, curved and branched tubes have been treated in this chapter. The velocity profiles of fully developed Newtonian flow in a straight circular

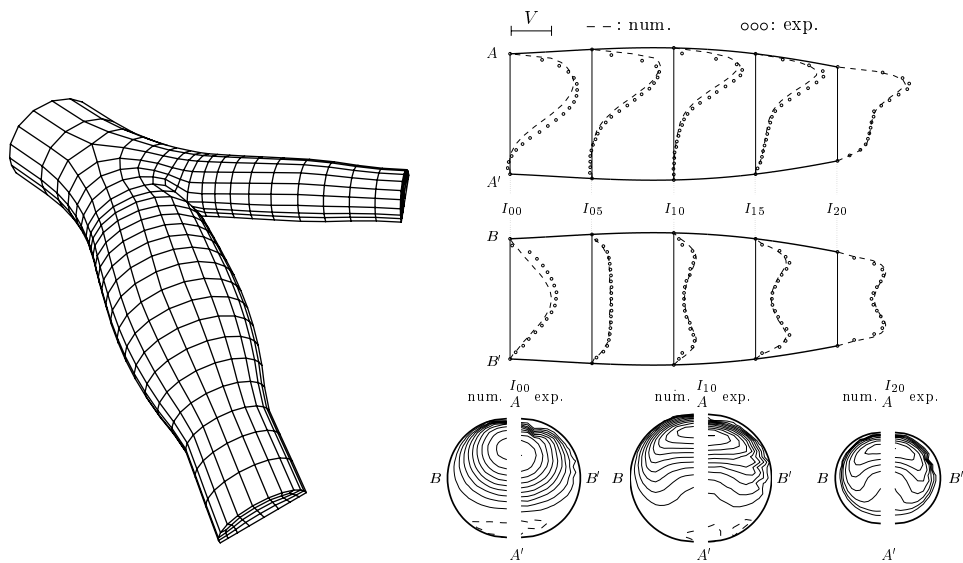


Figure 4.14: Computational (FEM) and experimental (LDA) velocity distributions of a steady flow in a model of the carotid artery bifurcation.

tube can easily be derived by integration of the Navier-Stokes equations in cylindrical coordinates using superposition of harmonics of the pressure pulse. Apart from a scale factor for the pressure, only one single parameter, the Womersley number  $\alpha = a\sqrt{\omega/\nu}$ , determines the character of the flow. For large values of this parameter the flow is dominated by inertia and flat velocity profiles are found oscillating  $90^\circ$  out of phase with the pressure gradient. For low values of  $\alpha$  the flow is dominated by viscous forces and a quasi static Poiseuille flow is found that is  $180^\circ$  out of phase with the pressure gradient. For arbitrary values of  $\alpha$  the velocity profiles are solutions of Bessel's function and can be interpreted as a composition of a viscosity dominated flow in the boundary layer and an inertia dominated flow in the core. The thickness of the boundary layer appears to depend on  $\alpha$  according to  $\delta/a = O(\alpha^{-1})$ .

The flow in curved tubes with curvature ratio  $\delta$  differs from that in straight tubes because also centrifugal forces are of importance. Due to these centrifugal forces, the pressure gradients in the bulk flow are not in equilibrium with the flow in the viscous boundary layers and a secondary flow is induced, resulting in a strongly disturbed axial flow. A new dimensionless parameter, the Dean number, defined as  $De = (a/R_0)^{1/2} Re$ , determines the importance of this secondary flow. The main features of the flow in branched tubes strongly resemble those of the flow in curved tubes.

## Chapter 5

# Mechanics of the vessel wall

### 5.1 Introduction

In the arterial system, the amplitude of the pressure pulse is that large that the arteries significantly deform during the cardiac cycle. This deformation is determined by the mechanical properties of the arterial wall. In this section an outline of the mechanical properties of the main constituents of the vessel wall and the wall as a whole is given taking the morphology as a point of departure. A simple linear elastic model for wall displacement due to change in transmural pressure will be derived.

## 5.2 Morphology

The vessel wall consists of three layers: the intima, the media and the adventitia. The proportions and composition of the different layers vary in different type of blood vessels. In figure 5.1 these layers and their composition are depicted schematically showing transversal sections through different kind of blood vessels.

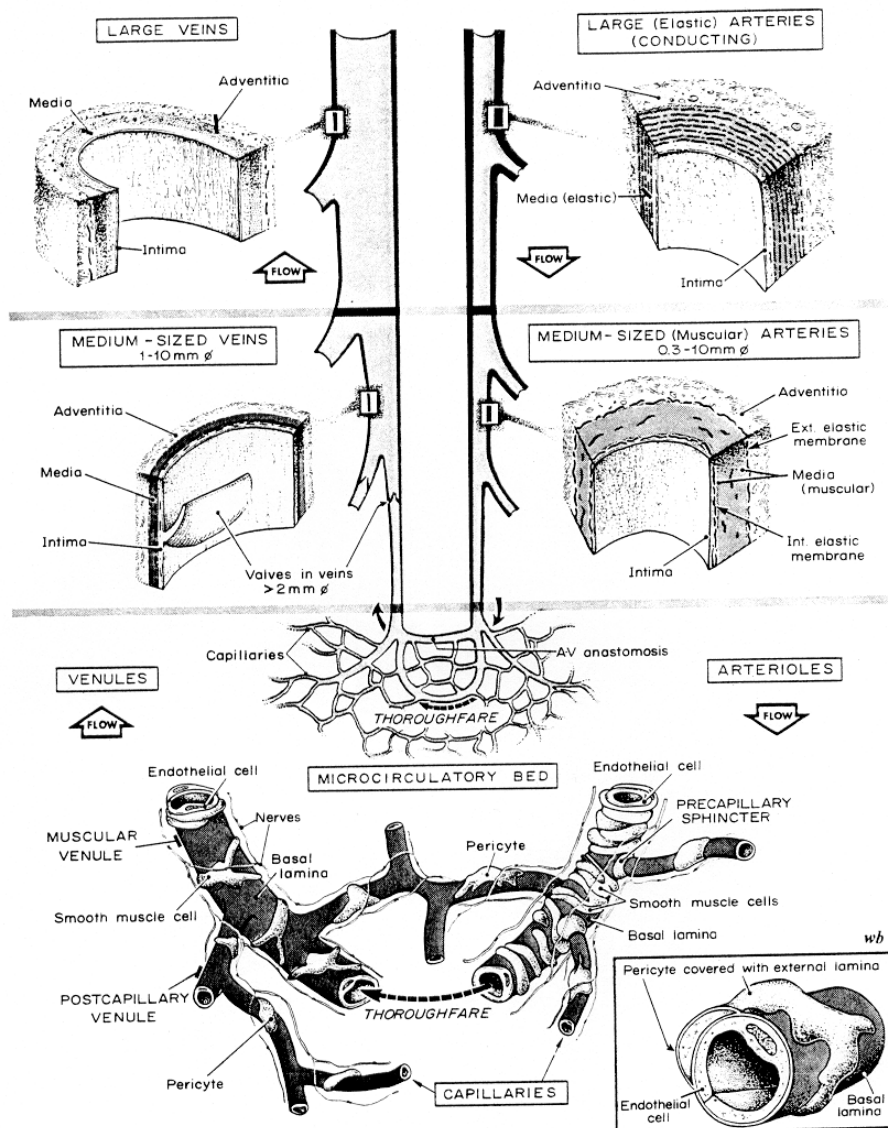


Figure 5.1: Morphology of principle segments of blood vessels in mammals (from Rhodin, 1980) .

**The intimal layer.** The intimal layer is the innermost layer of all blood vessels. This layer is composed of two structures, a single layer of endothelial cells and a thin subendothelial layer, separated by a thin basal lamina. The **endothelial cells** are flat and elongated with their long axis parallel to that of the blood vessel. They have a thickness of  $\pm 0.2 - 0.5 \mu\text{m}$ , except in the area of the nucleus, which protrudes slightly into the vessel. The endothelium covers all surfaces that come into direct contact with blood. It is important in regeneration and growth of the artery which is controlled by variations of wall shear stress and strain distributions induced by the blood flow and the wall deformation respectively. The **subendothelium layer** consists of a few collagenous bundles and elastic fibrils. Due to its relatively small thickness and low stiffness the intimal layer does not contribute to the overall mechanical properties of the vessel wall. An exception to this is found in the micro-circulation, where the intimal layer is relatively large. Here, however, mechanical properties are mainly determined by the surrounding tissue of the vessel.

**The tunica media.** The media is the thickest layer in the wall and shows large variation in contents in different regions of the circulation. It consists of elastic lamina and smooth muscle cells. In the human aorta and in large arteries, 40-60 of these lamina exist and almost no smooth muscle cells are found. These arteries therefor are often referred to as elastic arteries. Toward the periphery the number of elastic lamina decreases gradually and a larger amount of smooth muscle cells are found (muscular arteries). The elastic lamina (average thickness  $3 \mu\text{m}$ ) are concentric and equidistantly spaced. They are interconnected by a network of elastic fibrils. Thus structured, the media has great strength and elasticity. The smooth muscle cells are placed within the network of elastic fibrils and have an elongated, but irregular shape.

**The tunica adventitia.** The tunica adventitia of elastic arteries generally comprises only 10 % of the vascular wall. The thickness, however, varies considerably in different arteries and may be as thick as the media. The adventitia is composed of a loose connective tissue of elastin and collagen fibres in mainly longitudinal direction. The adventitia serves to connect the blood vessels to its surrounding tissue and in large arteries it harbors the nutrient vessels (arterioles, capillaries, venules and lymphatic vessels) referred to as *vaso vasorum*.

### 5.3 Mechanical properties

As described in the previous section, the main constituents of vascular tissue are elastin, collagen fibers and smooth muscle cells.

**Elastin** is a biological material with an almost linear stress-strain relationship (fig. 5.2). It has a Young's modulus of  $\approx 0.5 \text{ MPa}$  and remains elastic up to stretch ratios of  $\approx 1.6$  (Fung, 1993a). As can be seen from the stress-strain curves the material shows hardly any hysteresis.

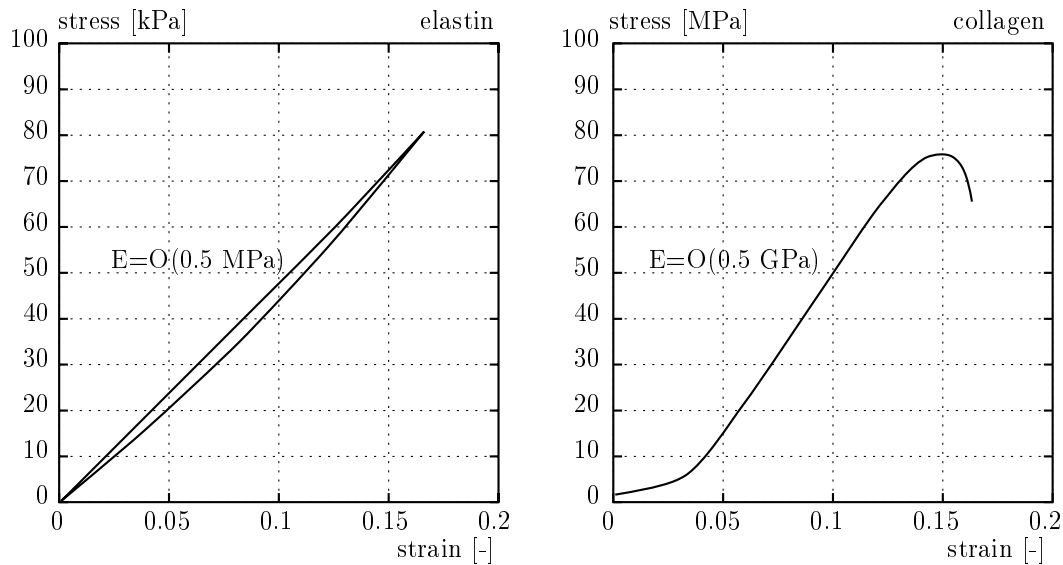


Figure 5.2: Left: Stress-strain relationships of elastin from the ligamentum nuchae of cattle. Right: Typical stress-strain relationship of collagen from the rabbit limb tendon. (Both after Fung, 1993a).

**Collagen** is a basic structural protein in animals. It gives strength and stability and appears in almost all parts of the body. The collagen molecule consists of three helically wound chains of amino-acids. These helices are collected together in microfibrils, which in their turn form subfibrils and fibrils. The fibrils have a diameter of 20-40 nm, depending on species and tissue. Bundles of fibrils form fibers, with diameters ranging from 0.2 to 12  $\mu\text{m}$ . The fibers are normally arranged in a wavy form, with typical "wavelengths" of 200  $\mu\text{m}$  (Fung, 1993a). Due to this waviness the stress-strain relationship shows a very low stiffness at small stretch ratios (fig. 5.2). The stiffness increases fast once the fibers are deformed to straight lines, the Young's modulus of the material then reaches  $\approx 0.5$  GPa. At further stretching, the material finally fails at 50-100 MPa longitudinal stress.

**Smooth muscle cells** appear in the inner part of the tunica media and are oriented longitudinally, circumferentially or helically. The Young's modulus is in the order of magnitude of the one of elastine ( $\approx 0.5$  MPa). When relaxed it is about 0.1 MPa and when activated it can increase to 2 MPa. Especially in the smaller arteries and arterioles they strongly determine the mechanical properties of the arterial wall and are responsible for the ability to regulate local blood flow.

### Elastic and Viscoelastic behavior

Due to the properties of its constituents, its specific morphology and its geometry, the arterial wall exhibits a non-isotropic nonlinear response to cyclic pressure loads. An important geometrical parameter is the ratio between diameter and thickness of the arterial wall. This ratio depends on the type of artery but is  $O(0.1)$  in many cases.

Moreover the vessels are tethered mainly longitudinal by the surrounding tissue. Due to these complex properties it formally is not possible to define a Young's modulus as can be done in linear elasticity theory. Still in order to obtain a global idea of the elastic behavior it is possible to lump all properties together as if the vessel wall was homogeneous. This can be done by measuring the stress strain relationship and use the result to define an *effective* Young's modulus. In figure 5.3 a typical stress strain relationship of a large artery is shown. The stiffness in longitudinal direction is higher then in circumferential direction especially at larger stretch ratios yielding a different effective incremental Young's modulus. Still the relation is non-linear due to the wavy form of the collagen fibres that consequently contribute to the stiffness only at higher stretch ratios. It will be clear that linear elasticity can not be applied straight forward. Linearization, however, about an equilibrium state (for instance the mean or diastolic pressure) yields a *linearized* or *incremental* effective Young's modulus that in many cases is appropriate the use in linear elasticity analysis.

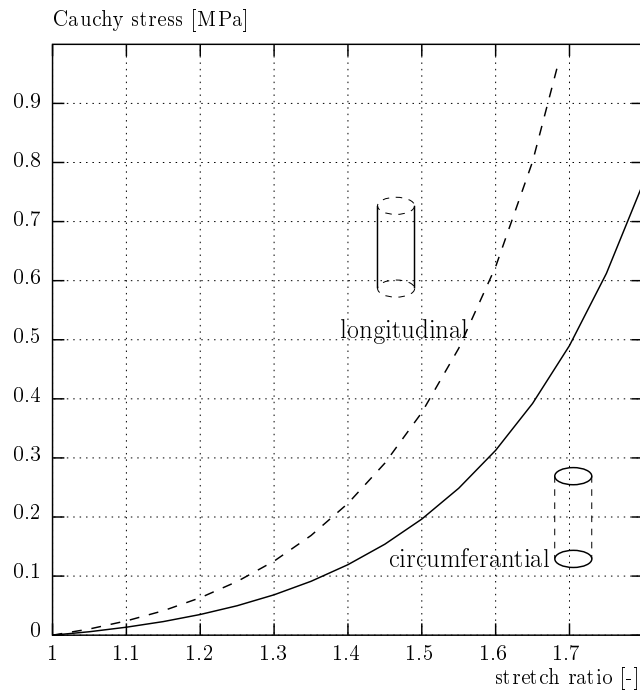


Figure 5.3: Typical stress-strain relationship (broken line = longitudinal, solid line = circumferential) of aortic wall material (after Kasyanov and Knet-s, 1974) .

Vascular tissue normally is viscoelastic. When a cyclic load is applied to it in an experiment, the load-displacement curve for loading differs from the unloading curve: hysteresis due to viscoelasticity is found ( see figure 5.2). Moreover, the curves change after several repetitions of the same loading/unloading cycle. After a certain number of repetitions, the loading-unloading curve doesn't change anymore, and the loading/unloading curves almost coincide. The state of the specimen then is called preconditioned (Fung *et al.*, 1979; Fung, 1993a). How well this state resembles

the in-vivo situation is not reported.

## 5.4 Incompressible elastic deformation

In section 2.2.4 it has been shown that in general elastic solids can be described by the constitutive equation  $\boldsymbol{\sigma} = -p\mathbf{I} + \boldsymbol{\tau}(\mathbf{B})$ . The most simple version of such a relation will be the one in which the extra stress  $\boldsymbol{\tau}$  linearly depends on the Finger tensor. Materials that obey such a relation are referred to as linear elastic or neo-Hookean solids. Most rubber like materials but also to some extent biological tissues like the arterial wall are reasonably described by such a neo-Hookean model.

### 5.4.1 Deformation of incompressible linear elastic solids

The equations that describe the deformation of incompressible linear elastic solids are given by the continuity equation (2.38) and the momentum equation (2.39) together with the constitutive equation:

$$\boldsymbol{\sigma} = -p\mathbf{I} + G(\mathbf{B} - \mathbf{I}) \quad (5.1)$$

with  $p$  the pressure and  $G$  the shear modulus. Note that the linear relation between the extra stress and the strain is taken such that if there is no deformation ( $\mathbf{B} = \mathbf{I}$ ) the strain measure  $\mathbf{B} - \mathbf{I} = \mathbf{0}$ . The momentum and continuity equations then read:

$$\begin{cases} \rho \frac{\partial \mathbf{v}}{\partial t} + \rho(\mathbf{v} \cdot \nabla)\mathbf{v} = \rho \mathbf{f} - \nabla p + G \nabla \cdot (\mathbf{B} - \mathbf{I}). \\ \nabla \cdot \mathbf{v} = 0 \end{cases} \quad (5.2)$$

After introduction of the non-dimensional variables  $\mathbf{x}^* = \mathbf{x}/L$ ,  $t^* = t/\theta$  and characteristic strain  $\gamma$ , the characteristic displacement is  $U = \gamma L$  and the characteristic velocity is  $V = U/\theta = \gamma L/\theta$ . Using a characteristic pressure  $p^* = p/p_0$ , the dimensionless equations for elastic deformation then become (after dropping the superscript \*):

$$\begin{cases} \frac{\rho \gamma L}{\theta^2} \frac{\partial \mathbf{v}}{\partial t} + \frac{\rho \gamma^2 L}{\theta^2} (\mathbf{v} \cdot \nabla)\mathbf{v} = \rho g \mathbf{f} - \frac{p_0}{L} \nabla p + \frac{\gamma G}{L} \nabla \cdot (\mathbf{B} - \mathbf{I}) \\ \nabla \cdot \mathbf{v} = 0 \end{cases} \quad (5.3)$$

Unfortunately in the solid mechanics community it is not common to use dimensionless parameters and we have to introduce them ourselves or use an example to show which of the terms are of importance in this equation. If we assume that we deform a solid with density  $\rho = O(10^3)[kg/m^3]$ , shear modulus  $G = O(10^5)[Pa]$  and characteristic length  $L = O(10^{-2})[m]$  with a typical strain  $\gamma = O(10^{-1})$  in a characteristic time  $\theta = O(1)[s]$ , the terms at the left hand side have an order of magnitude of  $O(1)[Pa/m]$  and  $O(10^{-2})[Pa/m]$ . The deformation forces at the right hand side, however, have an order of magnitude  $O(10^4)[Pa/m]$ . As a consequence the terms at the left hand side can be neglected. Gravity forces can not be neglected automatically but are often not taken into account because they work on the body

as a whole and do not induce extra deformation unless large hydrostatic pressure gradients occur. The momentum equation then reads:

$$\begin{cases} \nabla \cdot \boldsymbol{\sigma} = -\nabla p + G\nabla \cdot (\mathbf{B} - \mathbf{I}) = \mathbf{0} \\ \det(\mathbf{F}) = 1 \end{cases} \quad (5.4)$$

Note that the continuity equation is expressed in terms of the deformation tensor  $\mathbf{F}$  (see below). Equations (5.4) can be solved after applying boundary conditions of the form (see (2.43)):

$$\begin{aligned} & \text{in normal direction:} \\ & \quad \text{prescribed displacement:} & (\mathbf{u} \cdot \mathbf{n}) = u_{n\Gamma} \\ & \quad \text{or prescribed stress:} & (\boldsymbol{\sigma} \cdot \mathbf{n}) \cdot \mathbf{n} = (\mathbf{s} \cdot \mathbf{n}) \\ & \text{in tangential directions:} \\ & \quad \text{prescribed displacement:} & (\mathbf{u} \cdot \mathbf{t}_i) = u_{t_i\Gamma} \quad i = 1, 2 \\ & \quad \text{or prescribed stress:} & (\boldsymbol{\sigma} \cdot \mathbf{n}) \cdot \mathbf{t}_i = (\mathbf{s} \cdot \mathbf{t}_i) \end{aligned} \quad (5.5)$$

In linear elasticity the incompressibility constraint ( $\det(\mathbf{F}) = 1$ ) is oftenly circumvented by assuming the material to be (slightly) compressible. In that case it is convenient to decompose the deformation in a volumetric part and an isochoric part according to:

$$\mathbf{F} = J^{1/3} \tilde{\mathbf{F}} \quad (5.6)$$

with  $J$  the volume ratio defined by:

$$J = \det(\mathbf{F}) = \frac{dV}{dV_0} \quad (5.7)$$

Consequently  $\det(\tilde{\mathbf{F}}) = \det(J^{-1/3} \mathbf{I}) \cdot \det(\mathbf{F}) = 1$  and an equivalent neo-Hookean model can be taken according to:

$$\boldsymbol{\sigma} = \kappa(J - 1)\mathbf{I} + G(\tilde{\mathbf{B}} - \mathbf{I}) \quad (5.8)$$

with  $\kappa$  the compression modulus and  $\tilde{\mathbf{B}} = \tilde{\mathbf{F}} \cdot \tilde{\mathbf{F}}^c = J^{-2/3} \mathbf{F} \cdot \mathbf{F}^c$ .

#### 5.4.2 Approximation for small strains

For small strains  $\gamma$  (i.e.  $\|\nabla \mathbf{u}\| \approx \|\nabla^0 \mathbf{u}\| \ll 1$ ) the deformation tensor  $\mathbf{F}$  can be written as:

$$\mathbf{F} = (\nabla^0 \mathbf{x})^c = (\nabla^0(\mathbf{x}^0 + \mathbf{u}))^c = \mathbf{I} + (\nabla^0 \mathbf{u})^c \approx \mathbf{I} + (\nabla \mathbf{u})^c \quad (5.9)$$

The volume ratio for small deformations then yields:

$$J = \det(\tilde{\mathbf{F}}) \approx \det(\mathbf{I} + (\nabla \mathbf{u})^c) \approx 1 + \text{tr}(\nabla \mathbf{u}) \quad (5.10)$$

The isochoric part of the deformation then is given by:

$$\begin{aligned}
\tilde{\mathbf{F}} &= J^{-1/3} \mathbf{F} \\
&\approx (1 + \text{tr}(\nabla \mathbf{u}))^{-1/3} (\mathbf{I} + (\nabla \mathbf{u})^c) \\
&\approx (1 - \frac{1}{3} \text{tr}(\nabla \mathbf{u})) (\mathbf{I} + (\nabla \mathbf{u})^c)
\end{aligned} \tag{5.11}$$

This finally yields the isochoric Finger tensor:

$$\begin{aligned}
\tilde{\mathbf{B}} &= J^{-2/3} \mathbf{F} \cdot \mathbf{F}^c \\
&\approx (1 - \frac{2}{3} \text{tr}(\nabla \mathbf{u})) (\mathbf{I} + (\nabla \mathbf{u})^c) (\mathbf{I} + (\nabla \mathbf{u})^c)^c \\
&\approx \mathbf{I} + (\nabla \mathbf{u})^c + \nabla \mathbf{u} - \frac{2}{3} \text{tr}(\nabla \mathbf{u}) \mathbf{I}
\end{aligned} \tag{5.12}$$

The constitutive relation for compressible elastic deformation for small strains then reads:

$$\begin{aligned}
\boldsymbol{\sigma} &= \kappa \text{tr}(\nabla \mathbf{u}) \mathbf{I} + G((\nabla \mathbf{u})^c + \nabla \mathbf{u} - \frac{2}{3} \text{tr}(\nabla \mathbf{u}) \mathbf{I}) \\
&= (\kappa - \frac{2}{3} G) \text{tr}(\nabla \mathbf{u}) \mathbf{I} + G(\nabla \mathbf{u} + (\nabla \mathbf{u})^c)
\end{aligned} \tag{5.13}$$

Together with the definition of infinitesimal strain:

$$\boldsymbol{\epsilon} = \frac{1}{2} (\nabla \mathbf{u} + (\nabla \mathbf{u})^c) \tag{5.14}$$

we finally obtain:

$$\boldsymbol{\sigma} = (\kappa - \frac{2}{3} G) \text{tr}(\boldsymbol{\epsilon}) \mathbf{I} + 2G \boldsymbol{\epsilon} \tag{5.15}$$

It can readily be verified that consequently

$$\boldsymbol{\epsilon} = \frac{(1 + \mu)}{E} \boldsymbol{\sigma} - \frac{\mu}{E} \text{tr}(\boldsymbol{\sigma}) \mathbf{I} \tag{5.16}$$

with :

$$\kappa = \frac{E}{3(1 - 2\mu)} \quad G = \frac{E}{2(1 + \mu)}$$

or (5.17)

$$\mu = \frac{3\kappa - 2G}{6\kappa + 2G} \quad E = \frac{9\kappa G}{3\kappa + G}$$

Note that the Young's modulus  $E$  and Poisson ratio  $\mu$  can be determined by a tensile test. Using the expression for the strain given by (5.16) it follows that:

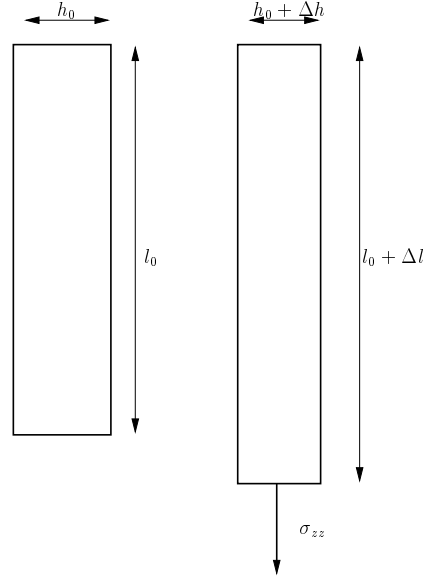
$$\epsilon_{zz} = \frac{\Delta l}{l_0} = \frac{1}{E} \sigma_{zz}$$

$$\epsilon_{xx} = \epsilon_{yy} = \frac{\Delta h}{h_0} = -\frac{\mu}{E} \sigma_{zz}$$

and consequently:

$$E = \frac{\sigma_{zz}}{\epsilon_{zz}}$$

$$\mu = -\frac{\epsilon_{xx}}{\epsilon_{zz}}$$



### 5.5 Wall motion

Consider a linear elastic thin walled tube with constant wall thickness  $h$ , density  $\rho_w$ , Young's modulus  $E$  and Poisson's ratio  $\mu$  (see figure 5.4).

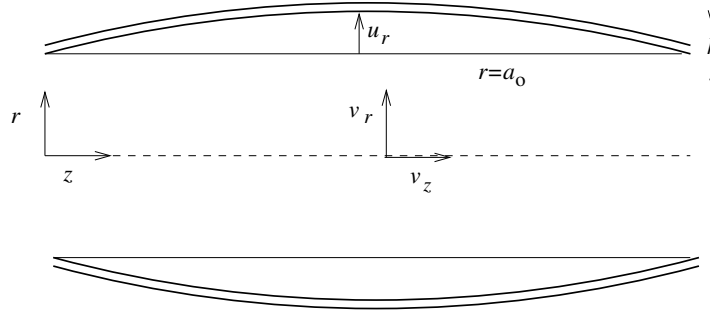


Figure 5.4: Distensible tube with radius  $a(z, t)$ , wall thickness  $h$

If the thickness of the wall is assumed to be that small that  $\sigma_{rr} = 0$ , the momentum equation in z-direction is given by:

$$\epsilon_{zz} = \frac{\partial u_z}{\partial z} = \frac{1}{E} (\sigma_{zz} - \mu \sigma_{\phi\phi}) \tag{5.18}$$

with  $u_z$  the wall displacement in axial direction. Assuming again axial restraint ( $u_z = 0$ ) then  $\epsilon_{zz} = 0$  and thus:

$$\sigma_{zz} = \mu \sigma_{\phi\phi} \tag{5.19}$$

In circumferential direction the strain  $\varepsilon_{\phi\phi}$  is given by:

$$\begin{aligned}\varepsilon_{\phi\phi} &= \frac{(a_0 + u_r)d\phi - a_0d\phi}{rd\phi} \approx \frac{u_r}{a_0} \\ &= \frac{1}{E}(\sigma_{\phi\phi} - \mu\sigma_{zz}) = \frac{\sigma_{\phi\phi}}{E}(1 - \mu^2)\end{aligned}\quad (5.20)$$

with  $u_r$  the wall displacement in radial direction. This implies the following expression for the circumferential stress:

$$\sigma_{\phi\phi} = \frac{E}{1 - \mu^2} \frac{u_r}{a_0} \quad (5.21)$$

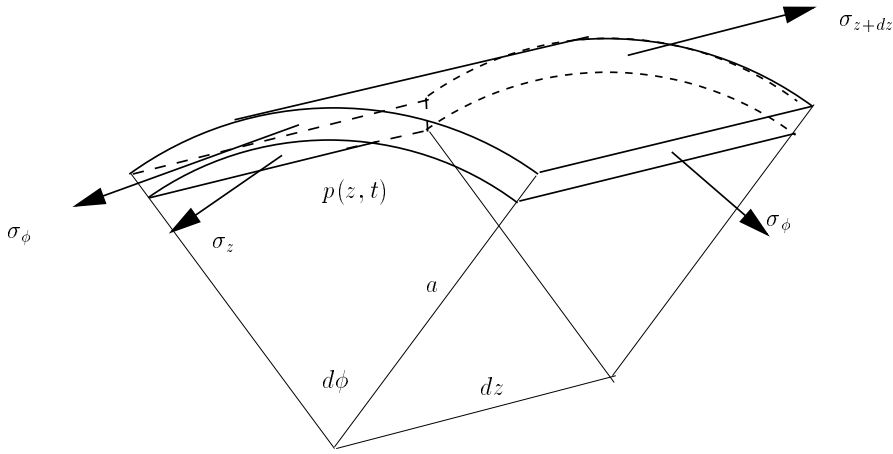


Figure 5.5: Stresses in tangential and circumferential direction.

If the tube is loaded with an internal (transmural) pressure  $p(z, t)$  the momentum equation in radial direction reads (see figure 5.5):

$$\rho_w a_0 d\phi h dz \frac{\partial^2 u_r}{\partial t^2} = p(z, t) a_0 d\phi dz - 2\sigma_{\phi\phi} \sin\left(\frac{1}{2}d\phi\right) h dz \quad (5.22)$$

Since  $\sin(d\phi) \approx d\phi$  this yields together with (5.21):

$$\rho_w h \frac{\partial^2 u_r}{\partial t^2} = p - \frac{hE}{(1 - \mu^2)} \frac{u_r}{a_0^2} \quad (5.23)$$

If we neglect inertia forces we obtain

$$u_r = \frac{(1 - \mu^2) a_0^2}{hE} p \quad (5.24)$$

The cross-sectional area of the tube is given by:

$$A = \pi(a_0 + u_r)^2 = \pi a_0^2 + 2\pi a_0 u_r + \pi u_r^2 \approx \pi a_0^2 + 2\pi a_0 u_r \quad (5.25)$$

This yields the compliance of the tube to be:

$$C = \frac{\partial A}{\partial p} = \frac{2\pi a_0^3}{h} \frac{(1 - \mu^2)}{E} \quad (5.26)$$

Oftenly instead of the compliance  $C$  the distensibility

$$D = \frac{1}{A_0} C = \frac{2a_0}{h} \frac{(1 - \mu^2)}{E} \quad (5.27)$$

is used. In the next chapter  $D$  will be used to derive expressions for the propagation of pressure waves in distensible tubes.

## 5.6 Summary

A short introduction to vessel wall mechanics based on morphology and material properties of the main constituents (elastine and collagen) is given. Although the constitutive behavior of vessel wall is anisotropic and visco-elastic simple linear elastic models based on thin walled tubes can be valuable. To this end, simple expressions for the compliance and distensibility of thin walled tubes are derived and related to parameters that can be derived from tensile tests.



## Chapter 6

# Wave phenomena in blood vessels

### 6.1 Introduction

In this chapter we will show that traveling pressure and flow waves are the result of the distensibility (or compliance) of the arteries (see chapter 1 equations (1.2),(1.3) and (1.4) or chapter 5 equations (5.26) and (5.27)) and the pulsatile character of the pressure. A typical relation between the pressure and cross-sectional area of an artery is given in figure 1.5 and shows that the compliance normally does not have a constant value but strongly depends on the pressure. In this chapter, however, only small area variations will be considered and a linear relation between the pressure amplitude and the vessel diameter will be assumed. Apart from wave propagation and the importance of viscous forces expressed in the value of the Womersley number  $\alpha$ , also wave reflection from arterial bifurcations or transitions in mechanical or geometrical properties will be dealt with. Moreover, attenuation of waves as a result of fluid viscosity and wall visco-elasticity will be discussed.

## 6.2 Pressure and flow

In the physiological introduction of this course (chapter 1) it is mentioned that the heart is a four-chambered pump that generates a pulsating pressure and flow (see figure 1.2). The frequency contents of the pressure and flow in the aorta is given in table 1.3.1 and shows that the pulsatile character of the pressure and flow can be described very well with the first 8 to 10 harmonics (see also figure 1.6). Moreover, in chapter 1 a simple (windkessel) model was introduced to describe the pressure/flow relation or impedance of the arterial system using the compliance  $C_e = dV/dp$  of the elastic arteries and the resistance  $R_p$  of the periferal arteries (see also equation 1.8):

$$q_a = C_e \frac{\partial p_a}{\partial t} + \frac{p_a}{R_p} \quad (6.1)$$

and with  $p_a = \hat{p}_a e^{i\omega t}$ ,  $q_a = \hat{q}_a e^{i\omega t}$ :

$$Z = \frac{p_a}{q_a} = \frac{R_p(1 - i\omega R_p C_e)}{1 + \omega^2 R_p^2 C_e^2} \quad (6.2)$$

In figure 6.1 the absolute value and argument of the impedance given by (6.2) is shown as a function of the harmonics. Experimental data (indicated with lines (Milnor, 1989)) show that the windkessel model does not predict accurate results especially for the phase of the higher harmonics. Moreover, as illustrated in figure (1.4), the pressure and flow waves change their shape with increasing distance from the heart. This is a result of traveling waves and never can be described by the windkessel model.

In order to describe the pressure and flow in terms of traveling waves (i.e.  $p = p(z, t)$  and  $q = q(z, t)$ ) the following complex notation will be used:

$$p(z, t) = \hat{p} e^{i(\omega t - kz)} \quad \text{and} \quad q(z, t) = \hat{q} e^{i(\omega t - kz)} \quad (6.3)$$

here  $\omega$  is the angular frequency,  $k = k_r + ik_i$  is the complex wave number and  $\hat{p} = |\hat{p}|e^{i\phi}$  denotes the complex amplitude. The actual pressure (c.q. flow) is defined as the real part of (6.3):

$$Re [p(z, t)] = |\hat{p}| e^{k_i z} \cos(\omega t - k_r z + \phi) \quad (6.4)$$

It will be clear that  $(-k_i)$  is a measure for the attenuation of the wave and that  $k_r = 2\pi/\lambda$  with  $\lambda$  the wavelength.

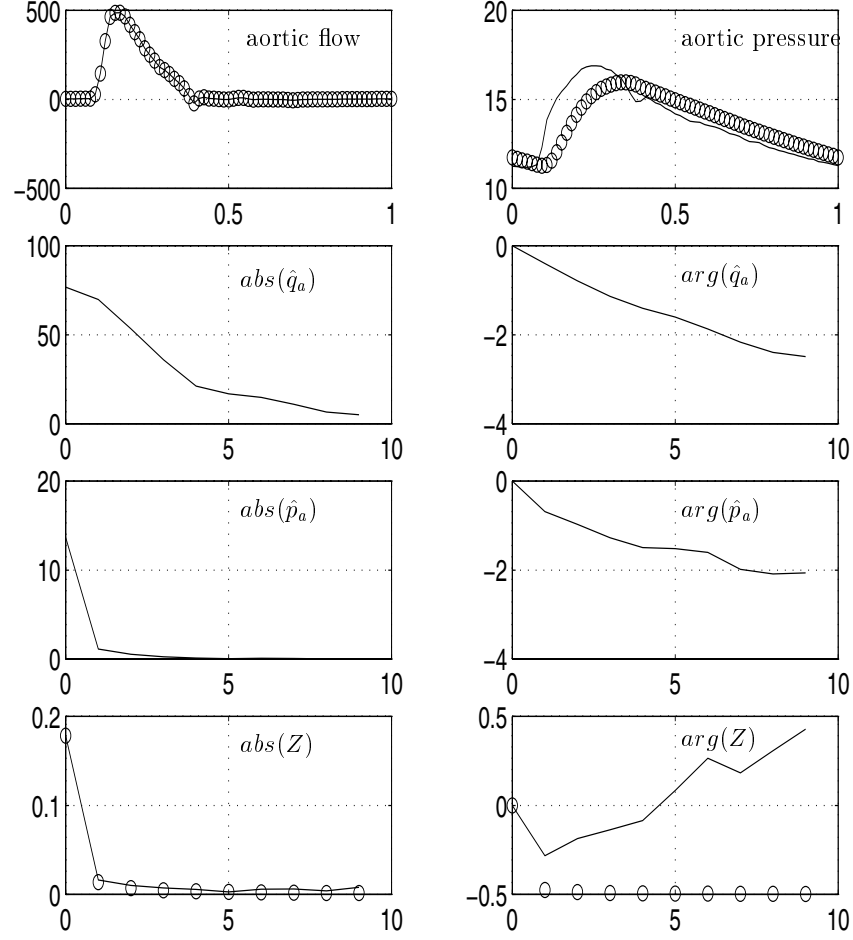


Figure 6.1: Absolute value and argument of the arterial impedance as computed with a windkessel model (o) and from experimental data (-).

### 6.3 Fluid flow

To analyze fully developed Newtonian flow in distensible tubes we consider the Navier-Stokes equations in a cylindrical coordinate system:

$$\left\{ \begin{array}{l} \frac{\partial v_r}{\partial t} + v_r \frac{\partial v_r}{\partial r} + v_z \frac{\partial v_r}{\partial z} = -\frac{1}{\rho} \frac{\partial p}{\partial r} + \nu \left( \frac{\partial}{\partial r} \left( \frac{1}{r} \frac{\partial}{\partial r} (r v_r) \right) + \frac{\partial^2 v_r}{\partial z^2} \right) \\ \frac{\partial v_z}{\partial t} + v_r \frac{\partial v_z}{\partial r} + v_z \frac{\partial v_z}{\partial z} = -\frac{1}{\rho} \frac{\partial p}{\partial z} + \nu \left( \frac{1}{r} \frac{\partial}{\partial r} \left( r \frac{\partial}{\partial r} (v_z) \right) + \frac{\partial^2 v_z}{\partial z^2} \right) \\ \frac{1}{r} \frac{\partial}{\partial r} (r v_r) + \frac{\partial v_z}{\partial z} = 0 \end{array} \right. \quad (6.5)$$

Since the velocity in circumferential direction equals zero ( $v_\phi = 0$ ), the momentum equation and all derivatives in  $\phi$ -direction are omitted. Due to the distensibility of

the tube, pressure and flow waves will propagate with a finite wave speed  $c = \omega/k_r$  and a typical wavelength  $\lambda = 2\pi/k_r$ . First a properly scaled dimensionless form of the Navier-Stokes equations will be derived. To this end the radial coordinates are made dimensionless using the mean radius of the tube, i.e.  $r' = r/a_0$ . The axial coordinates, however, must be scaled with the real part of the wave number  $k_r$ :  $z' = zk_r$  (see (6.3)). The axial velocity is made dimensionless with its characteristic value over a cross-section:  $v'_z = v_z/V$ . From the continuity equation it can be derived that the radial velocity then must be made dimensionless as:  $v'_r = (v_r/V)(1/k_r a_0)$ . The characteristic time  $t' = \omega t$  can be written as  $t' = (k_r c)t$  with  $c$  the wave speed. Together with a dimensionless pressure  $p' = p/(\rho V c)$  the dimensionless Navier-Stokes equations read:

$$\left\{ \begin{array}{l} \frac{\partial v'_r}{\partial t'} + \frac{V}{c} \left( v'_r \frac{\partial v'_r}{\partial r'} + v'_z \frac{\partial v'_r}{\partial z'} \right) = \\ \quad - \frac{1}{k_r^2 a_0^2} \frac{\partial p'}{\partial r'} + \frac{1}{\alpha^2} \left( \frac{\partial}{\partial r'} \left( \frac{1}{r'} \frac{\partial}{\partial r'} (r' v'_r) \right) + a_0^2 k_r^2 \frac{\partial^2 v'_r}{\partial z'^2} \right) \\ \frac{\partial v'_z}{\partial t'} + \frac{V}{c} \left( v'_r \frac{\partial v'_z}{\partial r'} + v'_z \frac{\partial v'_z}{\partial z'} \right) = \\ \quad - \frac{\partial p'}{\partial z'} + \frac{1}{\alpha^2} \left( \frac{1}{r'} \frac{\partial}{\partial r'} \left( r' \frac{\partial}{\partial r'} (v'_z) \right) + a_0^2 k_r^2 \frac{\partial^2 v'_z}{\partial z'^2} \right) \\ \frac{1}{r'} \frac{\partial}{\partial r'} (r' v'_r) + \frac{\partial v'_z}{\partial z'} = 0 \end{array} \right. \quad (6.6)$$

Besides the Womersley parameter  $\alpha = a_0 \sqrt{\omega/\nu}$  the dimensionless parameters that play a role in this equation are the speed ratio  $S = V/c$  and the circumference-to-wavelength ratio  $G = a_0 k_r = 2\pi a_0/\lambda$ . Under the assumptions that the wave velocity  $c$  is much larger than the fluid velocity  $V$ , the wavelength  $\lambda$  is much larger than the tube radius  $a_0$ , i.e.:

$$S = \frac{V}{c} \ll 1, \quad G^2 = (k_r a_0)^2 = \left( \frac{2\pi a_0}{\lambda} \right)^2 \ll 1 \quad (6.7)$$

it can readily be shown that the equations of motion reduce to:

$$\left\{ \begin{array}{l} \frac{\partial p}{\partial r} = 0 \\ \frac{\partial v_z}{\partial t} = -\frac{1}{\rho} \frac{\partial p}{\partial z} + \nu \frac{1}{r} \frac{\partial}{\partial r} \left( r \frac{\partial v_z}{\partial r} \right) \\ \frac{1}{r} \frac{\partial}{\partial r} (r v_r) + \frac{\partial v_z}{\partial z} = 0 \end{array} \right. \quad (6.8)$$

If we search for harmonic solutions with angular frequency  $\omega$  and wave number  $k$ :

$$p = \hat{p} e^{i(\omega t - kz)} \quad (6.9)$$

and

$$v_z = \hat{v}_z(r)e^{i(\omega t - kz)} \quad (6.10)$$

substitution in equation (6.8) yields exactly the same differential equation for  $\hat{v}_z$  as in the case of a rigid tube given in equation (4.45). If we further assume that the wall motion is axially restrained, which is thought to be relevant *in vivo* (Pedley, 1980), also the boundary condition for  $\hat{v}_z$  is not different from the one in rigid tubes but now must be applied in a linearized way at  $r = a_0$ . It will be clear that in that case we obtain exactly the same Womersley solution given by equation (4.45). Substitution of:

$$\frac{\partial \hat{p}}{\partial z} = -ik\hat{p} \quad (6.11)$$

yields:

$$\hat{v}_z(r) = \frac{k}{\rho\omega} \left[ 1 - \frac{J_0(i^{3/2}\alpha r/a_0)}{J_0(i^{3/2}\alpha)} \right] \hat{p} \quad (6.12)$$

In Womersley (1957) a relation similar to (6.12) is derived, however without the assumption of axial constraint. In that case the second term in the brackets is multiplied with an extra parameter that only slightly differs from unity. The wall shear stress is equal to the wall shear stress for rigid tubes and is defined by equation (4.58). The wave number  $k$  still has to be determined and depends on the properties of the arterial wall. In the next section the wall motion will be analyzed, again assuming axial restraint.

## 6.4 Wave propagation

### 6.4.1 Derivation of a quasi one-dimensional model

In order to obtain an expression for the wave number introduced in the previous section, a quasi one-dimensional wave propagation model for pressure and flow waves will be derived. To this end the Leibnitz formulae (or Reynolds transport theorem) will be used to integrate the equations of motion given in (6.8). This formulae was derived in chapter 2 (equation 2.32). A more suitable form for the application in this chapter is:

$$\frac{d}{dz} \int_0^{a(z)} s(r, z) dr = \int_0^{a(z)} \frac{\partial s(r, z)}{\partial z} dr + s(a, z) \frac{\partial a}{\partial z} \Big|_a \quad (6.13)$$

See also figure 6.2.

Application to the second term of the continuity equation in (6.8) integrated over the radius:

$$2\pi \left[ \int_0^{a(z)} \frac{1}{r} \frac{\partial}{\partial r} (rv_r) r dr + \int_0^{a(z)} \frac{\partial v_z}{\partial z} r dr \right] = 0 \quad (6.14)$$

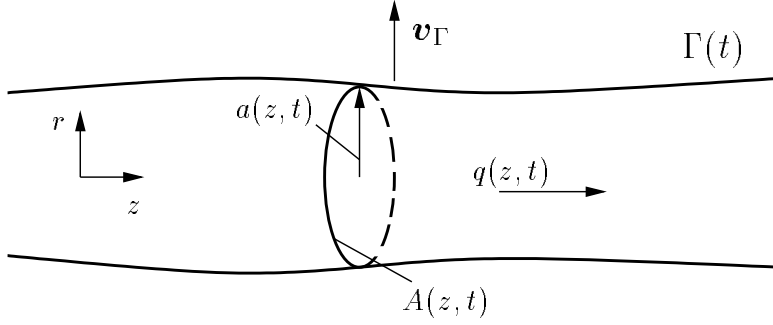


Figure 6.2: Flow  $q(z, t)$  in a distensible tube with moving wall  $\Gamma(t)$  and cross-sectional area  $A(z, t)$ .

yields:

$$2\pi \int_0^{a(z)} \frac{\partial r v_r}{\partial r} dr + 2\pi \frac{\partial}{\partial z} \int_0^{a(z)} v_z r dr - 2\pi v_z r \frac{\partial a}{\partial z} \Big|_a = 0 \quad (6.15)$$

or:

$$2\pi r v_r \Big|_0^a + \frac{\partial q}{\partial z} - 2\pi v_z(a, t) a \frac{\partial a}{\partial z} \Big|_a = 0 \quad (6.16)$$

and thus:

$$2\pi a \left( v_r(a, t) - v_z(a, t) \frac{\partial a}{\partial z} \Big|_a \right) + \frac{\partial q}{\partial z} = 0 \quad (6.17)$$

with  $q = q(z, t)$  the flow through the cross-section. Rewriting the first term in terms of the cross-sectional area  $A(z, t) = \pi a^2(z, t)$ , finally the integrated continuity equation reads:

$$\frac{\partial A}{\partial t} + \frac{\partial q}{\partial z} = 0 \quad (6.18)$$

This equation is formally derived but will be clear immediately from figure 6.2 if we write  $[A(z, t + dt) - A(z, t)]dz + [q(z + dz, t) - q(z, t)]dt = 0$ .

In a similar way the momentum equation in axial direction can be integrated:

$$2\pi \int_0^{a(z,t)} \frac{\partial v_z}{\partial t} r dr = -2\pi \int_0^{a(z,t)} \frac{1}{\rho} \frac{\partial p}{\partial z} r dr + 2\pi \nu \int_0^{a(z,t)} \frac{\partial}{\partial r} \left( r \frac{\partial v_z}{\partial r} \right) dr \quad (6.19)$$

Application of the Leibnitz formulae to the first term yields:

$$2\pi \frac{\partial}{\partial t} \int_0^{a(z,t)} v_z r dr - 2\pi v_z v_r r \Big|_0^a = -\frac{A}{\rho} \frac{\partial p}{\partial z} + 2\pi \nu r \frac{\partial v_z}{\partial r} \Big|_0^a \quad (6.20)$$

The second term in the left hand side of this equation vanishes if a longitudinal restraint of the wall motion ( $v_z(a) = 0$ ) is assumed. The second term in the right

hand side can be written in terms of the wall shear stress defined in equation (4.48). The integrated momentum equation then reads:

$$\rho \frac{\partial q}{\partial t} + A \frac{\partial p}{\partial z} = -\frac{2A\tau}{a} \quad (6.21)$$

Together with the expression for the wall shear stress given in (4.58) and linearisation of the  $A \frac{\partial p}{\partial z}$  term we finally obtain:

$$\rho \frac{\partial q}{\partial t} + A_0 \frac{\partial p}{\partial z} = -f_0 q \quad (6.22)$$

with  $f_0$  a friction function defined as:

$$f_0(\omega) = i\omega\rho \frac{F_{10}(\omega)}{1 - F_{10}(\omega)} \quad (6.23)$$

The linearized one-dimensional equations that describe the pressure and flow in distensible tubes under the assumption that  $V/c \ll 1$ ,  $(2\pi a/\lambda)^2 \ll 1$  and under the assumption that the wall motion is longitudinally constrained thus are given by:

$$\begin{cases} C_0 \frac{\partial p}{\partial t} + \frac{\partial q}{\partial z} = 0 \\ \rho \frac{\partial q}{\partial t} + A_0 \frac{\partial p}{\partial z} = -f_0 q \end{cases} \quad (6.24)$$

with  $C_0$  the linearized compliance given by:

$$C_0 = \left( \frac{\partial A}{\partial p} \right)_{p=p_0} \quad (6.25)$$

Alternatively using the mean velocity  $\bar{v}$  instead of the flow  $q = A\bar{v}$ :

$$\begin{cases} D_0 \frac{\partial p}{\partial t} + \frac{\partial \bar{v}}{\partial z} = 0 \\ \rho \frac{\partial \bar{v}}{\partial t} + \frac{\partial p}{\partial z} = -f_0 \bar{v} \end{cases} \quad (6.26)$$

with  $D_0$  a linearized distensibility given by:

$$D_0 = \frac{1}{A_0} \left( \frac{\partial A}{\partial p} \right)_{p=p_0} \quad (6.27)$$

In the next section we will derive the wave number  $k$  for inviscid, viscosity dominated and general flow (i.e. large, small and intermediate values of the Womersley parameter  $\alpha$ ).

### 6.4.2 Wave speed and attenuation constant

The linearized one-dimensional mass and momentum equations for unsteady viscous flow through a distensible tube has been derived by integrating the continuity and momentum equations over a cross-section of the tube assuming the wave-length to be large compared to the diameter of the tube and the phase velocity of the wave to be large compared to the mean fluid velocity. Moreover it is assumed that the motion of the tube wall is restrained longitudinally. Due to the linearity assumed, the resulting equations (6.18) and (6.22) can be solved in the frequency domain by substituting harmonic solutions

$$p(\omega, z, t) = \hat{p}(\omega, 0)e^{i(\omega t - kz)} \quad (6.28)$$

$$q(\omega, z, t) = \hat{q}(\omega, 0)e^{i(\omega t - kz)} \quad (6.29)$$

$$A(\omega, z, t) = \hat{A}(\omega, 0)e^{i(\omega t - kz)} \quad (6.30)$$

where  $\hat{p}(\omega, 0)$ ,  $\hat{q}(\omega, 0)$  and  $\hat{A}(\omega, 0)$  are the complex amplitudes representing both the amplitude and the phase of the waves measured at location  $z = 0$ ,  $\omega$  is the angular frequency and  $k(\omega)$  is the wave number ; a complex number defined by:

$$k(\omega) = \frac{\omega}{c} - i\frac{\gamma(\omega)}{\lambda} \quad (6.31)$$

Here  $c$  denotes the phase velocity of the waves and the wave length is given by  $\lambda = 2\pi c/\omega$ . The exponential decrease of the amplitude of the waves is described by the attenuation constant  $\gamma(\omega) = -2\pi k_i/k_r$ .

Viscoelastic wall behavior is described by an experimentally determined constitutive relationship between the cross-sectional area  $\hat{A}$  and the complex amplitude  $\hat{p}$ :

$$\hat{A} = C(\omega)\hat{p} \quad (6.32)$$

where  $C(\omega)$  is the dynamic compliance. For thin walled visco-elastic tubes this relationship can also be derived from equations (5.26) using a complex Young's modulus  $E = E_r + iE_i$ .

#### Large Womersley number flow

For large Womersley parameters the flow will be inviscid and the friction function  $f_0$  can be neglected. Substitution of (6.28-6.30) in (6.24) yields:

$$\begin{cases} i\omega C(\omega)\hat{p} - ik(\omega)\hat{q} = 0 \\ -ik(\omega)A_0\hat{p} + i\omega\rho\hat{q} = 0 \end{cases} \quad (6.33)$$

with solution:

$$k_0(\omega) = \pm\sqrt{\frac{\omega^2\rho C(\omega)}{A_0}} = \pm\frac{\omega}{c_0} \quad (6.34)$$

where the positive (negative) sign holds for waves traveling in the positive (negative)  $z$ -direction and  $c_0$  denotes the Moens-Korteweg wave speed given by:

$$c_0(\omega) = \sqrt{\frac{A_0}{\rho C(\omega)}} = \sqrt{\frac{1}{\rho D_0(\omega)}}. \quad (6.35)$$

Note that the subscript  $_0$  is used in  $k_0$  and  $c_0$  in order to obey conventions in literature despite the fact that  $k_\infty$  and  $c_\infty$  would be more meaningful since  $\alpha \rightarrow \infty$ . For thin walled tubes the Moens-Korteweg wave speed can be derived from 5.26) and reads:

$$c_0 = \sqrt{\frac{1}{\rho} \frac{hE}{2a_0(1-\mu^2)}} \quad (6.36)$$

Note that the wave number  $k_0 = \omega/c_0$  is a real number expressing that the phase velocity  $c$  equals the Moens-Korteweg wave speed and that the attenuation constant  $\gamma$  equals zero:

$$\alpha \rightarrow \infty : \quad c(\omega) = c_0, \quad \gamma(\omega) = 0. \quad (6.37)$$

As there is no friction and the compliance is assumed to be real (no visco-elasticity), no attenuation ( $\gamma(\omega) = 0$ ) of the wave will occur. The corresponding wave equation can be derived from (6.24): after elimination of the flow and keeping in mind that the friction function is neglected we obtain the differential equation:

$$\frac{\partial^2 p}{\partial t^2} - \frac{1}{\rho D_0} \frac{\partial^2 p}{\partial z^2} = 0 \quad (6.38)$$

This is a wave equation with wave speed  $c_0 = \sqrt{1/\rho D_0}$ . So for large  $\alpha$  and real values for the distensibility  $D_0$  the pressure wave travels without damping in  $z$ -direction. Equation (6.33) can also be solved with respect to the ratio  $\hat{q}/\hat{p}$  between the flow and the pressure:

$$Y_0 = \frac{\hat{q}}{\hat{p}} = C(\omega) \frac{\omega}{k(\omega)} = \pm \frac{A_0}{\rho c_0} \quad (6.39)$$

This ratio is referred to as the admittance  $Y_0$  and is equal to the reciprocal value of the impedance:

$$Y \equiv \frac{1}{Z} \equiv \frac{\hat{q}}{\hat{p}} \quad (6.40)$$

As  $k(\omega)$  represents two waves (one wave traveling in positive  $z$ -direction ( $k > 0$ ) and one wave traveling in negative  $z$ -direction ( $k < 0$ )) there are two flow and pressure waves: forward traveling waves  $q_f = +Y p_f$  and backward traveling waves  $q_b = -Y p_b$ . The total pressure and flow is the sum of these waves  $p(z, t) = p_f(z, t) + p_b(z, t)$  resp.  $q(z, t) = q_f(z, t) + q_b(z, t)$ .

### Small Womersley number flow

For small Womersley parameters the flow will be dominated by viscous forces and the friction function  $f_0$  can be approximated by its Poiseuille value  $f_0 = 8\eta/a_0^2$  whereas the instationary inertia forces in the momentum equation can be neglected. Substitution of (6.28-6.30) in (6.24) yields:

$$\begin{cases} i\omega C(\omega)\hat{p} - ik(\omega)\hat{q} = 0 \\ -ik(\omega)A_0\hat{p} + \frac{8\eta}{a_0^2}\hat{q} = 0 \end{cases} \quad (6.41)$$

and has a non-trivial solution if:

$$k(\omega) = \pm \sqrt{\frac{-8i\eta\omega C(\omega)}{A_0 a_0^2}} = \pm \frac{\omega}{c_0} \sqrt{\frac{-8i}{\alpha^2}} = \pm \frac{2(1-i)}{\alpha} k_0 \quad (6.42)$$

where the positive (negative) sign now holds for waves traveling in the positive (negative)  $z$ -direction and  $c_0$  denotes the Moens-Korteweg wave speed.

Now the wave number is a complex number and the phase velocity  $c$  and attenuation constant  $\gamma$  are given by:

$$\alpha \rightarrow 0: \quad c(\omega) = \frac{1}{2}\alpha c_0, \quad \gamma(\omega) = 2\pi. \quad (6.43)$$

As the real and imaginary part of the wave number are equal, the wave is damped critically. This can also be seen from (6.24): after elimination of the flow and keeping in mind that the instationary inertia forces can be neglected we obtain the differential equation:

$$\frac{\partial p}{\partial t} = \frac{A_0 a_0^2}{8\eta C_0} \frac{\partial^2 p}{\partial z^2} = \frac{a_0^2}{8\eta D_0} \frac{\partial^2 p}{\partial z^2} \quad (6.44)$$

This is a diffusion equation with diffusion coefficient  $D = a_0^2/8\eta D_0$ . So for small  $\alpha$  the wave equation reduces to a diffusion equation showing critical damping of the pressure in  $z$ -direction. This phenomena is responsible for the large pressure drop that is found in the micro-circulation where the Womersley parameter is low as a result of the small diameters of the vessels.

The admittance  $Y$  now is a complex number given by:

$$Y = \pm \frac{A_0}{\rho c_0} \frac{i+1}{4} \alpha = \frac{i+1}{4} \alpha Y_0 \quad (6.45)$$

### Arbitrary Womersley number flow

Substitution of equations (6.28-6.30), (6.32) and (6.23) in equations (6.18) and (6.22) yields:

$$\begin{cases} i\omega C(\omega)\hat{p} - ik(\omega)\hat{q} = 0 \\ -ik(\omega)A_0\hat{p} + (i\omega\rho + f_0)\hat{q} = 0 \end{cases} \quad (6.46)$$

After putting the determinant of the resulting set to zero the following expression for the wave number  $k$  is found:

$$k(\omega) = \pm \frac{\omega}{c_0} \sqrt{\frac{1}{1 - F_{10}(\omega)}} = \pm k_0 \sqrt{\frac{1}{1 - F_{10}(\omega)}} \quad (6.47)$$

Note that the wave number is again complex due to the friction function  $f_0$  as defined in equation (6.23) or due to the visco-elasticity of the tube expressed in a complex value for the compliance  $C(\omega)$ . The phase velocity  $c = \omega/k_r$  and attenuation constant  $\gamma = -2\pi k_i/k_r = -\lambda k_i$  can be derived from (6.47) and are given in figure 6.3.

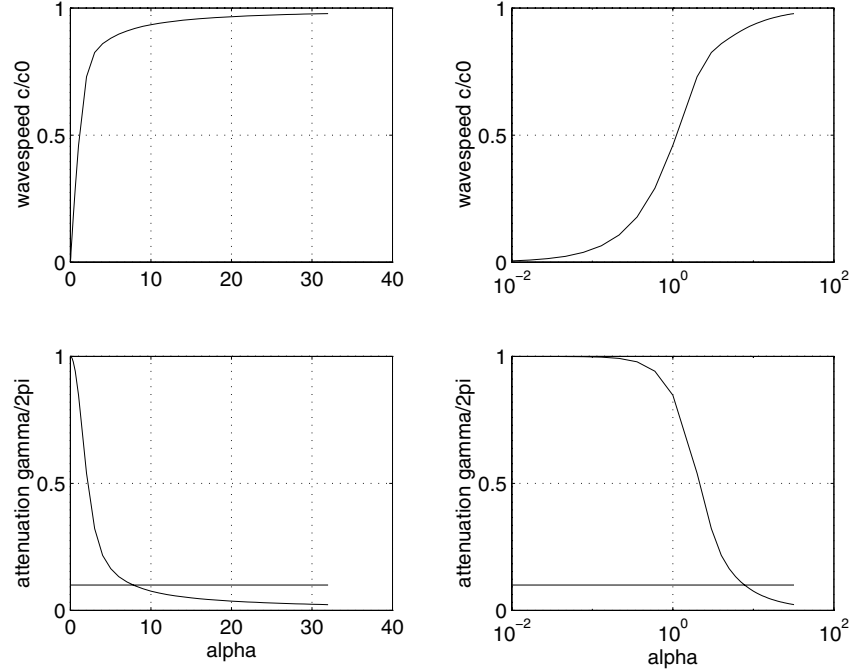


Figure 6.3: Phase velocity  $c/c_0$  and attenuation constant  $\gamma/2\pi$  as a function of  $\alpha$

It has been mentioned that viscoelastic tubes will yield a complex compliance. From experiments it is shown that the viscous part of the modulus is about 0.1 to 0.2 times the elastic part so  $E = E_r(1 + if_v)$  with the fraction  $f_v \approx 0.15$ . For large  $\alpha$  the visco-elasticity then will give a imaginary part in the wave number according to:

$$k = \frac{\omega}{c_0} \frac{1}{\sqrt{1 + if_v}} \approx k_0(1 - \frac{1}{2}if_v) \quad (6.48)$$

This line is indicated in figure 6.3 and shows that for larger  $\alpha$  (high frequencies and large arteries) the visco-elastic properties of the wall are the main cause for the attenuation of the pressure waves.

Finally the admittance can be derived as:

$$Y = \frac{k_0}{k} Y_0 \quad (6.49)$$

and is given in figure 6.4.

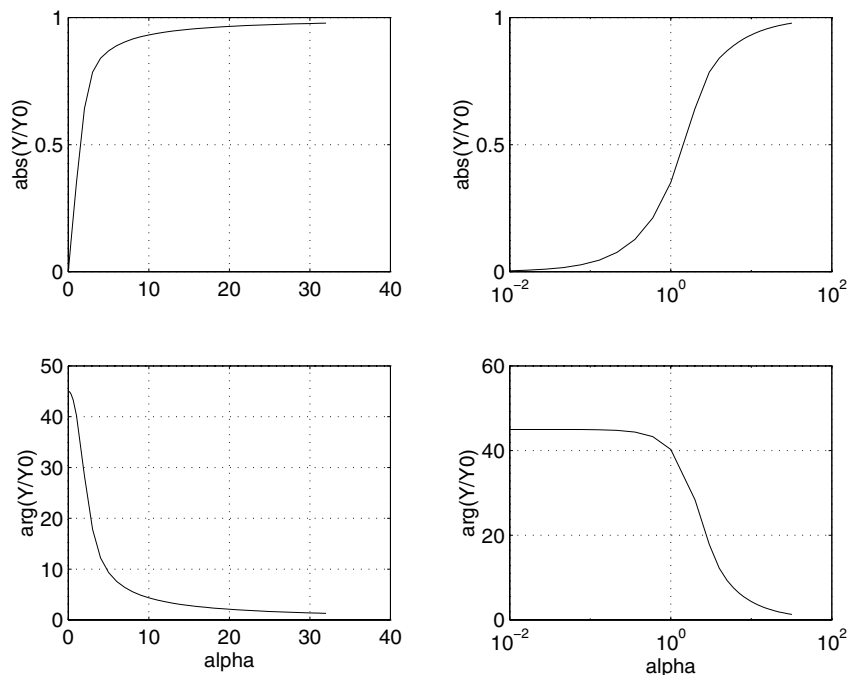


Figure 6.4: Absolute value and argument of  $Y/Y_0$  as a function of  $\alpha$ .

### Propagation of a pressure pulse in homogeneous tubes

As an example in figure 6.5 the propagation of pressure waves in an elastic (left) and a visco-elastic (right) tube are computed. For this computation the following characteristic data for the carotid artery are used:

$\eta$	$3.5 \cdot 10^{-3}$	$Pa \cdot s$	viscosity
$a_0$	$3 \cdot 10^{-3}$	$m$	radius
$h$	$a_0/10$	$m$	wall thickness
$\rho$	$10^3$	$kg \cdot m^{-3}$	density of fluid
$E$	$4.5 \cdot 10^5$	$N \cdot m^{-2}$	Young's modulus
$\mu$	0.5	-	Poisson's ratio

For the viscoelastic tube, the Young's modulus was taken to be  $E(1 + 0.2i)$ . Using equation (5.27) the distensibility and thus the compliance is determined. The wave number then was computed using equations (6.47) and (6.35). The incident pressure pulse is given as:

$$p(0, t) = e^{-\left(\frac{t-0.25}{0.1}\right)^2} \quad (6.50)$$

Clearly the damping of the wave due to viscous forces (i.e. wall shear stress) and viscoelastic properties of the wall can be distinguished.

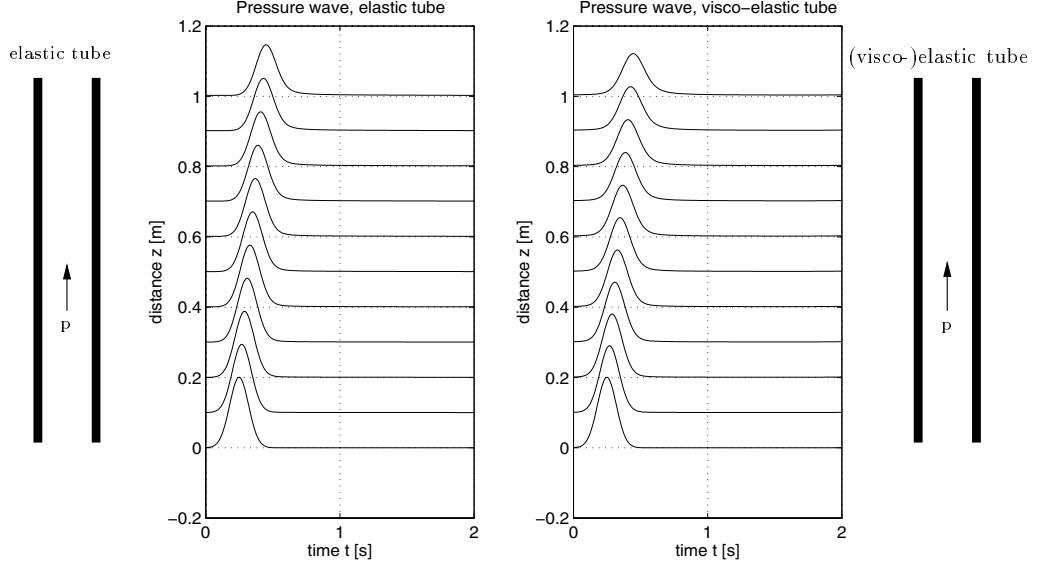


Figure 6.5: Propagation of pressure waves in an elastic tube (left) and a visco-elastic ( $E = E(1 + i * 0.2)$ ) tube (right).

## 6.5 Wave reflection

### 6.5.1 Wave reflection at discrete transitions

We will refer to transitions which are highly compact as discrete transitions. In these cases the length of the transition is so small compared to the wave length of the waves so that there is no difference in pressure or rate of flow between both ends of the transition, and the reflection phenomena can be described based on the equations of continuity of pressure and rate of flow across the transition. Figure 6.6 shows a discrete transition as might be formed by an increase or decrease in wall thickness at  $z = L$ . If the incident pressure and flow wave are represented by  $p_i$  and  $q_i$  respectively, the reflected waves by  $p_r$  and  $q_r$ , and the transmitted waves by  $p_t$  and  $q_t$ , continuity of pressure and rate of flow at a transition at location  $z = L$  can be expressed as:

$$p_i(\omega, L, t) + p_r(\omega, L, t) = p_t(\omega, L, t) \quad (6.51)$$

$$q_i(\omega, L, t) + q_r(\omega, L, t) = q_t(\omega, L, t) \quad (6.52)$$

The ratio between a single traveling pressure wave and its corresponding flow waves is dependent on the impedance  $Z$  or admittance  $Y$  of the tube. An expression for the impedance or admittance can be obtained by substituting equations (6.28-6.30) and (6.32) in equation (6.18):

$$Y(\omega) = \frac{1}{Z(\omega)} = \frac{\hat{q}(\omega, z)}{\hat{p}(\omega, z)} = \frac{\omega C(\omega)}{k(\omega)} \quad (6.53)$$

Note that normally the admittance is defined for waves traveling in positive  $z$ -direction i.e.  $k > 0$ . In that case the flow amplitude is given by  $\hat{q} = +Y\hat{p}$ . For  $k < 0$  the wave is traveling in negative  $z$ -direction and for an admittance defined for positive  $k$  we have a flow amplitude  $\hat{q} = -Y\hat{p}$ .

Substitution of equation (6.53) in equations (6.51) and (6.52) results in expressions for the reflection coefficient  $\Gamma_0$  and the transmission coefficient  $T_{01}$ :

$$\Gamma_0(\omega) = \frac{\hat{p}_r(\omega, L)}{\hat{p}_i(\omega, L)} = \frac{Y_0(\omega) - Y_1(\omega)}{Y_0(\omega) + Y_1(\omega)} \quad (6.54)$$

$$T_{01}(\omega) = \frac{\hat{p}_t(\omega, L)}{\hat{p}_i(\omega, L)} = \frac{2Y_0(\omega)}{Y_0(\omega) + Y_1(\omega)} \quad (6.55)$$

where  $Y_0$  is the admittance of the tube proximal to the transition, and  $Y_1$  the admittance of the tube distal to the transition. The propagation of an incident wave  $p_i = \hat{p}_i(\omega, 0)e^{i(\omega t - k_0 z)}$  in a tube with a discrete transition at  $z = L$  can be expressed as:

$$\left\{ \begin{array}{l} z < L : \\ p(\omega, z, t) = p_i(\omega, z, t) + p_r(\omega, z, t) \\ \qquad \qquad \qquad = \hat{p}_i(\omega, 0)e^{-ik_0(\omega)z} \left[ 1 + \Gamma_0(\omega)e^{-2ik_0(\omega)(L-z)} \right] e^{i\omega t} \\ z > L : \\ p(\omega, z, t) = p_t(\omega, z, t) \\ \qquad \qquad \qquad = \hat{p}_i(\omega, 0)e^{-ik_0(\omega)L} T_{01}(\omega)e^{-ik_1(\omega)(z-L)} e^{i\omega t} \end{array} \right. \quad (6.56)$$

As an example we consider the wave reflection of a transition formed by a sudden increase and a sudden decrease of the wall thickness ( $h(z < L) = a/10$  while  $h(z > L) = a/5$  and  $h(z > L) = a/20$  respectively). The resulting wave propagation for  $L = 0.5$  is given in fig 6.6.

From these figures it can be seen that a sudden decrease in wall thickness and thus a sudden increase of the distensibility or stiffness ( $Eh$ ) of the wall leads to a negative reflection of the incident wave and a transmitted wave with a decreased pressure amplitude and a decreased wave speed. For a sudden decrease of the stiffness the opposite phenomena occur.

In a similar way as in equation (6.56) expressions can be obtained for the reflection and transmission coefficient of a bifurcation of uniform tubes (see figure 6.7) at  $z = L$ , here referred to as a discrete bifurcation. In that case continuity of pressure and flow yields:

$$p_i(\omega, L, t) + p_r(\omega, L, t) = p_{t_1}(\omega, L, t) = p_{t_2}(\omega, L, t) \quad (6.57)$$

$$q_i(\omega, L, t) + q_r(\omega, L, t) = q_{t_1}(\omega, L, t) + q_{t_2}(\omega, L, t) \quad (6.58)$$

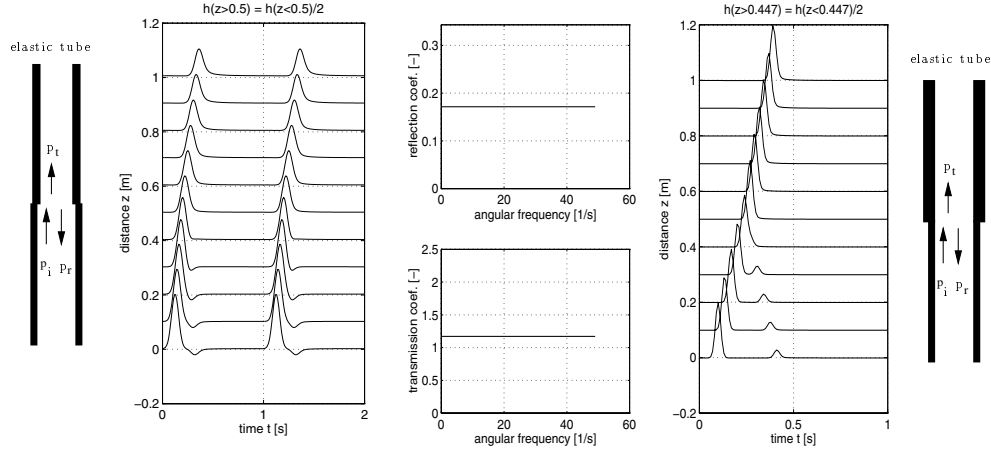


Figure 6.6: Wave reflection and propagation at discrete transitions formed by a sudden increase (left) and decrease (right) of the wall thickness.

resulting in:

$$\Gamma_0(\omega) = \frac{\hat{p}_r(\omega, L)}{\hat{p}_i(\omega, L)} = \frac{Y_0(\omega) - (Y_1(\omega) + Y_2(\omega))}{Y_0(\omega) + (Y_1(\omega) + Y_2(\omega))} \quad (6.59)$$

$$T_{01}(\omega) = \frac{\hat{p}_{t1}(\omega, L)}{\hat{p}_i(\omega, L)} = \frac{2Y_0(\omega)}{Y_0(\omega) + (Y_1(\omega) + Y_2(\omega))} \quad (6.60)$$

$$T_{02}(\omega) = \frac{\hat{p}_{t2}(\omega, L)}{\hat{p}_i(\omega, L)} = T_{01}(\omega) \quad (6.61)$$

Here  $p_{t1}$  and  $p_{t2}$  are the waves transmitted into the daughter tubes, and  $Y_1$  and  $Y_2$  are the impedances of these daughter tubes. Expressions for the pressure waves are similar to the ones given for the discrete transition in equations (6.56).

In figure 6.7 the wave reflection caused by a bifurcation of a tube with radius  $a_0$  into two tubes with respectively radius  $a_1$  and  $a_2$  is given for  $a_0 : a_1 : a_2 = 1 : 1 : 1$  (left) and  $a_0 : a_1 : a_2 = 3 : 2.1 : 1.8$  (right). One can observe a negative and a positive reflection of the incident wave due to the fact that  $a_0^2 < a_1^2 + a_2^2$  and  $a_0^2 > a_1^2 + a_2^2$  respectively and a wave speed which is slightly higher in the branch with the smallest radius.

Note that the transmission and reflection coefficients given in equations (6.54-6.55) and (6.60-6.61) are special cases of a general N-way junction with:

$$p_i(\omega, L, t) + p_r(\omega, L, t) = p_{t_j}(\omega, L, t) \quad (j = 1, \dots, N) \quad (6.62)$$

$$q_i(\omega, L, t) + q_r(\omega, L, t) = \sum_{j=1}^N q_{t_j}(\omega, L, t) \quad (6.63)$$

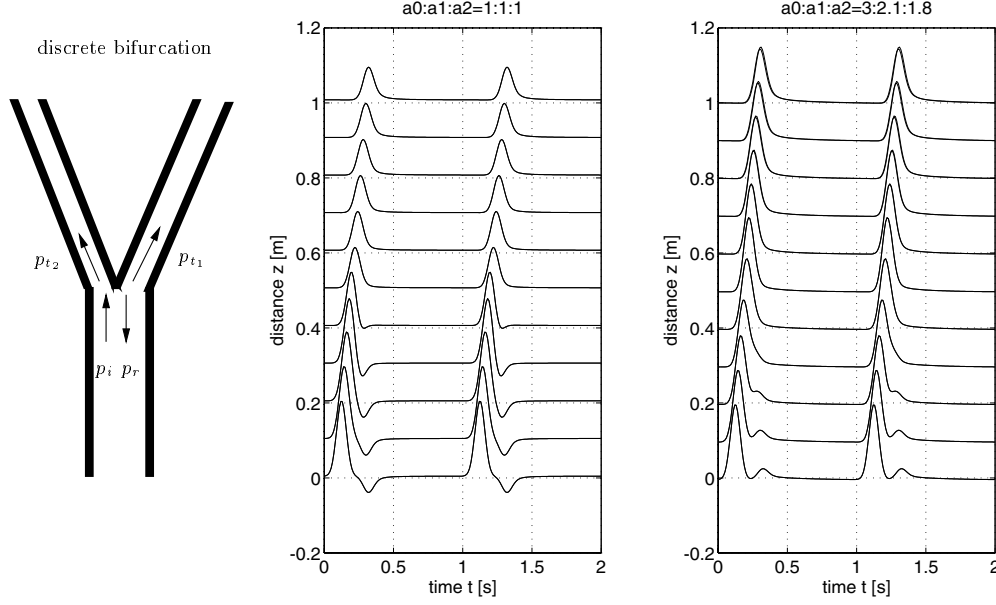


Figure 6.7: Wave reflection and propagation at a discrete bifurcation.

resulting in:

$$\Gamma_0(\omega) = \frac{\hat{p}_r(\omega, L)}{\hat{p}_i(\omega, L)} = \frac{Y_0(\omega) - \sum_{j=1}^N Y_j(\omega)}{Y_0(\omega) + \sum_{j=1}^N Y_j(\omega)} \quad (6.64)$$

$$T_{0j}(\omega) = \frac{\hat{p}_{t_j}(\omega, L)}{\hat{p}_i(\omega, L)} = \frac{2Y_0(\omega)}{Y_0(\omega) + \sum_{j=1}^N Y_j(\omega)} \quad (j = 1, \dots, N) \quad (6.65)$$

### 6.5.2 Multiple wave reflection: effective admittance

Consider two N-way junctions at a distance  $L_{mn}$  apart from each other as given in figure 6.8.

At junction  $n$  we have:

$$\Gamma_n = \frac{Y_{mn} - \sum_{j=1}^{N_n} Y_{nj}^e}{Y_{mn} + \sum_{j=1}^{N_n} Y_{nj}^e} \quad T_{nj} = \frac{2Y_{mn}}{Y_{mn} + \sum_{j=1}^{N_n} Y_{nj}^e} \quad (6.66)$$

where  $Y_{nj}^e$  is the effective admittance of section  $nj$  at location  $n$ . If there are no reflected waves in section  $nj$  then  $Y_{nj}^e = Y_{nj}$ .

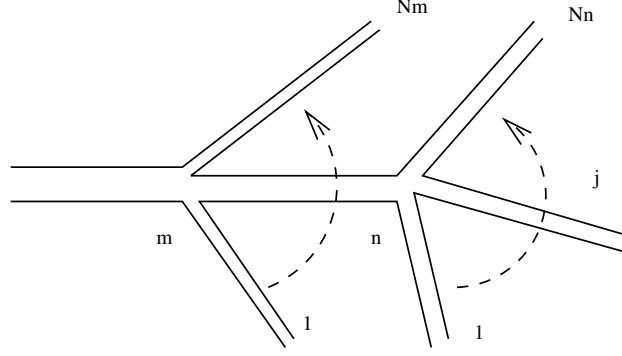


Figure 6.8: Multiple junctions.

At junction  $m$  we have:

$$\Gamma_m = \frac{Y_m - \sum_{n=1}^{N_m} Y_{mn}^e}{Y_m + \sum_{n=1}^{N_m} Y_{mn}^e} \quad T_{mn} = \frac{2Y_m}{Y_m + \sum_{j=1}^{N_m} Y_{mj}^e} \quad (6.67)$$

with:

$$Y_{mn}^e = \frac{\hat{q}(\omega, L_1)}{\hat{p}(\omega, L_1)} = Y_{mn} \frac{e^{ik_{mn}L_{mn}} - \Gamma_n e^{-ik_{mn}L_{mn}}}{e^{ik_{mn}L_{mn}} + \Gamma_n e^{-ik_{mn}L_{mn}}} \quad (6.68)$$

In this way it is possible to compute the pressure and flow in a complete transmission line network, starting from a distal impedance going back to the aorta. An example of such a computation is given in figure 6.9 where the input impedance at the aorta is given as a function of the frequency. A minimum of  $|Z|$  is found corresponding with a phase angle of zero. In (Milnor, 1989) this is attributed to a reflection from the aorta bifurcation.

The reflection mentioned above can be explained from the expression we obtain after substitution of (6.66) in (6.68) yields:

$$Y_{mn}^e = Y_{mn} \frac{\sum_{j=1}^{N_n} Y_{nj}^e + iY_{mn} \tan(k_{mn}L_{mn})}{Y_{mn} + i \sum_{j=1}^{N_n} Y_{nj}^e \tan(k_{mn}L_{mn})} \quad (6.69)$$

For  $k_{mn}L_{mn} = 0, \pm\pi, \pm2\pi, \dots$  we find  $Y_{mn}^e = \sum_{j=1}^{N_n} Y_{nj}^e$  and the section  $mn$  has no influence. These phenomena are illustrated in figure 6.10 showing the impedance  $Z_{mn}^e/Z_0$  in a tube with characteristic impedance  $Z_0 = Z_{mn}$  as a function of the frequency and distance from a termination with impedance  $Z_T^e = 4Z_0$ . Also the effect of attenuation is shown.

From expression (6.68) (or 6.69) we can see that for  $k_{mn}L_{mn} \ll 1$  we simply have  $e^{\pm ikL} = 1$  and after substitution of (6.66):

$$Y_{mn}^e = Y_{mn} \frac{1 - \Gamma_n}{1 + \Gamma_n} = \sum_{j=1}^{N_n} Y_{nj}^e \quad \text{if } k_{mn}L_{mn} \ll 1 \quad (6.70)$$

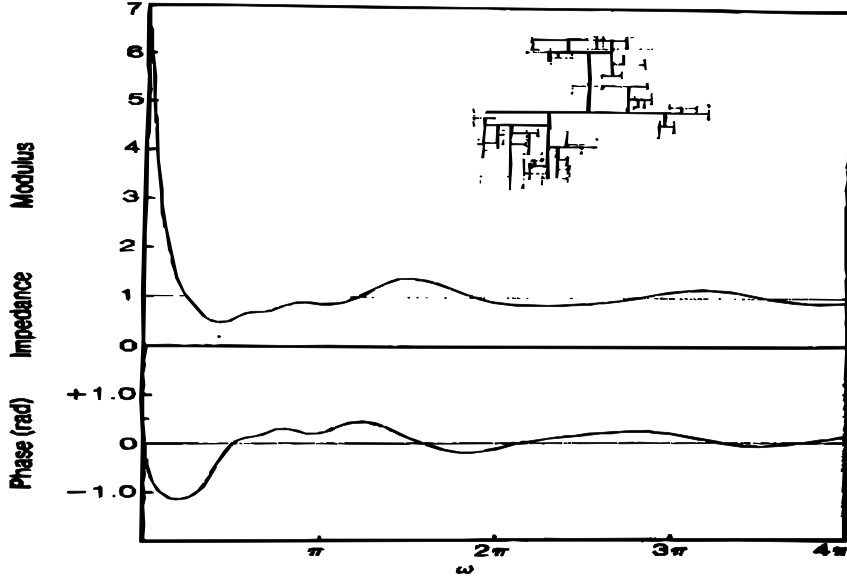


Figure 6.9: Input impedance at the aorta as a function of the frequency Milnor (1989).

as if the section  $mn$  did not exist. If, however,  $k_{mn}L_{mn}$  is small but still large enough that first order terms can not be neglected (i.e.  $k_{mn}^2L_{mn}^2 \ll 1$ ) we have:

$$Y_{mn}^e = Y_{mn} \frac{1 + ik_{mn}L_{mn} - \Gamma_n(1 - ik_{mn}L_{mn})}{1 + ik_{mn}L_{mn} + \Gamma_n(1 - ik_{mn}L_{mn})} \quad (6.71)$$

and after substitution of (6.66):

$$Y_{mn}^e = Y_{mn} \frac{ik_{mn}L_{mn}Y_{mn} + \sum_{j=1}^{N_n} Y_{nj}^e}{Y_{mn} + ik_{mn}L_{mn} \sum_{j=1}^{N_n} Y_{nj}^e} \quad \text{if } k_{mn}^2L_{mn}^2 \ll 1 \quad (6.72)$$

If we neglect terms of  $\mathcal{O}(k^2L^2)$  we obtain:

$$Y_{mn}^e = \sum_{j=1}^{N_n} Y_{nj} + ik_{mn}L_{mn}Y_{mn} \left[ 1 - \left( \frac{\sum_{j=1}^{N_n} Y_{nj}^e}{Y_{mn}} \right)^2 \right] \quad (6.73)$$

From this we can see that for intermediate long transitions only the phase of the admittance and not its absolute value is changed (see also Pedley, 1980).

So far, no attention was paid to reflections originating from peripheral vascular beds. However, these reflection phenomena might play an important role and can easily be taken into account. In the presence of reflected waves in the distal parts of a

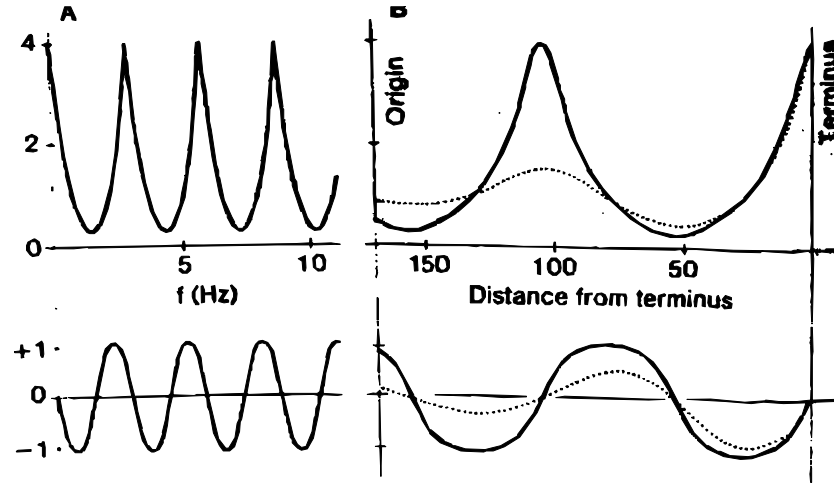


Figure 6.10: Effective impedance as a function of the frequency (left) and distance from termination (right) with (...) and without (-) attenuation Milnor (1989).

discrete transition, the reflection and transmission coefficient at an N-way junction read:

$$\Gamma_0(\omega) = \frac{Y_0 - \sum_{j=1}^N \frac{1-\Gamma_j^d}{1+\Gamma_j^d} Y_j}{Y_0 + \sum_{j=1}^N \frac{1-\Gamma_j^d}{1+\Gamma_j^d} Y_j} \quad (6.74)$$

$$T_{0j}(\omega) = \frac{2Y_0}{Y_0 + \sum_{j=1}^N \frac{1-\Gamma_j^d}{1+\Gamma_j^d} Y_j} \quad (j = 1, \dots, N) \quad (6.75)$$

This result can directly be derived from the results for distal sections without reflection by replacing the admittance by its effective admittance using the reflection coefficients  $\Gamma_j^d$  of the distal sections at the junction (see 6.70). So the reflection from the distal vascular system is represented by the reflection coefficients  $\Gamma_j^d$ . These have to be determined from experimental data or can be estimated by modeling the distal part as a transition to an appropriate output impedance.

### 6.5.3 Vascular impedance and cardiac work

The importance of wave phenomena in the vascular system and the corresponding vascular impedance is clearly illustrated if we want to investigate the mechanical work done by the left ventricle. For each cardiac cycle this work is the integral over time of the pressure flow product:

$$W = \int_{t_0}^{t_0+T} pqdt \quad (6.76)$$

This integral consists of two parts. The first part is the steady flow power  $W_s$  which is determined by the resistance  $R_0$  of the vascular system (mainly the peripheral

resistance) defined as the ratio between the mean pressure and the mean flow  $R_0 = p_0/q_0$ . The second part is the oscillatory flow power  $W_0$  following from (6.76) and the vascular impedance for each harmonic  $n$  ( $Z_n = |Z_n|exp(i\theta_n)$ ). So:

$$W = \frac{1}{2} \sum_{n=1}^N q_n^2 |Z_n| \cos \theta_n + q_0^2 R_0 \quad (6.77)$$

In Milnor (1989) the following values can be found:

	$q_0^2 R_0$	$\sum_n$
left ventricle	1400	200
right ventricle	155	73

For the systemic circulation the contribution of the higher harmonics to the total work is relatively low. This is due to the fact that  $\cos \theta_n \ll 1$ . As the value of  $Z_n$  directly influences the work that has to be done by the heart, knowledge of the influence of age, medicine and other factors on the value of  $Z_n$  is of great clinical importance.

## 6.6 Summary

In this chapter, linearized wave equations that govern the pressure and flow traveling through the arterial system are derived. For large values of the Womersley parameter these equations yield the Moens-Korteweg wave speed. For small values of the Womersley parameter a diffusion equation can be derived expressing perfusion flow in small arteries. For intermediate (arbitrary) values of the Womersley parameter wave speed and admittance can be expressed in terms of those derived for the Moens-Korteweg waves. Reflection of waves at discrete transitions are derived from continuity of pressure and rate of flow and allow determination of multiple wave reflection and the definition of effective admittance in order to determine vascular impedance and cardiac work.

## Chapter 7

# Non-Newtonian flow in blood vessels

### 7.1 Introduction

After a brief introduction to methods to measure fluid properties, in this chapter sequentially constitutive equations for Newtonian flow, generalized Newtonian flow, viscoelastic flow and the flow of suspensions will be dealt with. It will be shown that the viscosity of blood is shear and history dependent as a result of the presence of deformation and aggregation of the red blood cells that are suspended in plasma. The consequence of this non-Newtonian behavior on the velocity profiles in steady and pulsatile flow will be illustrated.

## 7.2 Mechanical properties of blood

Blood is a complex fluid consisting of blood cells suspended in plasma. The rheological behavior strongly depends in the properties of the suspended particles. In this section some of the main aspects of blood rheology are given starting from a short description of the morphology.

### 7.2.1 Morphology

**Plasma** is the continuous liquid medium in which the blood cells are suspended. It is an aqueous saline solution with proteins. The outline of the composition of the plasma is given in table 7.1. The density of plasma is  $1.03 \cdot 10^3 \text{ kg/m}^3$ . If denaturation of the proteins is avoided, plasma behaves like a Newtonian fluid with a dynamic viscosity of  $\eta = 1.2 \cdot 10^{-3} \text{ Pa} \cdot \text{s}$ .

The inorganic constituents of the plasma are a governing factor in various transport processes and generate an osmotic pressure of about  $8 \cdot 10^5 \text{ Pa}$  (equivalent to a 0.9% sodium chlorine solution by weight). The proteins have various functions and can be divided into three groups:

**fibrinogen** : a large, asymmetric molecule which is intimately concerned with the coagulation of blood. Although the concentration of fibrinogen is low, due to its asymmetry, it attributes significantly to the elevated viscosity of plasma.

**albumin** : a small molecule which is important for the osmotic pressure of the proteins.

**globulins** : a relatively symmetric molecule which is involved in transport of lipids and antibody reactions.

Apart from the buffering function of all the proteins, both fibrinogen and the globulins are involved in the aggregation of the erythrocytes.

An outline of the composition of suspended **blood cells** is given in table 7.2.

The red blood cells, or erythrocytes, occupy 45 % of the blood volume and dominate the rheological behavior of blood.

**erythrocytes** : form the dominant particulate matter of blood. The volume concentration of the erythrocytes, called haematocrite, is about 45 %. The density of the erythrocytes is  $1.08 \cdot 10^3 \text{ kg/m}^3$ . The erythrocyte is a biconcave discoid and the main dimensions are given in figure 7.2.1. The membrane of the erythrocytes has a thickness of 80 nm and consists of a phospholipid bilayer. This bilayer is covered with albumin at the outside and with another layer of protein, spectrin, at the inside. The spectrin layer is a skeletal protein and supports the lipid bilayer. The liquid interior of the erythrocyte is a saturated solution of hemoglobin (32 % by weight), behaving like a Newtonian fluid with a dynamic viscosity of  $\eta = 6 \cdot 10^{-3} \text{ Pa} \cdot \text{s}$ . The hemoglobin ( $MW = 68.000$ ) is a protein complex, consisting of an  $Fe^{2+}$  complex, the haem group, surrounded by amino acid molecules. The haem group is essential for transport processes

material	concentration <i>g/100ml</i>	molecular weight $*10^{-3}$	molecular dimension <i>nm</i>
<b>water</b>	90-92		
<b>proteins</b>			
albumin	3.3-4.0	69	15x4
$\alpha_1$ -globulins	0.31-0.32	44-200	
$\alpha_2$ -globulins	0.48-0.52	150-300	
$\beta$ -globulins	0.78-0.81	90-1300	20-50
$\gamma$ -globulins	0.31-0.32	160-320	23x4
fibrinogen	0.34-0.43	400	50-60x3-8
<b>inorganic constituents</b>			
cations			
sodium	0.31-0.34		
potassium	0.016-0.021		
calcium	0.009-0.011		
magnesium	0.002-0.003		
anions			
chloride	0.36-0.39		
bicarbonate	0.20-0.24		
phosphate	0.003-0.004		

Table 7.1: Composition of plasma.

cells	number per $mm^3$	unstressed shape and dimension $\mu m$	volume % in blood %
erythrocytes	$4 - 6 * 10^6$	biconcave disc 8x1-3	45
leucocytes	$4 - 11 * 10^3$	roughly spherical 7-22	1
platelets	$2.5 - 5 * 10^5$	rounded or oval 2-4	

Table 7.2: blood cells

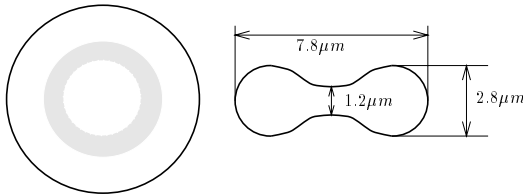


Figure 7.1: Size and dimension of the erythrocytes.

for it can bind oxygen and carbon dioxide and gives blood its red color. The origin of the biconcave shape of the erythrocytes is a source of dispute. For a review of possible explanations, one is referred to Fung (1993b). An important consequence of the biconcave shape is the ability of the erythrocytes to change shape without changing the surface area. This enables the erythrocyte to pass through capillaries with a diameter smaller than  $8 \mu m$ . Another phenomena, closely linked to the deformability of the erythrocyte, is the rotation of the membrane around the liquid interior in a shear flow (tank-threading movement, Schmid-Schönbein *et al.* (1971)). The erythrocytes aggregate face to face if they are brought in contact with each other at low shear rates (figure 7.2.2). These aggregates are known as rouleaux and are formed under the influence of bridging macromolecules, especially fibrinogen. At near zero shear rates, secondary aggregation of the rouleaux occurs, leading to formation of a rouleaux network.

**leucocytes** : are far less numerous than the erythrocytes (1 to 1000) and hereby they have only a marginal influence on the rheological properties of blood. The shape is spherical with a diameter of  $7 - 22 \mu m$ .

**platelets** : The volume concentration of the **platelets** is 0.3 % and there is one platelet for every 10 erythrocytes. The platelets are small oval bodies with a phospholipid membrane and an interior that resembles the interior of regular cells. This includes a cytoskeleton, giving the platelet a much higher rigidity than the erythrocyte. If the platelets are brought in contact with adenosine diphosphate (ADP) they aggregate and a thrombus can be formed. The process of thrombus formation is very complex and various agents are involved.

### 7.2.2 Rheological properties of blood

The composition of blood, as well as the properties of the constituents, lead to a complex macroscopic behavior of blood. The research on the flow behavior of blood can be divided into two classes: one involved with the viscometric flow of blood and another dealing with blood flow in tubes. The viscometric studies are mainly focused on obtaining constitutive equations for blood. Generally, these constitutive

equations can be used to relate stresses to deformation rates. In viscometry however, homogeneity the fluid and a constant shear rate is assumed and from several studies it can be concluded that this assumption does not hold for blood or concentrated suspensions in general. The studies of blood and blood analog fluids in tube flow show that the concentration distribution is inhomogeneous and that the velocity distribution is governed by the non-Newtonian properties of blood.

### Rheometry

The properties of fluids can be measured in a rheometer. In a rheometer, a well defined flow is generated and the forces, exerted by the fluid, are used to characterize its properties. The most commonly used flow is one in which the stress and shear is homogeneous. This simple shear can be generated by sliding one plate over another. The gap between the plates is filled with the fluid under investigation (see figure 7.2). In practice, a viscometer may consist of two rotating co-axial cylinders of which the radii  $R_i$  and  $R_o$  differ slightly such that  $h = R_o - R_i \ll R_i$  (Couette device). If the outer cylinder rotates, say with a steady angular velocity  $\Omega_c$  the forces of viscosity in the fluid will exert a moment  $M$  on the inner cylinder that can be measured. The velocity  $V = \Omega_c R_o$  locally can be considered to be unidirectional and is given by:

$$v_1 = \frac{\partial v_1}{\partial x_2} x_2 \equiv \dot{\gamma} x_2 \quad (7.1)$$

with  $\dot{\gamma} = V/h$  the shear rate. For this configuration the following expressions for the velocity gradient, rate of deformation and vorticity tensor can be found easily:

$$L = \begin{pmatrix} 0 & \dot{\gamma} & 0 \\ 0 & 0 & 0 \\ 0 & 0 & 0 \end{pmatrix} = D + \Omega \quad (7.2)$$

with

$$D = \frac{1}{2} \begin{pmatrix} 0 & \dot{\gamma} & 0 \\ \dot{\gamma} & 0 & 0 \\ 0 & 0 & 0 \end{pmatrix} \quad \text{and} \quad \Omega = \frac{1}{2} \begin{pmatrix} 0 & \dot{\gamma} & 0 \\ -\dot{\gamma} & 0 & 0 \\ 0 & 0 & 0 \end{pmatrix}, \quad (7.3)$$

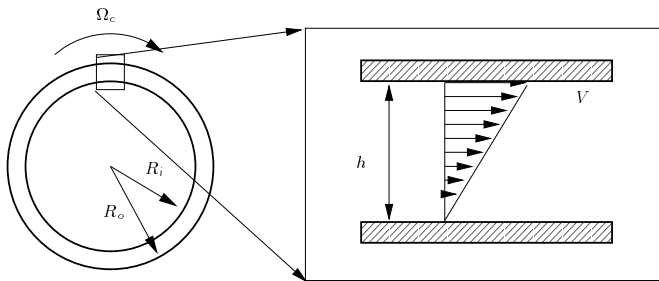


Figure 7.2: Simple shear flow as will be generated by a Couette device

### Viscosity measurements of blood

The deformability and the aggregation of the erythrocytes induce the complex behavior of blood in simple shear flow. At low shear rates, the erythrocytes tend to aggregate. These trains of rouleaux will increase the viscosity of the blood. Decreasing the shear rate even further, the rouleaux will form three dimensional structures, inducing an additional increase of the viscosity. If the shear rate is increased, the rouleaux break up and the erythrocytes align with the flow. Eventually, the shear rates will be high enough to deform the erythrocytes, thus decreasing the viscosity. The deformability and aggregation of the erythrocytes result in shear thinning behavior of blood in simple shear (figure 7.2.2). The deformability and the orientation of the rouleaux and the individual erythrocytes lead to the viscoelastic behavior of blood. They provide a mean of storing energy during flow. Thurston (1973) investigated the viscoelastic properties of blood in the linear viscoelastic regime and measured a significant elastic component in oscillatory blood flow.

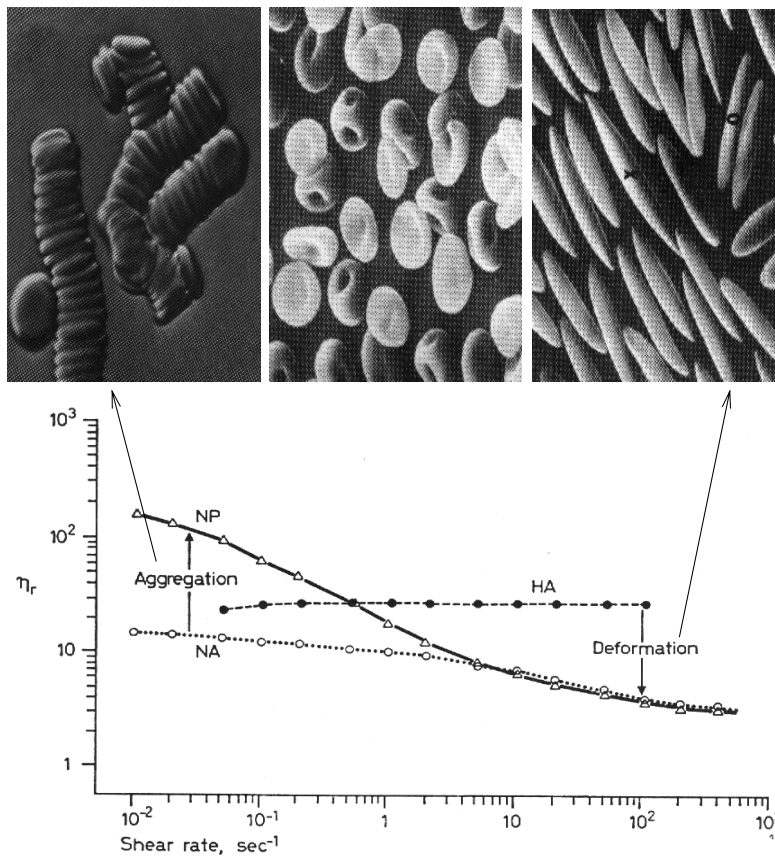


Figure 7.3: Aggregation (rouleaux), disaggregation and orientation of erythrocytes (top). Viscosity in steady shear of normal blood, blood with hardened erythrocytes (no deformation) and blood in a Ringer solution (no aggregation). From (Chien *et al.*, 1969).

## 7.3 Newtonian models

### 7.3.1 Constitutive equations

As indicated in the chapter 2, a constitutive equation for fluids may have the form

$$\boldsymbol{\sigma} = \boldsymbol{\sigma}(\dot{\mathbf{B}}) = \boldsymbol{\sigma}(2\mathbf{D}). \quad (7.4)$$

A general way to construct an arbitrary function  $\boldsymbol{\sigma}(2\mathbf{D})$  is to expand the function in a power series. This yields:

$$\boldsymbol{\sigma} = f_0\mathbf{D}^0 + f_1\mathbf{D}^1 + f_2\mathbf{D}^2 + f_3\mathbf{D}^3 + \dots \quad (7.5)$$

The Cayley Hamilton theorem (Chadwick, 1976) states that for (any symmetric) tensor  $\mathbf{D}$  it can be shown that:

$$\mathbf{D}^3 - I_D\mathbf{D}^2 + II_D\mathbf{D} - III_D\mathbf{I} = \mathbf{0} \quad (7.6)$$

Here  $I_D$ ,  $II_D$  and  $III_D$  are the invariants of  $\mathbf{D}$  defined as:

$$I_D = \text{tr}\mathbf{D} \quad (7.7)$$

$$= D_{11} + D_{22} + D_{33}$$

$$II_D = \frac{1}{2}(I_D^2 - \text{tr}\mathbf{D}^2) \quad (7.8)$$

$$= \begin{vmatrix} D_{11} & D_{12} \\ D_{21} & D_{22} \end{vmatrix} + \begin{vmatrix} D_{22} & D_{23} \\ D_{32} & D_{23} \end{vmatrix} + \begin{vmatrix} D_{33} & D_{31} \\ D_{13} & D_{11} \end{vmatrix}$$

$$III_D = \det\mathbf{D} \quad (7.9)$$

$$= \begin{vmatrix} D_{11} & D_{12} & D_{13} \\ D_{21} & D_{22} & D_{33} \\ D_{31} & D_{32} & D_{33} \end{vmatrix}$$

As a consequence any power series of  $\mathbf{D}$  can be written as:

$$\sum_k^K f_k\mathbf{D}^k = g_0\mathbf{D}^0 + g_1\mathbf{D}^1 + g_2\mathbf{D}^2 \quad (7.10)$$

With  $g_i$  scalar functions of the invariants of  $\mathbf{D}$ .<sup>1</sup>

Using this result in (7.5) yields

$$\boldsymbol{\sigma} = g_0\mathbf{D}^0 + g_1\mathbf{D}^1 + g_2\mathbf{D}^2 \quad (7.11)$$

If there is no deformation, for an incompressible fluid the Cauchy stress tensor must reduce to a hydrostatic pressure  $-p\mathbf{I}$ . As  $\mathbf{D}^0 = \mathbf{I}$ , it follows that  $g_0 = -p$ . For Newtonian fluids  $g_1$  is found to be a constant and  $g_2 = 0$ . If the dynamic viscosity is defined as  $\eta = g_1/2$ , the constitutive equation reads:

$$\boldsymbol{\sigma} = -p\mathbf{I} + 2\eta\mathbf{D} \quad (7.12)$$

---

<sup>1</sup>Note that for incompressible flows  $I_D = 0$ .

### 7.3.2 Viscometric results

If we substitute the expression for  $\mathbf{D}$  that was derived for simple shear (7.3) we obtain the following normal and shear stress for Newtonian fluid in a Couette flow device:

$$\sigma_{11} = \sigma_{22} = \sigma_{33} = -p \quad (7.13)$$

$$\tau = \sigma_{12} = \sigma_{21} = \eta\dot{\gamma} \quad (7.14)$$

There will be a linear relation between shear stress  $\tau$  and shear rate  $\dot{\gamma}$ . The viscosity is defined as the slope of the line. If the velocity  $V$  of the Couette device would vary in time but not that fast that inertia forces should be taken into account, then relation (7.14) indicates that for Newtonian fluids, the shear stress would follow instantaneously. This is in contradiction with viscoelastic fluids where a history dependent response would be found.

## 7.4 Generalized Newtonian models

### 7.4.1 Constitutive equations

One of the most striking properties of fluids that differ from Newtonian flow is the shear rate dependency of the viscosity. This shear rate dependency of the viscosity is generally found for polymeric liquids, emulsions and concentrated suspensions. In order to characterize such fluids a non-Newtonian scalar viscosity, dependent on the rate-of-strain tensor  $\dot{\gamma}$  can be introduced. The dependency on  $\dot{\gamma}$  must be such that the resulting constitutive equation does not depend on the coordinate system used. It has been shown that this is achieved if the three independent scalar invariants of  $\mathbf{D}$  are used (see equation 7.11).

Since  $tr(\mathbf{D}) = \nabla \cdot \mathbf{u}$ , for incompressible fluids  $I_D = 0$ . Further, experimental observations show that dependency on  $\mathbf{D}^2$  is rarely found (Macosko, 1994) so  $g_2$  in (7.11) is taken to be zero. Finally, data to fit these constitutive equations are obtained from simple shearing flows like in plane Couette flow. Therefore only for simple shear valuable forms for  $\eta$  can be found in literature. In that case from (7.3) it can be derived that  $det(\mathbf{D}) = 0$ . The generalized Newtonian constitutive equations then get the form:

$$\boldsymbol{\sigma} = -p\mathbf{I} + 2\eta(II_D)\mathbf{D} \quad (7.15)$$

From equation (7.9) it follows that for incompressible flows

$$II_D = -\frac{1}{2}(tr(\mathbf{D}^2)) = -|\dot{\gamma}|^2. \quad (7.16)$$

In other words, if we define the shear rate as the magnitude of the rate-of-strain tensor  $\dot{\gamma} = |\dot{\gamma}|$  the constitutive equations for incompressible generalized Newtonian fluids reduce to:

$$\boldsymbol{\sigma} = -p\mathbf{I} + 2\eta(\dot{\gamma})\mathbf{D} \quad (7.17)$$

The most important generalized Newtonian models are:

**Power-law model :**

In a power-law model the viscosity is assumed to depend on the shear rate according to:

$$\eta = \eta_0(\lambda\dot{\gamma})^{n-1} \quad (7.18)$$

with  $\eta_0$  the viscosity for  $\dot{\gamma} = 1/\lambda$ ,  $\lambda$  a time constant and  $n$  the power-law constant. If  $n > 1$  the fluid is called shear thickening and if  $n < 1$  the fluid is said to be shear thinning. Examples of shear thinning fluids are all kinds of polymer solutions and melts but also yogurt and blood. Shear thickening can be found in some concentrated suspensions of small particles. Note that the power-law model cannot describe the viscosity at very low and at very high shear rates as it goes to physically unrealistic values of 0 and  $\infty$  respectively.

**Carreau-Yasuda model :**

A more realistic model is given by:

$$\frac{\eta - \eta_\infty}{\eta_0 - \eta_\infty} = [1 + (\lambda\dot{\gamma})^a]^{(n-1)/a} \quad (7.19)$$

With  $\eta_0$  the viscosity at low shear rate,  $\eta_\infty$  the viscosity at high shear rate,  $\lambda$  a time constant and  $n$  the power-law constant. The parameter  $a$  determines the transition between the low-shear-rate region and the power-law region.

**Casson model :**

Bingham (1922) proposed a model in which a certain yield-stress  $\tau_0$  is needed in order to break networks of polymer chains (in polymer solutions and melts) or rouleaux (in blood) and induce any deformation at all. This can be expressed by the following equation:

$$\tau^{\frac{1}{m}} = \tau_0^{\frac{1}{m}} + (\eta_\infty \dot{\gamma})^{\frac{1}{m}} \quad (7.20)$$

For  $m = 1$  the model is called a Bingham model and for  $m = 2$  a Casson model. In terms of a shear dependent viscosity this can also be written as:

$$\eta = \eta_\infty \left[ 1 + \left( \frac{\tau_0}{\eta_\infty \dot{\gamma}} \right)^{\frac{1}{m}} \right]^m \quad (7.21)$$

Where  $\tau_0$  is some measure of  $\tau_0$  ( i.e.  $\tau_0 = |\tau_0|$  like  $\dot{\gamma} = |\dot{\gamma}|$ ). Originally, this model has been proposed for suspensions of spherical particles like paints but it has proven to be useful for blood flow as well.

**7.4.2 Viscometric results**

Equivalent to Newtonian fluids the following normal and shear stress for generalized Newtonian fluids is found in a Couette rheometer:

$$\sigma_{11} = \sigma_{22} = \sigma_{33} = -p \quad (7.22)$$

$$\tau = \sigma_{12} = \sigma_{21} = \eta(\dot{\gamma})\dot{\gamma} \quad (7.23)$$

As the stress must change sign if the viscometer rotates in the other direction,  $\tau$  must be an odd function of  $\dot{\gamma}$  and thus  $\eta(\dot{\gamma})$  must be an even function. This is clear from (7.16) where  $II_D = -|\dot{\gamma}|^2$ .

The viscosity may increase (shear thickening or dilatant) or decrease (shear thinning or pseudo-plast) with decreasing shear rate (see figure 7.4). As can be depicted from this figure several viscosity characteristics can be found and so the model that must be used to describe the shear rate dependency.

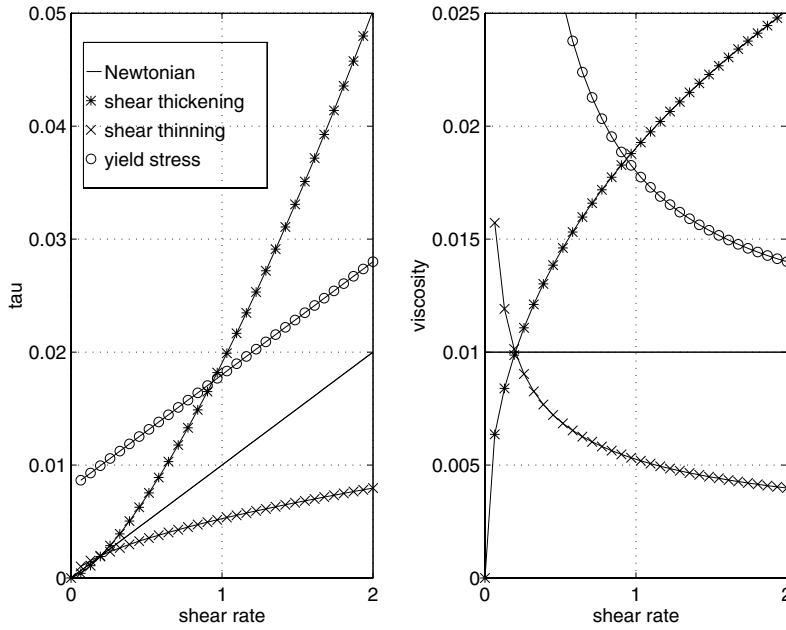


Figure 7.4: Relation between shear stress ( $\tau$ ) and shear rate  $\dot{\gamma}$  (left) and the viscosity ( $\eta$ ) as a function of the shear rate ( $\dot{\gamma}$ ) (right) for generalized Newtonian fluids.

The shear thinning effect will be illustrated on a tube flow with a small value of the Womersley parameter. Consider a fluid that obeys the power-law constitutive equation:

$$\eta = \eta_0(\lambda\dot{\gamma})^{n-1} \quad (7.24)$$

flowing through a rigid straight tube with its axis in  $z$ -direction. The momentum equation for fully developed flow then reads (see also (4.31)):

$$0 = -\frac{\partial p}{\partial z} + \frac{1}{r} \frac{\partial}{\partial r} (r\tau_{rz}) \quad (7.25)$$

Integration over the radius yields:

$$\tau_{rz} = \frac{1}{2} \frac{\partial p}{\partial z} r + \frac{C_1}{r} \quad (7.26)$$

The integration constant  $C_1$  must be zero to avoid that  $\tau_{rc}(0) \rightarrow \infty$ . On the other hand we know:

$$\tau_{rz} = \eta \frac{\partial v_z}{\partial r} = \eta_0 \left( \lambda \frac{\partial v_z}{\partial r} \right)^{n-1} \frac{\partial v_z}{\partial r} = \eta_0 \lambda^{n-1} \left( \frac{\partial v_z}{\partial r} \right)^n \quad (7.27)$$

Substitution in (7.26) yields

$$\frac{\partial v_z}{\partial r} = \left( \frac{\partial p}{\partial z} \frac{r}{\eta_0 \lambda^{n-1}} \right)^{1/n} \quad (7.28)$$

Again integration over  $r$  results in:

$$v_z(r) = \left( \frac{1}{\eta_0 \lambda^{n-1}} \frac{\partial p}{\partial z} \right)^{1/n} \frac{r^{1/n+1}}{1/n+1} + C_2 \quad (7.29)$$

The constant  $C_2$  follows from the boundary condition  $v_z(a) = 0$  and reads:

$$C_2 = - \left( \frac{1}{\eta_0 \lambda^{n-1}} \frac{\partial p}{\partial z} \right)^{1/n} \frac{a^{1/n+1}}{1/n+1} \quad (7.30)$$

The velocity profile for a power-law fluid in a straight tube thus reads:

$$v_z(r) = \left( \frac{\partial p}{\partial z} \frac{a}{\eta_0 \lambda^{n-1}} \right)^{1/n} \frac{a}{1/n+1} \left( 1 - \left( \frac{r}{a} \right)^{1/n+1} \right) \quad (7.31)$$

For shear thinning fluids this result in velocity profiles that are flattened compared to the profiles for Newtonian ( $n=1$ ) flow. In figure 7.5 the velocity profiles are given for different values of  $n$ .

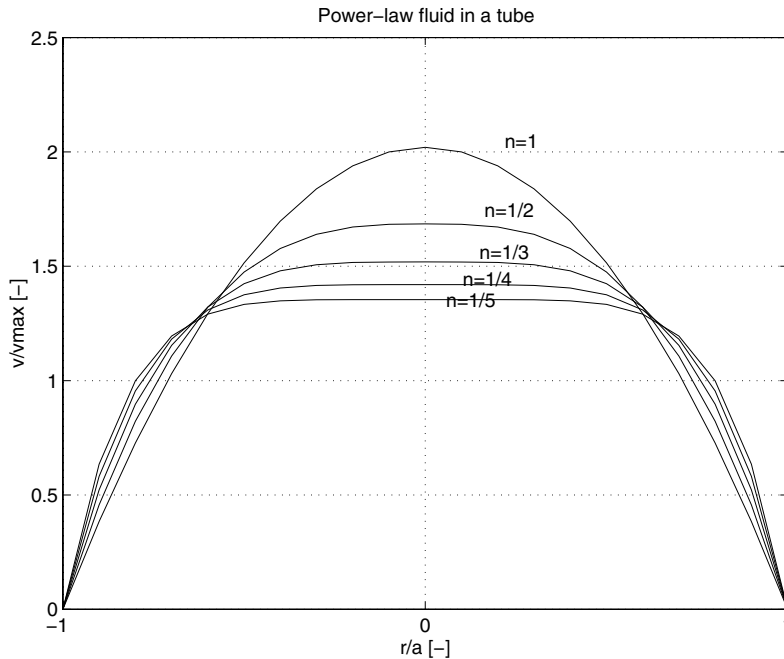


Figure 7.5: Velocity profile for several values of  $n$  of the power-law.

## 7.5 Viscoelastic models

### 7.5.1 Constitutive equations

If instationary inertia forces can be neglected, for (generalized) Newtonian fluids the momentary stress at a fixed location  $\boldsymbol{x}$ ,  $\tau(t)$  is determined by a momentary shear rate  $\dot{\gamma}(t)$  and is found to be  $\tau(t) = \eta(II_D)\dot{\gamma}(t)$ . Generalized Newtonian models can describe the shear rate dependency of viscosity quite well but can not describe time dependence in the response to deformation. This time dependency is illustrated clearly by the fact that some fluids return to their original form when the applied stress is released. These fluids do not only have viscous properties ( $\tau(t) = \tau(\dot{\gamma}(t))$ ) but show also elastic properties ( $\tau(t^0, t) = \tau(\gamma(t^0, t))$ ). This can be the result of the presence of long molecular chains or deformable particles which show an elastic relaxation after deformation. Note that the elastic response at a fixed location  $\boldsymbol{x}$  not only depends on the time but also on a reference time  $t^0$ . This, of course, originates from the fact that unlike the shear and strain rate, the shear and strain are defined with respect to a reference state. The relation between shear and shear rate can be expressed as:

$$\dot{\gamma}(t) = \frac{\partial \gamma(t^0, t)}{\partial t} \quad (7.32)$$

and

$$\gamma(t^0, t) = \int_{t^0}^t \dot{\gamma}(t'') dt'' \quad (7.33)$$

Constitutive equations for viscoelastic materials are often based on Boltzmann's superposition principle. Each increment in shear  $\delta\gamma_n$  at time  $t^n$  that is experienced by the material will induce a shear stress  $\tau_n$  which will be a function of time but will be independent of the shear stress that is induced by other increments in shear. So, like infinitesimal strains, also infinitesimal stresses are additive. The time dependence of the response to a shear rate increment at time  $t = t^n$  can be defined by a relaxation function  $G(t - t^n)$ . The relaxation function  $G(t - t^n)$  mostly is taken to be an exponential decay with time constant or characteristic relaxation time  $\lambda_0$  according to:

$$G(t - t^n) = G_0 e^{-\frac{1}{\lambda_0}(t - t^n)} \quad (7.34)$$

Following Boltzmann's superposition principle, the total shear stress at time  $t$  then is given by:

$$\tau(t) = \sum_n \delta\gamma_n G_0 e^{-\frac{1}{\lambda_0}(t - t^n)} \quad (7.35)$$

If we write

$$\delta\gamma_n(t) = \frac{\delta\gamma(t^n, t)}{\delta t} \delta t \approx \dot{\gamma}(t^n) \delta t \quad (7.36)$$

the following expression is found:

$$\tau(t) = \int_{-\infty}^t \dot{\gamma}(t') G_0 e^{-\frac{1}{\lambda_0}(t-t')} dt' \quad (7.37)$$

Partial integration yields:

$$\tau(t) = G_0 e^{-\frac{1}{\lambda_0}(t-t')} \gamma(t, t') \Big|_{-\infty}^t + \int_{-\infty}^t \frac{G_0}{\lambda_0} e^{-\frac{1}{\lambda_0}(t-t')} \gamma(t, t') dt' \quad (7.38)$$

Here the following definition has been used:

$$\gamma(t, t') = \int_{t'}^t \dot{\gamma}(t'') dt'' \quad (7.39)$$

Note that  $\gamma(t, t')$  expresses the shear that is experienced in the period of time between  $t'$  and  $t$  ( $t' < t'' < t$ ) and thus  $\gamma(t, t) = 0$ . As a consequence the first term in (7.38) vanishes. The shear stress then reduces to:

$$\tau(t) = \int_{-\infty}^t \frac{G_0}{\lambda_0} e^{-\frac{1}{\lambda_0}(t-t')} \gamma(t, t') dt' \quad (7.40)$$

A three-dimensional analog is known as the Lodge integral equation. It provides a general integral constitutive equation for viscoelastic fluids (see Macosko, 1994) and reads:

$$\boldsymbol{\sigma}(t) = \int_{-\infty}^t \frac{G_0}{\lambda_0} e^{-\frac{1}{\lambda_0}(t-t')} \mathbf{B}(t, t') dt' \quad (7.41)$$

In (7.40) the one-dimensional shear stress  $\tau(t)$  is replaced by the Cauchy stress  $\boldsymbol{\sigma}(t)$  and the shear  $\gamma(t, t')$  is replaced by the general measure  $\mathbf{B}(t, t')$ .

A corresponding differential form can be derived by differentiation of the Lodge integral equation (7.41). As the upper bound of the integral depends on  $t$  the Leibnitz formula is used:

$$\begin{aligned} \frac{d\boldsymbol{\sigma}(t)}{dt} &= \frac{G_0}{\lambda_0} e^{-\frac{1}{\lambda_0}(t-t')} \mathbf{B}(t, t') \Big|_{-\infty}^t + \\ &\int_{-\infty}^t \frac{G_0}{\lambda_0} e^{-\frac{1}{\lambda_0}(t-t')} \left( -\frac{1}{\lambda_0} \mathbf{B}(t, t') + \dot{\mathbf{B}}(t, t') \right) dt' \end{aligned} \quad (7.42)$$

The first term vanishes for  $t' = -\infty$  and yields  $(G_0/\lambda_0)\mathbf{B}(t, t) = (G_0/\lambda_0)\mathbf{I}$  for  $t' = t$ . The second part of the second term can be simplified with the aid of relation (2.25). So (7.42) reduces to:

$$\frac{d\boldsymbol{\sigma}}{dt} = \frac{G_0}{\lambda_0} \mathbf{I} - \frac{1}{\lambda_0} \boldsymbol{\sigma} + \mathbf{L} \cdot \boldsymbol{\sigma} + \boldsymbol{\sigma} \cdot \mathbf{L}^c \quad (7.43)$$

or:

$$\lambda_0 \left( \frac{d\boldsymbol{\sigma}}{dt} - \mathbf{L} \cdot \boldsymbol{\sigma} - \boldsymbol{\sigma} \cdot \mathbf{L}^c \right) + \boldsymbol{\sigma} = G_0 \mathbf{I} \quad (7.44)$$

Elimination of the hydrostatic part  $G_0 \mathbf{I}$  by substitution of  $\boldsymbol{\sigma} = \boldsymbol{\tau} + G_0 \mathbf{I}$  yields:

$$\lambda_0 (\dot{\boldsymbol{\tau}} - \mathbf{L} \cdot \boldsymbol{\tau} - \boldsymbol{\tau} \cdot \mathbf{L}^c - G_0 \mathbf{L} \cdot \mathbf{I} - G_0 \mathbf{I} \cdot \mathbf{L}^c) + \boldsymbol{\tau} = \mathbf{0} \quad (7.45)$$

and finally with

$$\mathbf{L} = (\nabla \mathbf{v})^c, \quad (7.46)$$

$$\mathbf{L} \cdot \mathbf{I} + \mathbf{I} \cdot \mathbf{L}^c = 2\mathbf{D}, \quad (7.47)$$

$$\eta_0 = G_0 \lambda_0 \quad \text{and} \quad (7.48)$$

$$\frac{d\boldsymbol{\tau}}{dt} = \frac{\partial \boldsymbol{\tau}}{\partial t} + \mathbf{v} \cdot \nabla \boldsymbol{\tau} \quad (7.49)$$

the differential form of the Lodge integral equation (7.41) is obtained and reads:

$$\lambda_0 \left\{ \frac{\partial \boldsymbol{\tau}}{\partial t} + \mathbf{v} \cdot \nabla \boldsymbol{\tau} - [(\nabla \mathbf{v})^c \cdot \boldsymbol{\tau} + \boldsymbol{\tau} \cdot (\nabla \mathbf{v})] \right\} + \boldsymbol{\tau} = 2\eta_0 \mathbf{D} \quad (7.50)$$

The term in between the brackets  $\{\}$  is called the upper convected time derivative of  $\boldsymbol{\tau}$ . The constitutive model is called the upper convected Maxwell (UCM) model and forms the basis of many other models that are proposed in literature.

After introduction of the non-dimensional variables:  $\mathbf{x}^* = \mathbf{x}/L$ ,  $\mathbf{v}^* = \mathbf{v}/V$ ,  $t^* = t/\theta$  and  $\boldsymbol{\tau}^* = \boldsymbol{\tau}L/\eta_0 V$  a dimensionless form of this equation is given by:

$$De \frac{\partial \boldsymbol{\tau}^*}{\partial t^*} + We [\mathbf{v}^* \cdot \nabla \boldsymbol{\tau}^* - (\nabla \mathbf{v}^*)^c \cdot \boldsymbol{\tau}^* - \boldsymbol{\tau}^* \cdot (\nabla \mathbf{v}^*)] + \boldsymbol{\tau}^* = \dot{\boldsymbol{\gamma}} \quad (7.51)$$

With the dimensionless numbers:

$$De = \frac{\lambda_0}{\theta} \quad \text{Deborah number} \quad (7.52)$$

$$We = \frac{\lambda_0 V}{L} \quad \text{Weissenberg number}$$

with  $De$  the Deborah number defined as the ratio of a characteristic relaxation time of the fluid  $\lambda_0$  to a characteristic time of the flow  $\theta$  and  $We$  the Weissenberg number defined as the ratio of a characteristic relaxation time of the fluid  $\lambda_0$  and a characteristic time measure of shear rate  $L/V$ .

If the Weissenberg number is small a linear viscoelastic (Maxwell) model is found according to:

$$De \frac{\partial \boldsymbol{\tau}^*}{\partial t^*} + \boldsymbol{\tau}^* = \dot{\boldsymbol{\gamma}} \quad (7.53)$$

or in dimensionfull form:

$$\lambda_0 \frac{\partial \tau}{\partial t} + \tau = \eta_0 \dot{\gamma} \quad (7.54)$$

with  $\eta_0$  the viscosity and  $\lambda_0$  a time constant (for deformation of red blood cells  $\lambda_0 = \mathcal{O}(0.1s)$ ). The presence of the time derivative term introduces an elastic contribution with elastic modulus  $\eta_0/\lambda_0$ . For large Deborah numbers this equation yields a constitutive equation for a simple Hookean solid with elastic modulus  $G = \eta_0/\lambda_0$ :

$$\tau = G\gamma \quad (7.55)$$

which only holds for small strains  $\gamma \ll 1$

Generalized upper convected Maxwell models use more then one relaxation time:

$$G(t - t^n) = \sum_{k=0}^K G_k e^{-\frac{t-t^k}{\lambda_k}} \quad (7.56)$$

Note that for viscoelastic solids at least one time constant  $\lambda_k = \infty$  must exist.

### 7.5.2 Viscometric results

The material behavior of viscoelastic fluids can be illustrated clearly by two experimental observations:

#### Response to a step input in the shear rate :

If we define the function  $S(t)$  as:

$$S(t) = \begin{cases} 0 & t < 0 \\ 1 & t \geq 0 \end{cases} \quad (7.57)$$

and a shear rate according to:

$$\dot{\gamma}(t) = \dot{\gamma}_0 S(t) \quad (7.58)$$

The corresponding stress then is found to be:

$$\tau(t) = \eta \dot{\gamma}_0 (1 - e^{-t/\lambda}) \quad \text{for } t > 0 \quad (7.59)$$

This indeed consists of two contributions:

**elastic** :  $\tau = (\eta/\lambda)\dot{\gamma}_0 t$  for  $t \ll \lambda$

**viscous** :  $\tau = \eta \dot{\gamma}_0$  for  $t \gg \lambda$

**Response to a sinusoidal oscillation in the shear rate :**

Consider a shear rate according to:

$$\dot{\gamma}(t) = \dot{\gamma}_0 e^{i\omega t} \quad (7.60)$$

The corresponding stress then is found to be:

$$\tau(t) = \tau_0 e^{-i\delta} e^{i\omega t} \quad (7.61)$$

We can define a complex viscosity:

$$\eta = \eta_v - i\eta_e = (\tau_0/\dot{\gamma}_0) e^{-i\delta} \quad (7.62)$$

with a viscous part  $\eta_v = (\tau_0/\dot{\gamma}_0) \cos(\delta)$  and an elastic part  $\eta_e = (\tau_0/\dot{\gamma}_0) \sin(\delta)$ . The phase shift  $\delta$  between the shear rate and shear stress is a measure for the importance of the elastic part of the response.

Both experimental observations are also illustrated in figure 7.6.

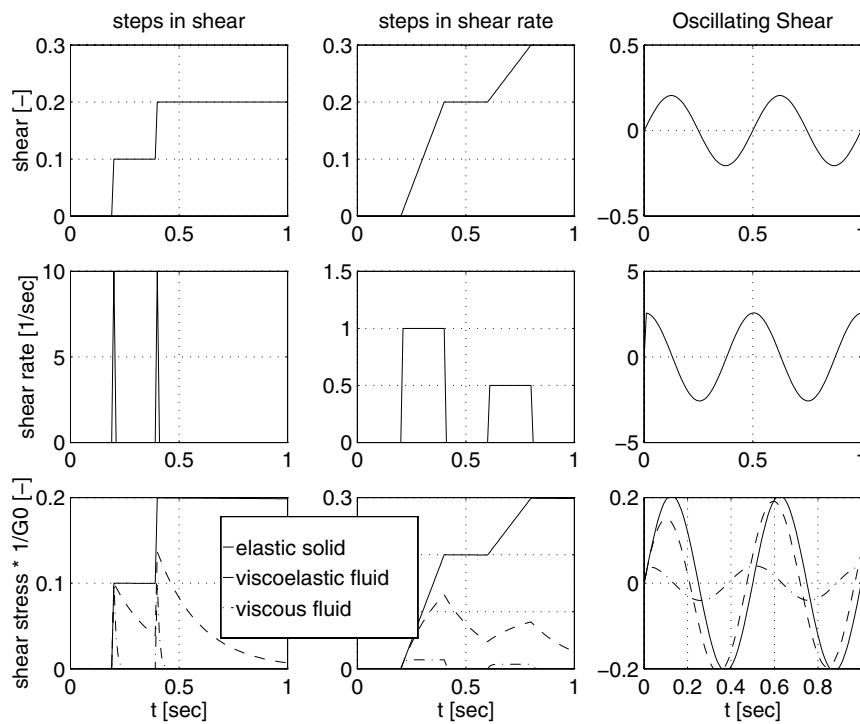


Figure 7.6: Response to steps in shear, steps in shear rate and sinusoidal shear rate

Fully developed viscoelastic flow in a tube is described by the momentum equation in z-direction:

$$\alpha^2 \frac{\partial v_z}{\partial t} = -\frac{\partial p}{\partial z} + \frac{1}{r} \frac{\partial}{\partial r} (r\tau_{rz}) \quad (7.63)$$

With the aid of:

$$\mathbf{v} = \begin{bmatrix} 0 \\ 0 \\ v_z \end{bmatrix} \quad \nabla \mathbf{v} = \begin{bmatrix} 0 & 0 & \dot{\gamma} \\ 0 & 0 & 0 \\ 0 & 0 & 0 \end{bmatrix} \quad (7.64)$$

with  $\dot{\gamma} = \frac{\partial v_z}{\partial r}$ . It can easily be verified that  $\mathbf{v} \cdot \nabla \boldsymbol{\tau} = \mathbf{0}$  and that the upper convected Maxwell model reduces to:

$$\begin{aligned} De \frac{\partial}{\partial t} \begin{bmatrix} \tau_{rr} & \tau_{r\phi} & \tau_{rz} \\ \tau_{\phi r} & \tau_{\phi\phi} & \tau_{\phi z} \\ \tau_{zr} & \tau_{z\phi} & \tau_{zz} \end{bmatrix} - We \begin{bmatrix} 0 & 0 & \tau_{rr}\dot{\gamma} \\ 0 & 0 & \tau_{\phi r}\dot{\gamma} \\ \tau_{rr}\dot{\gamma} & \tau_{r\phi}\dot{\gamma} & 2\tau_{zr}\dot{\gamma} \end{bmatrix} + \\ + \begin{bmatrix} \tau_{rr} & \tau_{r\phi} & \tau_{rz} \\ \tau_{\phi r} & \tau_{\phi\phi} & \tau_{\phi z} \\ \tau_{zr} & \tau_{z\phi} & \tau_{zz} \end{bmatrix} = \begin{bmatrix} 0 & 0 & \dot{\gamma} \\ 0 & 0 & 0 \\ \dot{\gamma} & 0 & 0 \end{bmatrix} \end{aligned} \quad (7.65)$$

Making use of symmetry of  $\boldsymbol{\tau}$  and assuming a stress free initial condition, this yields:

$$De \frac{\partial \tau_{rz}}{\partial t} + \tau_{rz} = \dot{\gamma} \quad (7.66)$$

and

$$De \frac{\partial \tau_{zz}}{\partial t} - 2We\dot{\gamma}\tau_{rz} + \tau_{zz} = 0 \quad (7.67)$$

We search for harmonic solutions:

$$v_z(r) = \hat{v}_z(r)e^{i\omega t}, \quad \frac{\partial p}{\partial z} = \frac{\partial \hat{p}}{\partial z}e^{i\omega t}, \quad \tau_{rz}(r) = \hat{\tau}_{rz}(r)e^{i\omega t} \quad (7.68)$$

Equation (7.66) in dimensionfull form then can be solved and yields the following relation between the shear stress and the shear rate:

$$\hat{\tau}_{rz} = \frac{\eta}{1 + i\omega\lambda} \dot{\gamma} \quad (7.69)$$

This shows that the solution of (7.63) for viscoelastic flow is exactly the same as the one for Newtonian flow except for the viscosity that in the viscoelastic case is a complex function according to:

$$\nu^* = \frac{\nu}{1 + i\omega\lambda} \quad (7.70)$$

The two dimensionless parameters thus are:

$$De = \omega\lambda \quad (7.71)$$

and

$$\alpha^* = a\sqrt{\frac{\omega(1 + iDe)}{\nu}} = (1 + iDe)^{1/2}\alpha \quad (7.72)$$

The solution of the velocity field will again be (see (4.45)):

$$\hat{v}_z(r) = \frac{i}{\rho\omega} \frac{\partial \hat{p}}{\partial z} \left[ 1 - \frac{J_0(i^{3/2}\alpha^*r/a)}{J_0(i^{3/2}\alpha^*)} \right] \quad (7.73)$$

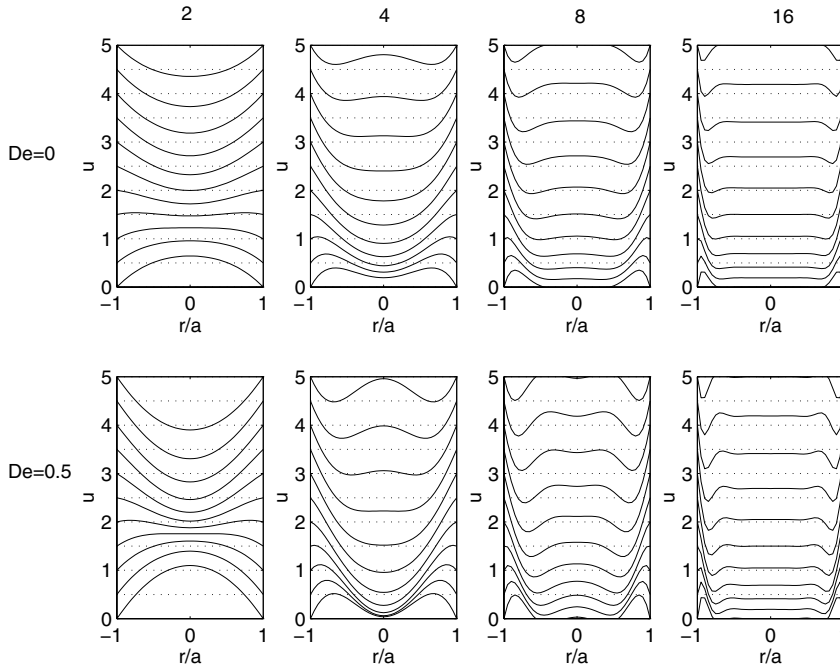


Figure 7.7: Velocity profiles for several values of  $De$  and  $\alpha$ .

but now with a complex value of  $\alpha$ . In figure 7.7 the velocity profiles are given for different values of  $De$  and  $\alpha$ .

Note that equation (7.67) shows that for viscoelastic fluids there will be a normal stress difference  $\tau_{rr} - \tau_{zz}$  that will be non-zero. This however does not influence the velocity profiles for fully developed flow.

## 7.6 Rheology of suspensions

### 7.6.1 Constitutive equations

A suspension can be considered as a homogeneous fluid if the dimension of the suspended particles is small with respect to the dimension of the flow channel. The viscosity of this homogeneous suspension will be a function of the concentration of suspended particles expressed in the volume fraction of particles  $\phi$ . If we bring particles in a Newtonian fluid with viscosity  $\eta_0$ , the effective viscosity  $\eta_s$  will increase. If we assume that the particles move with the fluid and do not deform, the shear rate in between the particles will be larger than the shear rate in a fluid without particles (see figure 7.8).

The way in which the viscous properties of the fluid change strongly depends on the concentration, shape and mechanical properties of the particles. A short overview of viscosity changes that are found for suspensions of particles in a Newtonian fluid will be given below:

#### **Rigid spheres - low concentration :**

A suspension of rigid spheres with a particle volume fraction  $\phi$  which is so low

that there is no interaction between the spheres will have a viscosity given by the Einstein relation:

$$\eta_s(\phi) = \eta_0(1 + 2.5\phi) \tag{7.74}$$

If the volume fraction  $\phi$  is larger than 0.01 the particles will interact and the viscosity will increase even more and the following modification appears to be useful for volume fractions up to  $\phi = 0.3$  (Batchelor, 1977):

$$\eta_s(\phi) = \eta_0(1 + 2.5\phi + 6.25\phi^2) \tag{7.75}$$

For volume fractions larger than 0.3 the suspension becomes non-Newtonian.

**Deformable spheres - low concentration :**

Also for suspensions of deformable spheres (f.i. droplets that keep their spherical shape due to surface tension) the viscosity will increase with the concentration. This increase, however, will be less than in a suspension with rigid spheres because the particles are able to deform due to the shear. The shear between the particles will be less. If  $\eta_d$  is the viscosity of the droplets that are suspended, the following relation has been derived by Taylor (Macosko, 1994):

$$\eta_s(\phi) = \eta_0 \left( 1 + \phi \left( \frac{1 + 2.5\eta_d/\eta_0}{1 + \eta_d/\eta_0} \right) \right) \tag{7.76}$$

Note that for rigid spheres ( $\eta_d \rightarrow \infty$ ) this relation reduces to the relation of Einstein. Due to elastic properties of the spheres, at large deformations the suspension may show viscoelastic properties.

**Rigid asymmetric particles - low concentration :**

The viscosity of suspensions of asymmetric rigid particles increases with increasing volume fraction and increasing asymmetry. The reason for this is that due to a competition of Brownian motion and shear stresses the particles will rotate and occupy all larger volume. For low concentrations the following relation is found:

$$\eta_s(\phi) = \eta_0(1 + K\phi) \tag{7.77}$$

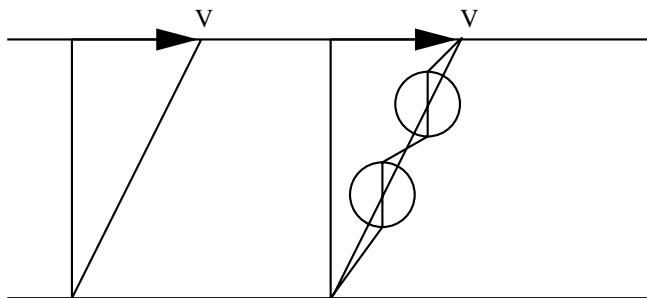


Figure 7.8: Simple shear in a homogeneous fluid and in a suspension

with  $K$  a number expressing the degree of asymmetry of the particles. If the shear rate increases it will be able to orient the particles and the viscosity decreases again. The suspension then will behave as a shear-thinning fluid. Quemada (1978) proposed the following model that combines the shear thinning properties with the volume fraction dependency:

$$\eta_s(\phi, \dot{\gamma}) = \eta_0 \left[ 1 - \frac{\phi}{2} \left( k_\infty + \frac{k_0 - k_\infty}{1 + (\dot{\gamma}/\dot{\gamma}_c)^q} \right) \right]^{-2} \quad (7.78)$$

with parameters  $\eta_0, k_0, k_\infty, \dot{\gamma}_c$  and  $q$ .

### Deformable asymmetric particles - low concentration :

Also deformable asymmetric particles will rotate in a shear flow but they will be able to change their shape in such a way that they will experience less friction. The viscosity, hereby, will be lower then for rigid asymmetric particles. Also here at large deformations the suspension may exhibit viscoelasticity.

### Rigid or deformable particles - high concentration :

At higher concentration the particles may form a more or less continuous structure like trees flowing in a river. Often a yield stress is needed to break this structure. For rigid particles this yield stress is determined by the volume fraction  $\phi$ .

As the rheological properties of suspensions of deformable and asymmetric particles, especially at high concentrations, are shear thinning and viscoelastic, they are mostly described by a viscoelastic model adopted from polymer liquids. If the particle concentration is relatively constant, i.e. the fluid is homogeneous, measurement of rheological properties as a function of the particle concentration can be used to fit these models.

If the particle size is not small compared to the flow channel (blood flow in the micro-circulation) particle migration and inhomogeneous viscosity must be taken into account. In the next chapter examples of such flows will be given.

## 7.6.2 Viscometric results

The influence of particles suspended in the fluid is summarized in figure 7.9

## 7.7 Rheology of whole blood

### 7.7.1 Experimental observations

#### Coagulation

Measurement of the rheological properties of blood are very difficult because of its coagulation properties. Almost all measurements are performed after addition of anticoagulants. Most important anticoagulants are heparin, sequestrine (EDTA) and acid-citrate-dextrose (ACD). It is assumed that these products do not alter the rheology of blood or at least have little effect.

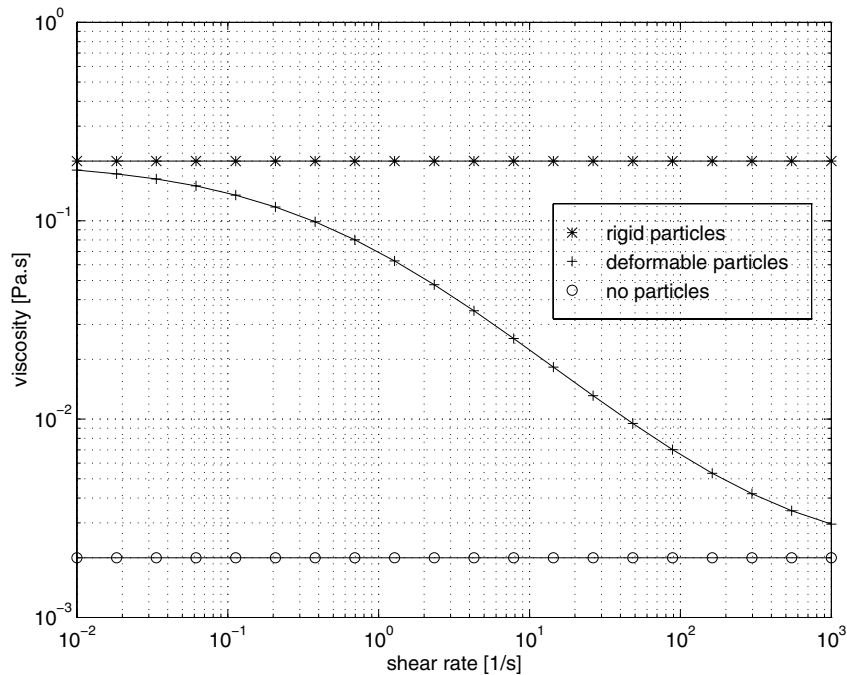


Figure 7.9: The influence of particles suspended in a Newtonian fluid

### Rheology of plasma

As mentioned in the first chapter of this course plasma behaves like a Newtonian fluid, with a dynamic viscosity of  $\eta = 1.2 \cdot 10^{-3} Pa \cdot s$ . To measure this value, contact with air resulting in denaturation of the proteins must be avoided.

### Hardened blood cells

Red blood cells can be hardened with aldehyde. A suspension of hardened cells in an albumin-Ringer solution, that does not show aggregation because of the absence of globulins and fibrinogen, shows a Newtonian behavior with a viscosity that varies with the hematocrit in a way as is found for rigid particles (see figure 7.10 broken line). For a hematocrit of 45% this solution has a viscosity of about  $\eta = 3 \cdot 10^{-2} Pa \cdot s$ .

### Deformable blood cells

If we allow the blood cells to deform but still suppress aggregation, the viscosity decreases with respect to the viscosity of hardened cells according to the dotted line in figure (7.10). As mentioned in the previous section the suspension now shows shear thinning due to deformation and orientation of the cells at higher shear rates.

### Aggregation of blood cells

If also aggregation of the blood cells is possible, at very low shear rates formation of rouleaux will significantly increase the viscosity and will even result in a yield

stress with an order of magnitude equal to  $1 - 5 \cdot 10^{-3} Pa$ . At higher shear rates the rouleaux will break down and a behavior as is found for the albumin-Ringer solution will be found.

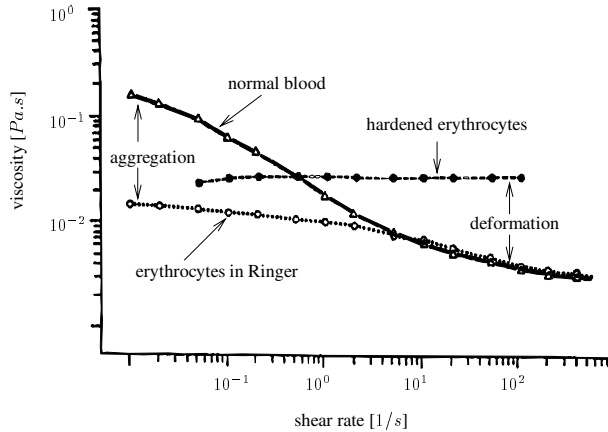
10<sup>3</sup>

Figure 7.10: Viscosity in steady shear of normal blood, blood with hardened erythrocytes (no deformation) and blood in a Ringer solution (no aggregation). From (Chien *et al.*, 1969).

### Viscoelastic properties of blood

The deformability and the orientation of the rouleaux and the individual erythrocytes lead to the viscoelastic behavior of blood. They provide a mean of storing energy during flow. Thurston (1973) investigated the viscoelastic properties of blood in the linear viscoelastic regime and measured a significant elastic component in oscillatory blood flow (figure 7.11).

McMillan *et al.* (1987) investigated the transient properties of blood in viscometric flow. They measured the shear stress generated by blood, subjected to a number of sequential steps in the shear rate. The overshoot in the shear stress was attributed to orientation of erythrocytes and aggregates. The delayed relaxation of the shear stress can be related to the viscoelastic properties of blood. The transient data can be used to compute time scales for the formation and break-up of rouleaux.

#### 7.7.2 Constitutive equations

The constitutive equation (7.50) is a relation between  $\tau$  and  $\dot{\gamma}$ . More complex relations can be obtained using more than one time constant and superposition of simple models. Also non-linear relations letting e.g.  $\dot{\gamma} = \dot{\gamma}(\tau \cdot \tau)$ ,  $\eta = \eta(\dot{\gamma})$  or

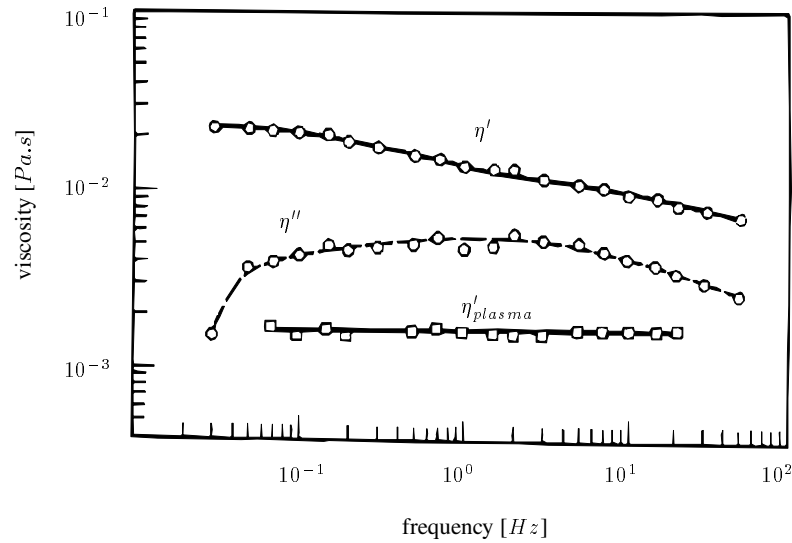


Figure 7.11: The elastic ( $\eta''$ ) and the viscous ( $\eta'$ ) component of the complex viscosity of blood as a function of frequency in oscillatory shear.

non-constant structure dependent time scales  $\lambda = \lambda(\dot{\gamma})$  are used (see e.g. Bird *et al.* (1987)). For blood Rosenblatt (1988) proposed the constitutive equation:

$$\lambda(P) \left\{ \frac{d\boldsymbol{\tau}}{dt} - [(\nabla \mathbf{v})^c \cdot \boldsymbol{\tau} + \boldsymbol{\tau} \cdot (\nabla \mathbf{v})] \right\} + \boldsymbol{\tau} = \eta_0(P) \dot{\boldsymbol{\gamma}} \quad (7.79)$$

with  $P$  a structure parameter defined as the fraction of red cells that are aggregated satisfying the structure kinetics:

$$\frac{\partial P}{\partial t} + \mathbf{v} \cdot \nabla P = k(1 - P) - \alpha \dot{\boldsymbol{\gamma}} P \quad (7.80)$$

Here  $k$  represents the formation of aggregates and  $\alpha \dot{\boldsymbol{\gamma}}$  represents a shear dependent loss of aggregates. A challenge for the future will be to evaluate this kind of models experimentally for complex flows and to incorporate them into numerical methods for time-dependent three-dimensional flow simulations.

## 7.8 Summary

In this chapter the basic equations that have been derived in the chapter 2 to construct constitutive relations of non-Newtonian and viscoelastic fluids have been used to describe the rheological properties that can be derived from rheometrical measurements. It has been shown that the shear-thinning behavior that is found for blood can be well described by a generalized Newtonian model where the shear stress is generally related to the rate of deformation tensor. Using the Cayley-Hamilton theorem it follows that for shear flow of incompressible fluids the general dependency of shear stress and the rate of deformation reduces to a simple shear

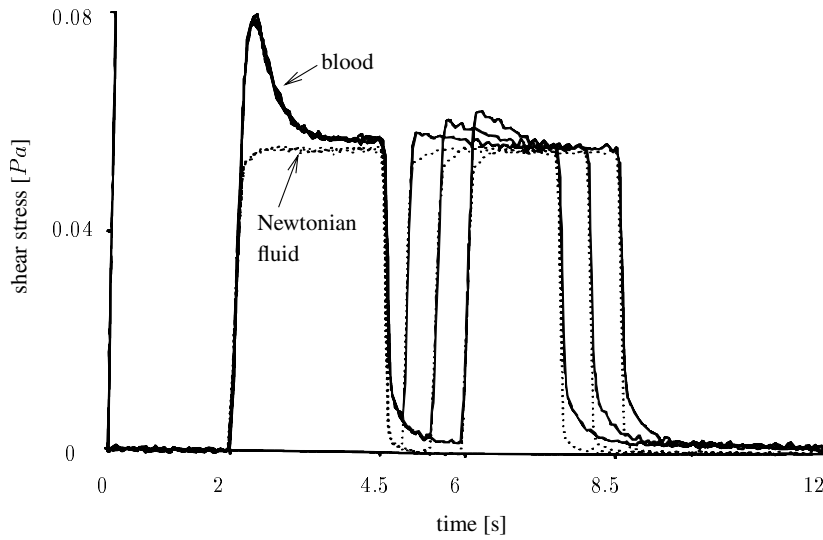


Figure 7.12: *Transient behavior of blood after step in shear rate.*

dependency of the viscosity that for Newtonian fluids is taken to be a constant. Power-law, Carreau-Yasuda and Casson models have been mentioned as examples of generalized Newtonian models. Viscoelasticity has been introduced using a simple exponential relaxation function and a shear dependency of the stress based on Boltzmann's superposition principle. From this the upper-convected Maxwell differential model for viscoelastic fluids is derived and two important dimensionless numbers are defined: the Deborah number, defined as the ratio between the relaxation time and the characteristic time of the fluid motion, and the Weissenberg number, defined as the product of the relaxation time and the characteristic shear rate. Finally it has been shown that suspensions may show non-Newtonian viscoelastic properties depending on the volume fraction, shape and deformability of the suspended particles.

Non-Newtonian shear-thinning properties of blood are most important in tubes with small diameters and result in flattened velocity profiles as compared to the Newtonian profiles. For fully developed flow viscoelastic properties can be incorporated by introduction of a complex Womersley number defined by  $\alpha^* = \sqrt{1 + iDe\alpha}$ ,  $De$  being the Deborah number.

## Chapter 8

# Flow patterns in the micro-circulation

### 8.1 Introduction

The circulatory system with vessels of a diameter  $D_v$  smaller than  $500\mu m$  is denoted as the micro-circulation. The flow in the micro-circulation is relatively simple from geometrical point of view since the entrance lengths are relatively short (see table 8.1) and almost everywhere the flow may be considered as a fully developed flow. Moreover, the Womersley number is relatively low (see table 8.1) so that the flow may be considered to be quasi-static. Finally the steady component is relatively large compared to the higher harmonics of the flow and hereby the diameter of the tubes may be considered to be constant in time. It must be noted that vasodilatation and vasoconstriction is not considered and beyond the scope of this section.

	$D[\mu m]$	$L[mm]$	$V[mm/s]$	$Re[-]$	$L_e/D[-]$	$\alpha[-]$
small arteries	70-500	10	40	5	0.25	1
arterioles	10-70	2	5	0.1	0.005	0.1
capillaries	4-10	1	1	0.005	0.0003	0.01
venules	10-110	2	4	0.1	0.005	0.15
small veins	110-500	10	20	3	0.15	1

Table 8.1: Dimensions and dimensionless numbers in the micro-circulation

Taking in account the consideration given above the governing equations that describe the flow are given by the steady Stokes equations:

$$\frac{\eta}{r} \frac{\partial}{\partial r} \left( r \frac{\partial v}{\partial r} \right) = \frac{\partial p}{\partial z} \quad (8.1)$$

Still the flow is more complex than Poiseuille flow as a result of the fact that the diameter  $D_c$  of the red blood cells suspended in the plasma is that large that the fluid can not be considered as a homogeneous fluid anymore. As will be elucidated in

the next sections, the flow in the micro-circulation can be divided into three regimes: small arteries and small veins ( $D_v > 2D_c$ ), arterioles and venules ( $D_c < D_v < 2D_c$ ) and capillaries ( $D_v < D_c$ ).

## 8.2 Flow in small arteries and small veins: $D_v > 2D_c$

If the ratio of the vessel diameter  $D_v$  and the cell diameter  $D_c$  is large, we may assume that the fluid in the core of the vessel is a homogeneous suspension of particles. The concentration of the particles in the core is constant and hereby the core will have a viscosity  $\eta_c$ . At the vessel wall, however, the concentration of particles will be lower due to the fact that they can not penetrate through the wall. A possible concentration profile then will look like the one depicted in figure 8.1. At a distance smaller than half the cell diameter  $\frac{1}{2}D_c$  the concentration is assumed to be zero  $c(a - \frac{1}{2}D_c < r < a) = 0$ . The concentration in the core is assumed to be constant  $c(r < a - \frac{1}{2}D_c) = c_c$ . With the definition  $a_c = a - \frac{1}{2}D_c$  this yields:

$$c = \begin{cases} c_c & 0 < r < a_c \\ 0 & a_c < r < a \end{cases} \quad (8.2)$$

The viscosity then will be also a function of the radius according to:

$$\eta = \begin{cases} \eta_c & 0 < r < a_c \\ \eta_p & a_c < r < a \end{cases} \quad (8.3)$$

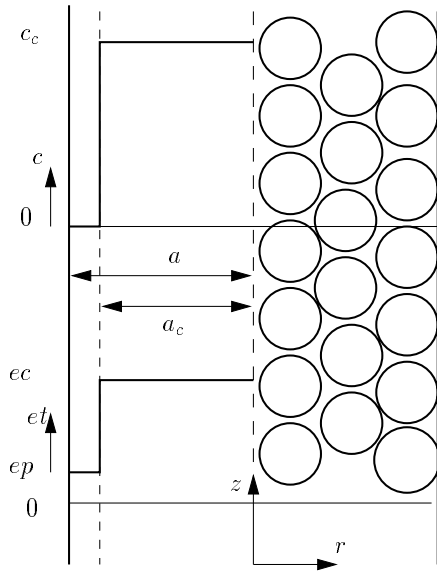


Figure 8.1: Particle concentration  $c$  and viscosity  $\eta$  in a tube with diameter  $D_v > 2D_c$ .

### 8.3 Velocity profiles

The velocity profiles can be computed from the momentum equations:

$$\begin{cases} \frac{\partial}{\partial r} \left( r \eta_c \frac{\partial v}{\partial r} \right) = r \frac{\partial p}{\partial z} & 0 < r < a_c \\ \frac{\partial}{\partial r} \left( r \eta_p \frac{\partial v}{\partial r} \right) = r \frac{\partial p}{\partial z} & a_c < r < a \end{cases} \quad (8.4)$$

Integration from 0 to  $r$  assuming the stress to be constant over the interface  $r = a_c$ , again integration from 0 to  $r$  assuming the velocity to be constant over the interface and substitution of the boundary conditions at  $r = a$  yields:

$$\begin{cases} v(r) = \frac{r^2 - a_c^2}{4\eta_c} \frac{\partial p}{\partial z} + \frac{a_c^2 - a^2}{4\eta_p} \frac{\partial p}{\partial z} & 0 < r < a_c \\ v(r) = \frac{r^2 - a^2}{4\eta_p} \frac{\partial p}{\partial z} & a_c < r < a \end{cases} \quad (8.5)$$

or with the dimensionless radius  $\xi = r/a$  and the dimensionless core diameter  $\lambda_c = a_c/a$ :

$$\begin{cases} v(\xi) = -\frac{a^2}{4\eta_c} (\lambda_c^2 - \xi^2) \frac{\partial p}{\partial z} + \frac{a^2}{4\eta_p} (\lambda_c^2 - 1) \frac{\partial p}{\partial z} & 0 < \xi < \lambda_c \\ v(\xi) = -\frac{a^2}{4\eta_p} (1 - \xi^2) \frac{\partial p}{\partial z} & \lambda_c < \xi < 1 \end{cases} \quad (8.6)$$

This function is plotted in figure 8.2 for several values of the dimensionless core radius  $\lambda_c$ . The profiles consist of two parts, one part (in the core) is a parabolic profile with a curvature that coincides with the profile of a fluid with a viscosity equal to the viscosity of the core fluid. The layer ( $\lambda < \xi < 1$ ) at the boundary corresponds with a profile that coincides with the profile of a fluid with plasma viscosity  $\eta = \eta_p$ . This combination results in a velocity profile that is flattened in the core with respect to the profile of pure plasma (see figure 8.2).

#### 8.3.1 Flow

The flow can easily be computed from the velocity profile by integration over the tube diameter and yields:

$$q = q_c + q_p = -\frac{\pi a^4}{8\eta_p} \left( 1 - \left( 1 - \frac{\eta_p}{\eta_c} \right) \lambda_c^4 \right) \frac{\partial p}{\partial z} \quad (8.7)$$

#### 8.3.2 Effective viscosity

If we compare the flow (8.7) with the flow of a homogeneous fluid with viscosity  $\eta_e$  yielding the same longitudinal impedance, we have:

$$\eta_e = \eta_p \frac{1}{1 - \left( 1 - \frac{\eta_p}{\eta_c} \right) \lambda_c^4} \quad (8.8)$$

In figure 8.3 the relative effective viscosity  $\eta_e/\eta_p$  is given as a function of the relative core diameter  $\lambda_c$  and the vessel radius  $a$ .

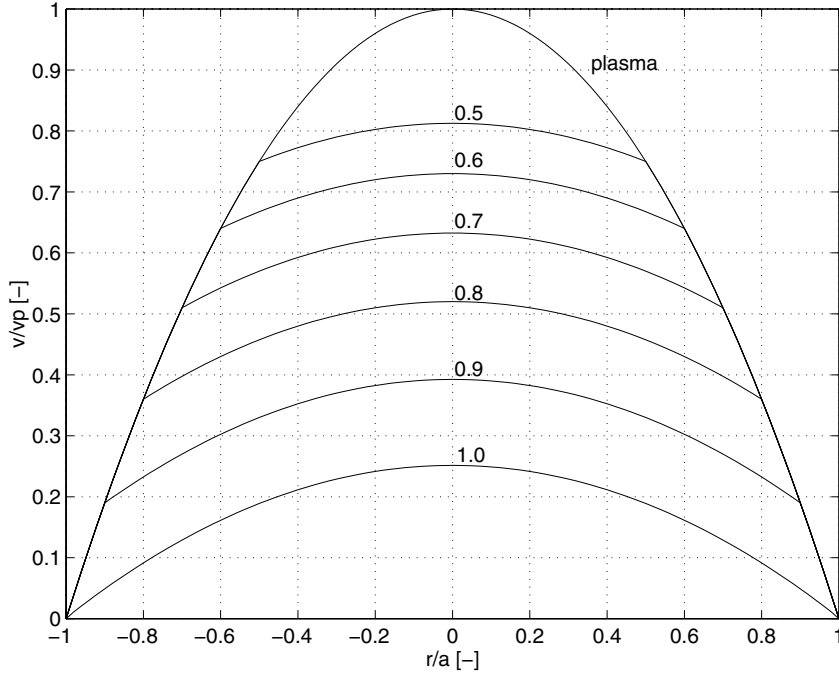


Figure 8.2: Velocity profile for several  $\lambda_c$  in a tube with diameter  $D_v > 2D_c$

### 8.3.3 Concentration

If we assume that the blood that flows through the vessel that is considered is supplied by a buffer with hematocrit  $c_0$ , then the concentration in the core  $c_c$  can be derived from:

$$c_o q = c_c q_c \quad (8.9)$$

and thus:

$$\frac{c_c}{c_0} = \frac{q}{q_c} = 1 + \frac{1 + \lambda_c^4 - 2\lambda_c^2}{\frac{\eta_p}{\eta_c} \lambda_c^4 - 2\lambda_c^4 + 2\lambda_c^2} \quad (8.10)$$

As can be seen from figure 8.3 the concentration in the core increases with decreasing  $\lambda_c$  or radius  $a$ .

The mean concentration, however, will decrease with decreasing  $\lambda_c$  according to:

$$\bar{c} = \frac{1}{\pi a^2} \int_0^a 2\pi r c(r) dr = \frac{2}{a^2} \int_0^{a_c} c_c r dr = c_c \lambda_c^2 \quad (8.11)$$

This shows us that if we want to measure the hematocrit by counting the particles that move with a flow through a small tube, the concentration will be underestimated. Actually figure 8.3 shows that the fraction of plasma in the core decreases with decreasing  $\lambda_c$  or diameter  $a$ .

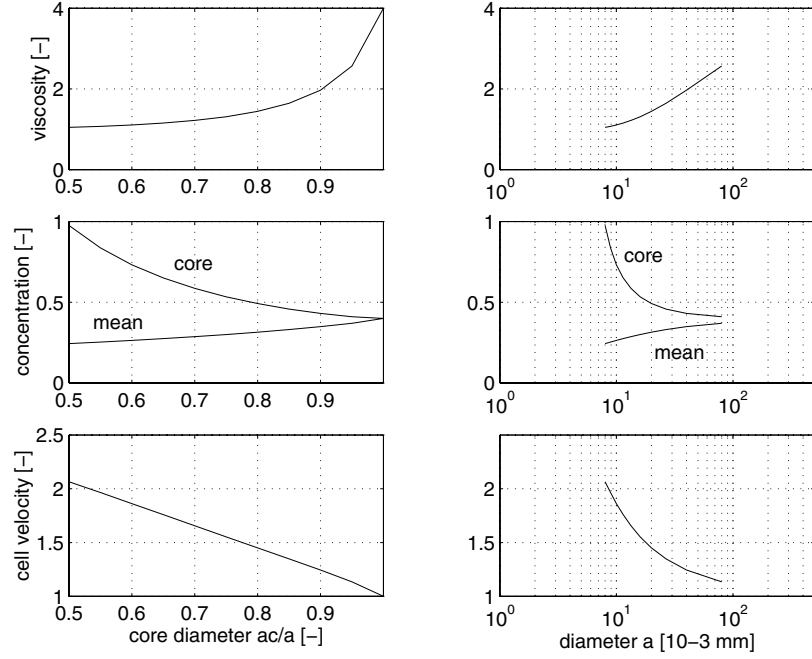


Figure 8.3: Relative viscosity  $\eta_e/\eta_p$  (top), concentration  $c_c$  and  $c_m$  (middle) and relative cell velocity  $v_{cell}/v_{plasma}$  (bottom) as a function of the relative core diameter  $\lambda_c$  (left) and tube radius  $a$  (right) in a tube with diameter  $D_v > 2D_c$

### 8.3.4 Cell velocity

In order to determine the velocity of the cells relative to the velocity of the surrounding plasma we compute the volume flow of cells:

$$q_{cell} = 2\pi \int_0^a vcrdr = \bar{v}_{cell}\bar{c}\pi a^2 \quad (8.12)$$

The volume flow of plasma is:

$$q_{plasma} = 2\pi \int_0^a v(1-c)dr = \bar{v}_{plasma}(1-\bar{c})\pi a^2 \quad (8.13)$$

The ratio between both flows is given by the hematocrit  $c_0$  according to:

$$\frac{q_{plasma}}{q_{cell}} = \frac{1-c_0}{c_0} \quad (8.14)$$

This yields (see also figure 8.3):

$$\frac{\bar{v}_{cell}}{\bar{v}_{plasma}} = \frac{c_0}{1-c_0} \frac{1-\bar{c}}{\bar{c}} \quad (8.15)$$

## 8.4 Flow in arterioles and venules : $D_c < D_v < 2D_c$

If the vessel diameter is in between 1 and 2 times the cell diameter, the cells have to move in a single train (see figure 8.4). The velocity in the core hereby will be constant. Similar to what has been shown in the previous section for vessels with a diameter larger then  $2D_c$  the velocity, flow, effective viscosity, effective concentration and cell velocity can be computed. As the central core behaves as a solid cylinder, it can be seen as a fluid with an infinite viscosity. The equations that are derived in the previous section can be simplified for the case that  $\eta_c \rightarrow \infty$ . Note that in the previous section with decreasing diameter the influence of the plasma layer increased. In this section, for smaller diameters, decreasing the diameter will also decrease the influence of the plasma layer.

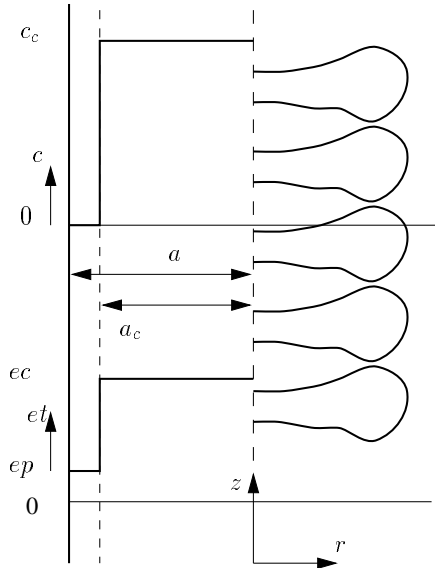


Figure 8.4: Particle concentration  $c$  and viscosity  $\eta$  in a tube with diameter  $D_c < D_v < 2D_c$ .

### 8.4.1 Velocity profiles

The velocity can be derived from (8.6) using  $\eta_c \rightarrow \infty$ .

$$\begin{cases} v(\xi) = \frac{a^2}{4\eta_p}(\lambda_c^2 - 1)\frac{\partial p}{\partial z} & 0 < \xi < \lambda_c \\ v(\xi) = -\frac{a^2}{4\eta_p}(1 - \xi^2)\frac{\partial p}{\partial z} & \lambda_c < \xi < 1 \end{cases} \quad (8.16)$$

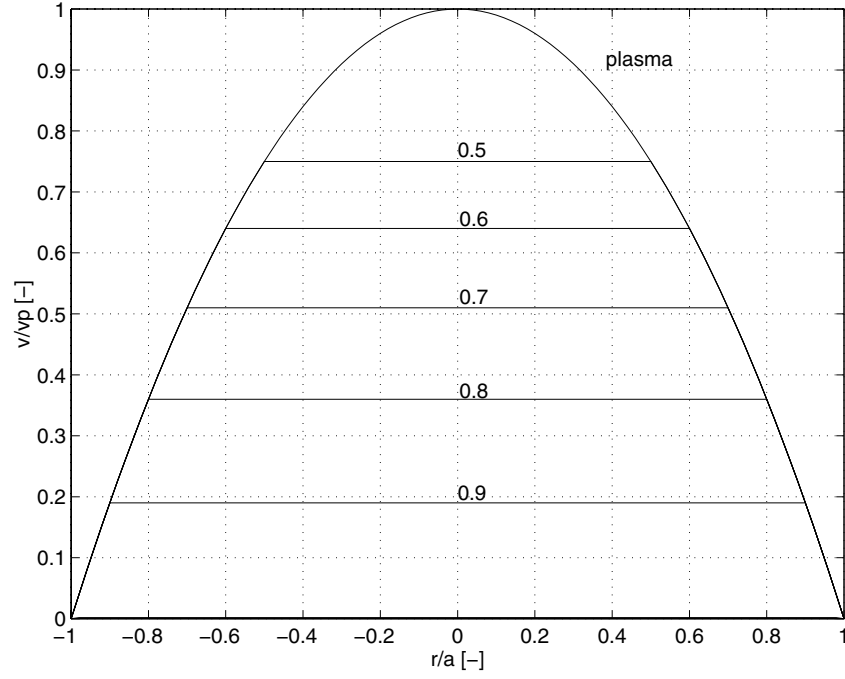


Figure 8.5: Velocity profile for several  $\lambda_c$  in a tube with diameter  $D_v > 2D_c$

### 8.4.2 Flow

The flow again can be derived from the velocity profiles and can be computed from (8.7) using  $\eta_c \rightarrow \infty$ .

$$q = q_c + q_p = -\frac{\pi a^4}{8\eta_p} (1 - \lambda_c^4) \frac{\partial p}{\partial z} \quad (8.17)$$

### 8.4.3 Effective viscosity

The effective viscosity then will be:

$$\eta_e = \eta_p \frac{1}{1 - \lambda_c^4} \quad (8.18)$$

### 8.4.4 Concentration

$$\frac{c_c}{c_0} = 1 + \frac{1 + \lambda_c^4 - 2\lambda_c^2}{-2\lambda_c^4 + 2\lambda_c^2} = 1 + \frac{1 + \lambda_c^2}{2\lambda_c^2} \quad (8.19)$$

and

$$\bar{c} = c_c \lambda_c^2 \quad (8.20)$$

### 8.4.5 Cell velocity

$$\frac{\bar{v}_{cell}}{\bar{v}_{plasma}} = \frac{c_0}{1 - c_0} \frac{1 - \bar{c}}{\bar{c}} \quad (8.21)$$

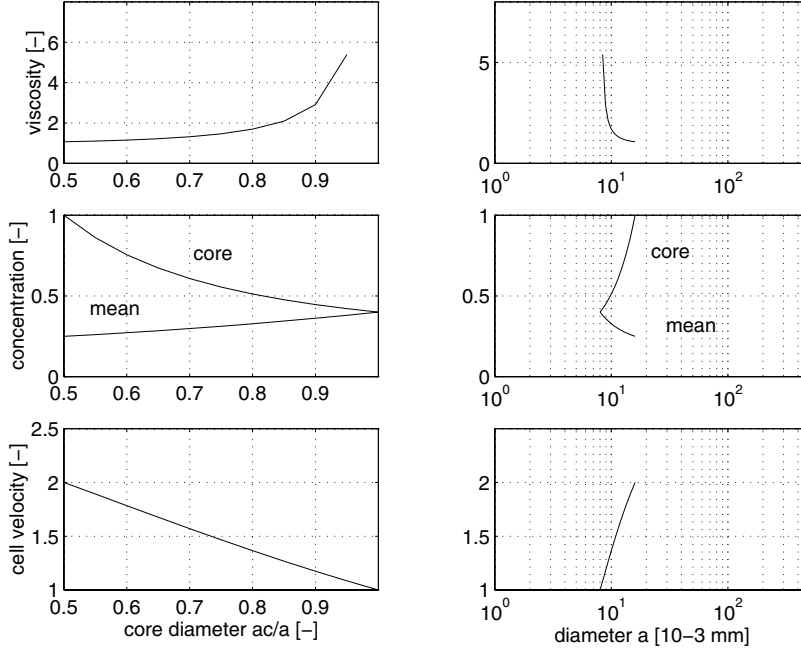


Figure 8.6: Relative viscosity  $\eta_e/\eta_p$  (top), concentration  $c_c$  and  $c_m$  (middle) and relative cell velocity  $v_c/v_p$  (bottom) as a function of the relative core diameter  $\lambda_c$  (left) and tube radius  $a$  (right) in a tube with diameter  $D_v > 2D_c$

## 8.5 Flow in capillaries: $D_v < D_c$

In the capillaries, both the vessel wall and the red blood cells deform in order enable a flow: the diameter of the undeformed capillaries is smaller than the diameter of the undeformed red cells. This deformation and some important parameters that are used in models that describe the flow in capillaries are given in figure 8.5. If it is assumed that the deformation of the cell and the deformation of the wall are proportional to the local pressure, a cell with a parabolic shape is defined by:

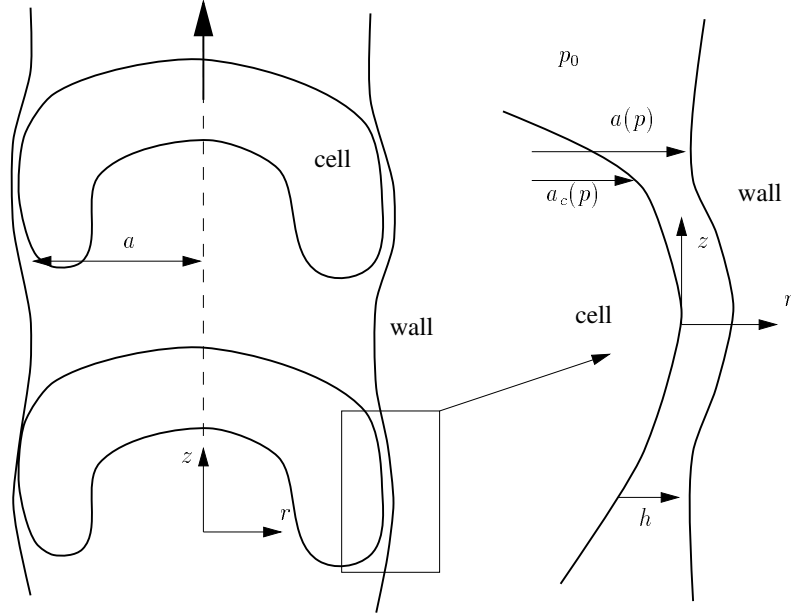
$$a_c(p) = a_c(p_0) - \frac{1}{2}kz^2 - \beta(p - p_0) \quad (8.22)$$

The location of the wall then will be given by:

$$a(p) = a(p_0) + \alpha(p - p_0) \quad (8.23)$$

If we define  $h$  to be the thickness of the film in between the cell and the wall, it will be given by:

$$h(p) = a(p) - a_c(p) = (\alpha - \beta)(p - p_0) + \frac{1}{2}kz^2 \quad (8.24)$$


 Figure 8.7: Particle movement in a tube with diameter  $D_v < D_c$ .

For a small film-thickness ( $h \ll a_c$ ) a local Cartesian coordinate system can be used and the momentum equation reduces to:

$$\begin{cases} \frac{\partial p}{\partial z} = \mu \frac{\partial^2 v}{\partial r^2} \\ v(0) = \bar{v}_c \\ v(h) = 0 \end{cases} \quad (8.25)$$

This restricts the velocity to a function that is quadratic in  $r$ :

$$v = ar^2 + br + c \quad (8.26)$$

Together with the boundary conditions and the continuity equation:

$$\int_0^h v dr = \bar{v}_p \cdot h = \frac{1}{3}ah^3 + \frac{1}{2}bh^2 + \bar{v}_c h = \bar{u}_p h \quad (8.27)$$

This yields:

$$v = \bar{v}_c \left( 3 \frac{r^2}{h^2} - 2 \frac{r}{h} \right) + \bar{v}_p \left( -6 \frac{r^2}{h^2} + 6 \frac{r}{h} \right) \quad (8.28)$$

The pressure gradient then is given by:

$$\frac{\partial p}{\partial z} = \frac{6\eta_p}{h^2} \bar{v}_c + \frac{12\eta_p}{h^3} \bar{v}_p \quad (8.29)$$

It will be clear that the effective viscosity will increase enormously with decreasing artery diameter.

## **8.6 Summary**

In the micro-circulation, the size of the red blood cells is not small compared to the radius of the tube and models can be derived where the difference in concentration and motion of the individual cells are incorporated by introducing a jump in the viscosity. Also in these cases flattened velocity profiles are found even if non-Newtonian properties are not included as a result of the lower viscosity at the wall.

# Bibliography

- Abramowitz, M. and Stegun, I. (1964). *Handbook of Mathematical functions*. Dover Publications, Dover.
- Batchelor, G. (1967). *An Introduction to Fluid Mechanics*. Cambridge University Press, Cambridge.
- Batchelor, G. K. (1977). The effect of brownian motion on the bulk stress in a suspension of spherical particles. *J. Fluid Mech.*, **83**, 97–117.
- Bingham, E. (1922). *Fluidity and Plasticity*. McGraw-Hill, New York.
- Bird, R., Stewart, W., and Lightfoot, E. (1960). *Transport phenomena*. John Wiley & Sons, New York.
- Bird, R., Armstrong, R., and Hassager, O. (1987). *Dynamics of Polymer Liquids*. John Wiley & Sons, New York.
- Chadwick, P. (1976). *Continuum Mechanics*. John Wiley & Sons, New York.
- Chien, S., Usami, S., Dellenback, R. J., and Gregersen, M. I. (1969). Shear-dependent deformation of erythrocyts in rheology of human blood. *American Journal of Physiology*, **219**, 136–142.
- Collins, W. M. and Dennis, S. C. R. (1975). The steady motion of a viscous fluid in a curved tube. *Q.J.Mech. Appl. Math*, **28**, 133–156.
- Fung, Y. (1993a). *Mechanical Properties and Active Remodeling of Blood Vessels*, chapter 8, pages 321–391. In Fung (1993b), 2<sup>nd</sup> edition.
- Fung, Y., Fronek, K., and Patitucci, P. (1979). Pseudoelasticity of arteries and the choice of its mathematical expression. *American Journal of Physiology*, **237**, H620–H631.
- Fung, Y. C. (1993b). *Biomechanics, Mechanical Properties of Living Tissues*. Springer Verlag, New York Berlin Heidelberg, 2<sup>nd</sup> edition.
- Guyton, A. C. (1967). *Textbook of Medical Physiology*. Saunders.
- Kasyanov, V. and Knet-s, I. (1974). Deformation energy function of large human blood vessels. *Mekhanika Polimerov*, **1**, 122–128.

- Macosko, C. W. (1994). *Rheology, principles, measurements and applications*. VCH publishers, Inc., New York.
- McMillan, D., Strigberger, J., and Utterback, N. (1987). Rapidly recovered transient flow resistance: a newly discovered property of blood. *Am. J. Physiol.*, **253**, 919–926.
- Milnor, W. R. (1989). *Hemodynamics*. Williams & Wilkins, Baltimore, Hong Kong, London, Sidney.
- Pedley, T. (1980). *The fluid mechanics of large blood vessels*. Cambridge University Press, Cambridge.
- Quemada, D. (1978). Rheology of concentrated disperse systems. ii. a model for non-newtonian shear viscosity in steady flows. *Rheol. Acta*, **17**, 632–642.
- Rhodin, J. A. G. (1980). *Architecture of the Vessel Wall*, chapter 1, pages 1–31.
- Rosenblatt, J. S. (1988). *The rheology of blood: a structured fluid approach based on rouleau behaviour*. Ph.D. thesis, University of California, Berkeley.
- Schlichting, H. (1960). *Boundary Layer Theory*. McGraw-Hill, New York.
- Schmid-Schönbein, H., Wells, R., and J. Goldstone (1971). Fluid drop-like behavior of erythrocytes- disturbance in pathology and its quantification. *Biorheology*, **7**, 227–234.
- Thurston, G. (1973). Frequency and shear rate dependence of viscoelasticity of human blood. *Biorheology*, **10**, 375–381.
- Ward-Smith, A. (1980). *Internal fluid flow*. Oxford.
- Womersley, J. R. (1957). The mathematical analysis of the arterial circulation in a state of oscillatory motion. Technical report wadc-tr-56-614, Wright Air Development Center.

# Index

- admittance, 71–73
  - effective, 78
- aggregation, 103
- albumin, 84
- arterial system, 4, 5
  - dimensions, 4
- arteries
  - aorta, 3
  - pulmonary, 2
- arterioles
  - pulmonary, 2
- atrium
  - left, 2
  - right, 2
- Bernoulli equation, 30
- Bessel functions, 35
- blood
  - generalized Newtonian models, 90
  - Newtonian models, 89
  - plasma, 84
  - rheology, 86, 102
  - viscoelastic models, 94
  - viscosity, 88
- Boltzmann's superposition principle, 94
- boundary layer
  - thickness, 40
- boundary layer flow, 30
- branched tube
  - flow, 49
- capillary system, 5
  - dimensions, 4
- cardiac work, 81
- cardiovascular system, 2
- Careau-Yasuda model, 91
- Casson model, 91
- Cauchy stress tensor, 16
- Cauchy-Green deformation tensor, 18
- circulation
  - pulmonary, 2
  - systemic, 2, 4
- coagulation, 102
- collagen, 53
- compliance, 7, 11, 60, 69
- compression modulus, 57
- constitutive equations, 20
- continuity equation, 22
- contraction
  - atrial, 3
  - ventricular, 3
- curved tube
  - steady entrance flow, 41
  - steady fully developed flow, 45
  - unsteady fully developed flow, 47
- Dean number, 46
- Deborah number, 96
- deformation
  - Cauchy-Green deformation tensor, 18
  - deformation gradient tensor, 16, 17
  - Finger tensor, 18
  - linear elastic, 56
  - neo-Hookean, 56
  - rate of deformation tensor, 19, 20
  - shear, 18
  - stretch, 17
- diastole, 3
- Dirichlet conditions, 24
- discrete transitions, 75
- displacement
  - displacement vector, 16
- distensibility, 7, 61, 69
- distensible tube
  - fluid flow, 65
- distensible tubes

- wave propagation, 67
- effective viscosity, 109, 113
- elastic solids, 20
- elastin, 53
- endothelial cells, 5, 53
- entrance flow
  - curved tube, 41
  - rigid tube, 39
- entrance length
  - oscillating flow, 41
  - steady flow, 40
- equations of motion, 21
- erythrocytes, 84
- Euler equations, 29
- extra stress tensor, 20
- fibrinogen, 84
- Finger tensor, 18
- flow
  - aortic, 3
  - arterioles and venules, 112
  - branched tubes, 49
  - capillaries, 114
  - curved tube, 41
  - entrance, 39
  - Fourier decomposition, 8, 10
  - incompressible in-viscid, 29
  - incompressible boundary layer flow, 30
  - incompressible viscous, 28
  - irrotational, 30
  - Newtonian, 28
  - secondary flow in curved tube, 43
  - small arteries and veins, 108
- Froude number, 28
- fully developed flow
  - curved tube, 45
  - straight tube, 32
- Gauss-Ostrogradskii theorem, 22
- globulins, 84
- heart, 2
  - minute volume, 5
- impedance, 71
  - input, 12
    - longitudinal, 12, 38
    - transverse, 12
  - initial and boundary conditions, 24
  - Leibnitz formula, 22
  - leucocytes, 86
  - micro circulation, 5
  - micro-circulation, 107
  - Moens Korteweg wave speed, 71
  - momentum equation, 23
  - Navier-Stokes equations, 28
    - cylindrical coordinates, 32
    - dimensionless, 28
    - toroidal coordinates, 45
  - Neumann conditions, 24
  - Newtonian flow, 28
    - fully developed, 32
  - Newtonian fluids, 20
  - peripheral resistance, 11
  - plasma, 84
    - density, 84
    - viscosity, 84, 103
  - platelets, 86
  - Poisson ratio, 58
  - power-law model, 91
  - pressure
    - aortic, 3
    - Fourier decomposition, 8, 10
    - pulmonary, 3
    - systemic, 3
    - transmural, 6
    - ventricular, 3
  - Quemada model, 102
  - rate of deformation tensor, 20, 28
  - red blood cells
    - aggregation, 103
    - concentration, 110, 113
    - deformation, 103
    - viscosity, 84
  - reflection
    - multiple, 78
  - reflection coefficient, 76

- resistance
  - periferal, 5
- Reynolds number, 28
- Reynolds' transport theorem, 21
- rheology, 86
- rheology of blood, 102
- rheometry, 87
- Rosenblatt model, 105
- rotation tensor, 18
- secondary flow, 43
  - secondary boundary layer, 47
- shear, 18
- shear modulus, 20, 56
- smooth muscle cells, 54
- spin tensor, 20
- straight tube
  - entrance flow, 39
  - fully developed flow, 32
  - longitudinal impedance, 38
  - oscillating entrance flow, 41
  - steady entrance flow, 40
  - velocity profiles, 33
  - wall shear stress, 36
- streamlines, 29
- stress
  - state of, 16
  - stress tensor, 16
  - stress vector, 16
- stretch, 17
- stretching tensor, 18
- Strouhal number, 28
- suspensions, 100
  - Quemada model, 102
  - rheology, 100
- systole, 3
- transmission coefficient, 76
- valve
  - aortic, 3
  - mitral, 3
- vasoconstriction, 5
- vasodilatation, 5
- veins
  - venae cavae, 2
- velocity
  - velocity gradient tensor, 19
  - velocity vector, 19
- velocity profiles
  - arbitrary Womersley number, 34
  - large Womersley number, 34
  - rigid tube, 33
  - small Womersley number, 33
- venoconstriction, 5
- venous system, 5
  - dimensions, 4
- ventricle
  - left, 2
  - right, 2
- vessel wall
  - adventitia, 53
  - effective Young's modulus, 55
  - elastic behavior, 54
  - incremental Young's modulus, 55
  - intima, 52, 53
  - media, 53
  - morphology, 52
  - smooth muscle cells, 53
  - viscoelastic behavior, 55
  - Young's modulus, 55
- viscoelastic fluids, 20
- viscoelastic solids, 20
- viscosity
  - dynamic, 20
  - effective viscosity, 109, 113
- vorticity tensor, 20
- wall shear stress
  - rigid tubes, 36
- wave attenuation, 70
- wave number, 70
- wave reflection, 75
- wave speed, 65, 70
  - Moens Korteweg, 71
- waves
  - angular frequency, 64
  - attenuation constant, 70
  - complex amplitude, 64, 70
  - complex notation, 64
  - flow, 6
  - phase velocity, 70
  - pressure, 6

- wave attenuation, 70
- wave length, 64
- wave number, 64, 70
- wave speed, 70
- Weissenberg number, 96
- windkessel model, 11, 64
  - impedance, 64
- Womersley function
  - approximation, 37
  - definition, 36
- Womersley number
  - definition, 32
  - values in arteries, 33
- Womersley profiles, 35, 67
- Young's modulus, 58
  - complex modulus, 70